INSTITUTO DE QUÍMICA

PROGRAMA DE PÓS-GRADUAÇÃO EM GEOCIÊNCIAS - GEOQUÍMICA

PATRICIA DE SENA PIACSEK BORGES

VEGETATION AND OCEAN DYNAMICS OVER THE LAST 130 KYR: PALYNOLOGICAL RECORDS FROM A MARINE SEDIMENT CORE IN THE WESTERN EQUATORIAL ATLANTIC

NITERÓI

2020

VEGETATION AND OCEAN DYNAMICS OVER THE LAST 130 KYR: PALYNOLOGICAL RECORDS FROM A MARINE SEDIMENT CORE IN THE WESTERN EQUATORIAL ATLANTIC

Tese apresentada ao Curso de Pós-Graduação em Geociências da Universidade Federal Fluminense, como requisito parcial para a obtenção do Grau de Doutora. Área de Concentração: Geoquímica Ambiental.

Orientadora:
Prof.ª Dr.ª Ana Luiza Spadano Albuquerque

NITERÓI
2020

AGRADECIMENTOS

Agradeço à CAPES pela concessão da bolsa de estudos durante o período deste doutorado e por sua atuação no suporte da ciência brasileira.

Agradeço à minha orientadora Ana Luiza Spadano Albuquerque que me acolheu e orientou com muito carinho e dedicação. Sou muito grata por você ter aceitado me orientar e por todo o suporte e contribuições valiosas na construção da minha tese de doutorado e na minha construção como pesquisadora do paleoclima. Você é uma profissional inspiradora.

Agradeço aos demais professores e funcionários do Departamento de Geoquímica pela dedicação ao ensino de qualidade e por todo o conhecimento adquirido. Saliento a cooperação do professor Renato Campello Cordeiro que disponibilizou o uso do microscópio óptico Zeiss primo star, viabilizando o prosseguimento na contagem dos palinomorfos. Muito obrigada.

Agradeço ao querido amigo Igor Venancio pelas discussões construtivas e cooperação com o desenvolvimento da minha tese.

O desenvolvimento do meu doutorado foi contemplado com o aperfeiçoamento de um ano no Departamento de Palinologia e Dinâmica Climática da Universidade de Göttingen, na Alemanha. Agradeço ao professor Hermann Behling por pela dedicação e paciência de me ensinar a identificar os diversos tipos polínicos, por sua valiosa contribuição técnica na elaboração do meu doutorado, pela amizade e cordialidade. Agradeço a Fang Gu, pelo carinho do primeiro ao último dia da minha permanência no departamento e por toda a paciência que teve ao me ensinar identificar os diferentes cistos de dinoflagelados. Agradeço também à receptividade e amizade dos pesquisadores e funcionários do departamento, vocês facilitaram minha estadia na Alemanha e sou muito grata por ter conhecido todos vocês.

Agradeço à equipe do Laboratório de Oceanografia Operacional e Paleoceanografia (LOOP) e aos tantos amigos que me acompanharam ao longo desta árdua caminhada.

Agradeço à minha família que sempre incentivou as minhas escolhas profissionais.

Agradeço à Mariane Morgado.

Agradeço ao Cristiano Piacsek Borges, meu pai, por ser minha base, meu norte, e exemplo de ser humano. Sem você esse doutorado não sería possível. Te amo.

ACKNOWLEDGMENTS

I thank CAPES for the scholarship during the period of this doctorate and for supporting Brazilian science.

I thank my advisor Ana Luiza Spadano Albuquerque, for guiding me with great affection and dedication. Ana, I'm extremely grateful that you accepted to orientate me and for all the support and valuable contributions over the elaboration of my doctoral thesis and in my personal construction as a paleoclimate researcher. You are an inspiring professional.

I thank the other professors and employees of the Geochemistry Department for the dedication to improve the quality of teaching and for all the knowledge acquired. I would like to thank the cooperation of Professor Renato Campello Cordeiro, with my palynomorph counting. Thank you very much.

I thank my dear friend Igor Venancio for the constructive discussions and cooperation with the development of my thesis.

My development as a researcher was contemplated with one year in the Department of Palynology and Climate Dynamics at the University of Göttingen, in Germany. I thank the professor Hermann Behling for the dedication and patience to teach me to identify the different pollen types. Thanks for the technical contribution to my Ph.D., friendship, and benevolence. I thank Fang Gu for the affection from the first to the last day of my stay in the Department, for all the patience he had in teaching me to identify the different types of dinoflagellate cysts and valuable contributions. I'm also grateful for the receptivity and friendship of the researchers and employees of the Department of Palynology, you made my stay joyful, and I am very thankful to have met you all.

I thank the team of the Laboratory of Operational Oceanography and Paleoceanography (LOOP) and the friends who accompanied me along this arduous journey.

I thank my family, who always encouraged my professional choices.

I thank Mariane Morgado.

I thank my dear father, for being my foundation, my north, and an example as a human being. Without you, this Ph.D. would not be possible. I love you.

“When we try to pick out anything by itself, we find that it is bound fast by a thousand invisible cords that cannot be broken, to everything in the universe.” John Muir

“What's goin' on?”

RESUMO

As concentrações atuais de CO_2 atmosférico romperam a variabilidade natural dos últimos 800 kyrs do quaternário. O aquecimento global gerado por ações antropogênicas aumenta as incertezas quanto à disponibilidade hídrica nos continentes. A precipitação na região do nordeste do Brasil possui estreita relação com a presença da Zona de Convergência Intertropical (ZCIT). Compreender o padrão de precipitação no nordeste do Brasil sob diferentes condicionantes climáticas pode trazer luz à interpretação de projeções climáticas futuras. Dentro dessa perspectiva, analisamos os últimos 130 mil anos registrados no testemunho marinho GL-1248, sob influência da descarga do rio Parnaíba. O uso do testemunho sedimentar marinho e a identificação morfológica de palinomorfos (grãos de pólen e esporos e cistos de dinoflagelados) nos permitiu inferir oscilações ecológicas no continente, carreadas pela vazão do rio até o oceano adjacente, assim como mudanças autóctones da produtividade primária na superfície do oceano. A identificação do pólen e dos esporos foi realizada com base nas coleções de referência do Departamento de Palinologia e Dinâmica Climática da Universidade de Göttingen e na literatura. Os grãos de pólen foram agrupados de acordo com o bioma em que os tipos polínicos são encontrados em sua distribuição natural. Os cistos de dinoflagelados (dinocistos) foram agrupados em táxons autotrófico e heterotrófico devido suas diferentes demandas energéticas. Os palinomorfos identificados foram classificados em nível de família e quando possível em nível de espécie, e agrupados de acordo com sua funcionalidade ecológica. Ao longo do glacial, eventos milenares de intensa precipitação (Heinrich Stadials) marcaram transições da ZCIT sob o nordeste do Brasil. A resposta contrastante entre a vegetação de floresta tropical e de vegetação aberta foi modulada pela sensibilidade à disponibilidade hídrica. A presença prolongada da ZCIT e aumento da umidade da bacia hidrográfica do Parnaíba promoveram ganhos da floresta tropical e da biodiversidade da vegetação. No oceano adjacente, as assembleias de dinocistos despontaram um padrão glacial-interglacial nítido. O período glacial apresentou aumento dos organismos heterotróficos, favorecidos pelo aumento da robustez da pluma do rio Parnaíba em decorrência dos eventos de aumento da precipitação, assim como, pela e da proximidade de linha de costa à região do testemunho marinho. Deslocamentos da ZCIT reduzem a precipitação local e promovem o aumento da intensidade dos ventos alísios. Alinhado a isto, ocorre a expansão da vegetação aberta e aumento do revolvimento da camada de mistura do oceano, viabilizando mais nutrientes na zona fótica. Os períodos interglaciais apresentaram diferenças entre si, a vegetação de floresta tropical apresentou significante aumento da abundância relativa em meio ao estágio isotópico marinho (MIS) 5, sem inferências similares no MIS1. No oceano, duas assembleias de dinocistos autotróficos, que intercalaram a predominância ao longo do MIS5. Estas alterações possivelmente relacionadas com a mudança de intensidade dos ventos alísios e da disponibilidade de nutrientes na zona fótica. Compreender os mecanismos de interação climáticos e as suas implicações para os ecossistemas terrestre e marinho tem o potencial de otimizar as projeções climáticas, assim como otimizar medidas de mitigação dos impactos antropogênicos na região nordeste do Brasil.

Palavras-chave: Palinologia; Nordeste do Brasil; Zona de Convergência Intertropical; Glacial-Interglacial.

ABSTRACT

Current atmospheric CO_2 concentrations have disrupted the natural variability of the last 800 kyrs of the Quaternary period. The anthropogenic global warming increases the uncertainties regarding water availability on the continents. Precipitation in northeastern Brazil (NEB) is closely related to the presence of the Intertropical Convergence Zone (ITCZ). Understanding the rainfall pattern in NEB under different climatic conditions has the potential to improve the interpretation of climate projections. We analyzed the last 130kyrs recorded in the marine core GL-1248, retrieved from the continental slope and under the influence of the Parnaíba river discharge. Palynological analysis of pollen grains and spores and dinoflagellate cysts enables us to infer ecological oscillations on the continent, carried by the river outflow to the adjacent ocean, as well as autochthonous changes in primary productivity on the surface of the ocean. The identification of pollen and spores was carried out based on the reference collections of the Department of Palynology and Climate Dynamics at the University of Göttingen and the literature. Pollen grains were grouped according to the vegetation in which pollen types are found in their natural distribution. Dinoflagellate cysts (dinocysts) were grouped into autotrophic and heterotrophic taxa due to their different energy demands. The identified palynomorphs were classified at the family level and, when possible at the species level, grouped according to their ecological affinities. Over the glacial period, events of intense precipitation (Heinrich Stadials) are linked to ITCZ displacements over the NEB. The contrast in vegetation response (tropical forest and more open vegetation) was modulated by sensitivity to water availability. The prolonged presence of the ITCZ and increased humidity in the Parnaíba Hydrographic Basin provoke gains in the tropical forest and the biodiversity of the vegetation. In the adjacent ocean, assemblages of dinocysts have displayed a clear glacial-interglacial pattern. The glacial period showed an increase in heterotrophic organisms, favored by the robustness of the Parnaíba river plume because of increased precipitation events, as well as the proximity of the coastline to the marine core region. The ITCZ shifts from NEB reduce local precipitation and increase the strength of trade winds. In line with this, there was an expansion of the open vegetation and an increased wind-mix and provided nutrients in the photic zone. The interglacial periods showed differences between them, the tropical forest vegetation showed a significant increase in relative abundance in the middle of the marine isotopic stage (MIS) 5, without similar inferences in MIS1. In the ocean, two assemblages of autotrophic dinocysts, this interspersed the predominance throughout the MIS5. These changes are possibly related to the difference in the intensity of the trade winds and the availability of nutrients in the photic zone. Understanding the mechanisms of climate interaction and its implications for terrestrial and marine ecosystems has the potential to optimize climate projections, as well as optimize measures to mitigate anthropogenic impacts in NEB.

Keywords: Palynology; Northeastern Brazil; Intertropical Convergence Zone; Glacial-Interglacial.

LIST OF ABBREVIATIONS

AAIW	Antarctic Intermediate Water
AMOC	Atlantic Meridional Overturn Circulation
A	Autotrophic
Avg.	Average
Brig spp	*Brigantedinium spp*
CCA	Canonical-Correlation Analysis
CA	Correspondence Analysis
D. cha	*Dalella chathamensis*
D-O	Dansgaard–Oeschger
E. acu	*Echinidinium aculeatum*
E. del	*Echinidinium delicatum*
E. gra	*Echinidinium granulatum*
E. tra	*Echinidinium transparantum*
AR-5	Fifth assessment report
HS	Heinrich Stadials
H	Heterotrophic
HDI	Human Development Index
HCl	Hydrochloric acid
HF	Hydrofluoric acid
IRD	Ice-Rafted Debris
I. acu	*Impagidinium aculeatum*
I. par	*Impagidinium paradoxum*
I. pat	*Impagidinium patulum*
I. sph	*Impagidinium sphaericum*
I. str	*Impagidinium strialatum*
I. vel	*Impagidinium velorum*
IPCC	Intergovernmental Panel on Climate Change
ITCZ	Intertropical Convergence Zone
LG	Lapa Grange cave
LGM	Last Glacial Maximum
L. mac	*Lingulodinium machaerophorum*
M	Meters
MIS	Marine Isotopic Stages
N. lab	*Nematosphaeropsis labyrinthus*
Nd	Neodymium
NADW	North Atlantic Deep Water
NBC	North Brasilian Current
NBUC	North Brazil Undercurrent
NECC	North Equatorial Countercurrent
NE	Northeast
NEB	Northeastern Brazil
O. cen	*Operculodinium centrocarpum*
O. isr	*Operculodinium israelianum*
PMIP	Paleoclimate Modelling Intercomparison Project
PHB	Parnaíba hydrographic basin
P. dal	*Pentapharsodinium dalei*

P. zoh	*Polysphaeridium zoharyi*
P. ame	*Protoperidinium americanum*
P. ret	*Pyxidinopsis reticulata*
T	Reaction time
R-Cysts	Resistant cysts
RSL	Relative Sea-Level
SST	Sea surface temperature
S. nep.	*Selenopemphix nephroides*
S. qua	*Selenopemphix quanta*
S-Cysts	Sensible oxygen cysts
K	Sensitive cysts
SACW	South Atlantic Central Water
SEC	South Equatorial Current
SE	Southeast
S. ben	*Spiniferites bentorii*
S. mem	*Spiniferites membranaceus*
S. mir	*Spiniferites mirabilis*
S. pac	*Spiniferites pachydermus*
T. app	*Trinovantedinium applanatum*
TW	Tropical Water
T. van	*Tuberculodinium vancampoae*
UTCV	Upper Tropospheric Cyclonic Vortices
XRF	X-ray fluorescence
Yr	Year
Kyr	Thousand years
O. cen reduced	*Operculodinium centrocarpum reduced processes*
∆δ18Odut-rub	The difference between the stable oxygen isotopic composition of Globigerinoides ruber white and Neogloboquadrina dutertrei

LIST OF FIGURES

LIST OF TABLES

SUMMARY

1 INTRODUCTION

1.1 Motivation

Over the last decades, scientists have drilled into the ancient ice preserved beneath Antarctica Ice sheets and analyzed the composition of oxygen isotopes trapped air bubbles from the past atmosphere. Paleoclimatologists are able to determine the historical carbon dioxide concentrations and to reconstruct the correlation between CO_2 atmospheric levels and global temperature (EPICA, 2004; Jouzel *et al.*, 2007; Luthi *et al.,* 2008). A periodicity pattern of 100 kyrs was noticed between warm interglacial phases, denoting the eccentricity orbit imprint. The clockwork precision of orbital cycles guided the climatic variability under the predominance of eccentricity orbit over the past 800 kyrs. In addition, the alignment of the maximum obliquity and precession orbit patterns with a more circular orbit (maximum eccentricity) seems to trigger warm conditions on the Earth's climate by elevating the CO_2 levels at the atmosphere of the planet (Berger & Loutre, 2003). The transition between glacial and interglacial periods is followed by changing patterns of heat distribution around the planet earth, with specific conditions of precipitation and temperature for each period.

The oceans and the atmosphere currents systems work as heat conveyors, operating the Earth's climate in parallel by redistributing temperature and moisture around the world. The Atlantic Meridional Overturning Circulation (AMOC) is a system of ocean currents, modulated by a delicate balance of temperature and salinity effects on density. Fluctuations in AMOC strength throughout the quaternary period supported the successions of glacial and interglacial cycles (Haug *et al.,* 2004). Unsteady flow of the warm superficial waters from the equatorial Atlantic to high latitudes reduced the exchange of heat between the ocean and the atmosphere. Still, the AMOC weakening generates an unbalanced distribution of sea surface temperatures (SST) over the Atlantic Ocean, warming the Southern Ocean, and Antarctica. A secondary effect of warmer waters on the sea surface is the southward shift of the Intertropical Convergence Zone (ITCZ) (Ruddiman *et al*., 2001; Yoon & Zeng, 2010). The ITCZ consists of an atmospheric convection band of intense precipitation, and its seasonal migration is the result of atmospheric pressure gradients at the equator and the meridional temperature gradient (Webster & Fasullo, 2003). The subsequent effect of the southward shift of ITCZ is the rearranging of the current rainfall distribution, as the tradewinds path and vigor.

Most of the vegetation reconstructions in northeastern Brazil comprise the transition from the last glacial maximum to the Holocene. They were valuable for the paleoclimatic community and have inferred the plasticity of rainforest vegetation, expanding to current semi-semiarid regions (De Oliveira *et al.,* 1999; Dupont *et al.,* 2010; Bouimetarhan *et al.,* 2018). These studies indicated that the vegetation responded to changes in the regional precipitation system. Although, due to the scarce continental information in northeastern

Brazil during another interglacial period, beyond the Holocene, it is complicated to prevent comparisons with recent CO_2 levels. Coordinated with ITCZ shifts over northeastern Brazil, the cross-equatorial heat flow of AMOC and tradewinds pattern can be evaluated in the adjacent ocean. The paleoproductivity of the western equatorial Atlantic has been recorded over the last interglacial. Still, most of the marine sediment cores were retrieved from the Ceará Rise. The paleoproductivity over the Ceará Rise was under the intermittent influence of North Equatorial Countercurrent (NECC), without or with a reduced continental contribution (Rühlemann *et al.,* 1996; Mulitza *et al.,* 1998; Vink *et al*., 2002). Also, the resolution of these marine sediment cores does not infer paleoproductivity oscillations on millennial-scale events over the glacial period, with gaps of information about the ITCZ shifts and the implications of the trade winds in the vertical wind-mix.

Climate variations may have occurred because of changes in the planetary orbit, but the composition of the atmosphere has determined more considerable climatic changes. Without humans, the Earth would be on track to re-enter a glacial period sometime in the upcoming fifty thousand years (Loutre & Berger, 2003). Still, the current carbon dioxide levels indicate that we broke the tight link between the orbital cycles and the atmosphere. Vast amounts of greenhouse gases are emitted into the atmosphere daily, leading humans to exceed the natural CO_2 variability (300-180 ppm) of the quaternary period (Figure 1). The increment of anthropogenic greenhouse gas emissions will cause further warming and long-lasting changes in the components of the climate system, improving the probability of severe and irreversible impacts for ecosystems.

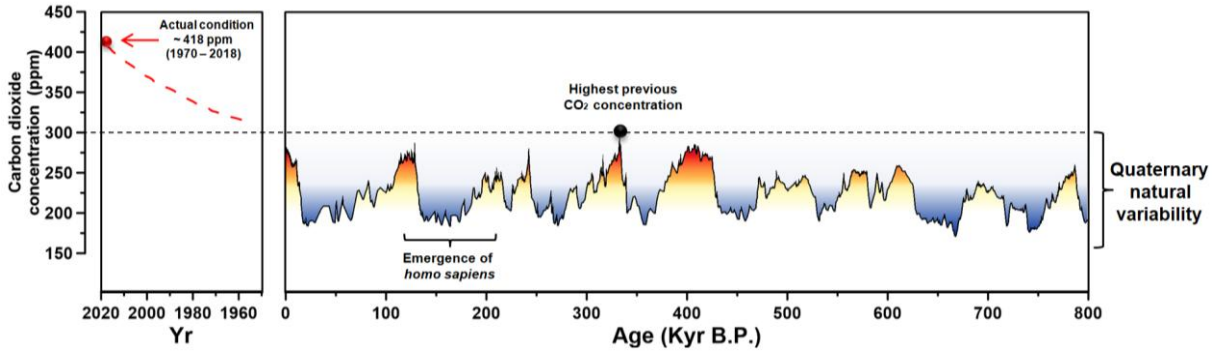

Figure 1 - Composite Antarctic CO_2 record (0-800 kyr before present) with current Mauna Loa readings. The figure indicates the quaternary natural variability, with 300ppm as the highest previous CO_2 concentration, and the anthropogenic effect post-industrial times, elevating greenhouse gas emissions to 400 ppm into the atmosphere.

The Intergovernmental Panel on Climate Change (IPCC) frequently warns about the consequences of anthropogenic greenhouse gas emissions on the Earth´s atmosphere. The report assessment intends to aware of the emergent risks for society, with suggestions to mitigate damage and to promote sustainable development. The numerical simulations of real-world systems are calibrated and validated by using observational data or analogies.

Several general climate models (GCM) simulate the increase of atmospheric CO_2 to produce customized scenarios and indicate the types of interventions that humans might do now and in the future. Therefore, even in scenarios where governments around the world work to limit and phase out greenhouse gas emissions, considered as the minimum (2.6) representative concentration pathway (RCP), the climate models predict a temperature increase of at least ~2°C. In scenarios with less aggressive action or with no action at all, maximum (8.5) RCP, the planet's average surface temperature goes up more than 6°C throughout the 21st century (Kirtman *et al.,* 2013). Simulations of GCM also points out to polar caps melting and further freshening of the northern Atlantic, reducing the strength of AMOC (Caesar *et al.,* 2018). As observed in the past, records of AMOC intensity changes have synchronic evidence with displacements in the equatorial precipitation band position.

Different rainfall patterns have the potential to improve the pluvial contrast between regions, altering biomes dispersion across the continents. The scientific community has a particular interest in the rainforest biome preservation, retainer of dense biodiversity, and one of the leading carbon sinks on the planet (Phillips, 2009). The rainforest biome is restricted to the equatorial band and inhabits in constant and specific climatic conditions of high precipitation and warm weather. The neotropical vegetation is the most significant land coverage of rainforest in the world, with unique biodiversity, and changes in rainfall patterns can lead to the loss of this vegetation, even accelerate global warming (Aragão *et al.,* 2014). Dryer biomes such as caatinga and cerrado borders with the Amazon rainforest (Figure 2) and the expansion of semi-arid areas or grassland fields is a climatological, ecological, and social concern.

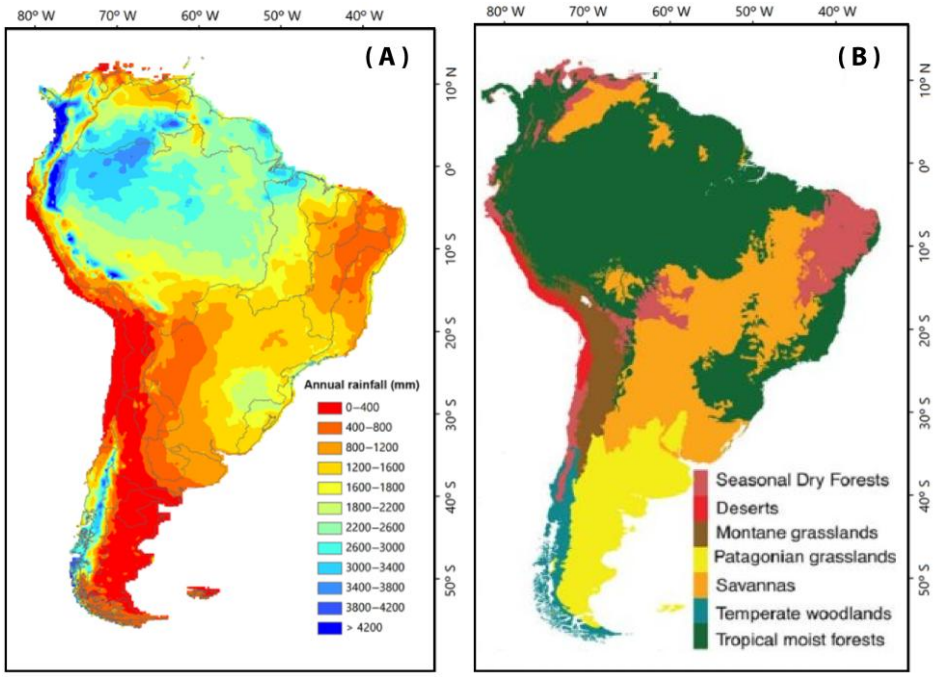

Figure 2: (A) Hydrological south America distribution, with the annual rainfall (mm), Alencar Siqueira *et al*. (2018); (B) Classification of Biome in South America, according to Olson *et al.* (2001).

Prolonged droughts have flow-on effects through plant species flourish and fruit production (Ogaya & Penuelas, 2007; Butt *et al.,* 2015). The consequences resonate on vertebrate and invertebrate fauna that relies on them (Harrison, 2000), decreasing biodiversity over the continents. Droughts in northeastern Brazil also affects the phytoplanktonic organisms in the adjacent ocean. The tropical surface waters are naturally oligotrophic as a result of the thermocline, which hampers more dense and nutrient-rich waters to reach the photic zone. In short, there are two main sources of nutrients for primary producers over the oligotrophic equatorial oceans: 1- The wind-mix revolves the water masses in the water column, providing nutrients in the photic zone. 2- Through the transport of rivers, carrying nutrients from the continent to the ocean (Sigman and Hain, 2012). The Parnaíba river is one of the most important rivers in northeastern Brazil. The river transports massive amounts of nutrients to its delta and enhances primary productivity, working as a CO_2 sink. Reduced rainfall over northeastern Brazil impacts the river discharge, shrinking the transport of nutrients to the adjacent ocean and altering the photosynthetic efficiency of phytoplankton organisms, and consequent deficits in the local fishery (Price *et al*., 2016; Mallin *et al*., 1993). The environmental degradation due to the semi-arid conditions in northeastern Brazil may trigger the impoverishment of the population with drastic implications to the exodus of this region. If the status quo does not change, the GCM simulations endorse the decrease of rainforest coverage over the 21st century (Figure 3) and alarm to severe storms and drought conditions over the world (Kirtman *et al.,* 2013). Regional climate models

are applied to understand the particularities and local effects of global warming. However, the broad range of variables considered simulating rain patterns and how each model moderates it creates divergences among distinct regional models. In the Northern and Northeastern Brazil, uncertainties permeate how precipitation anomaly will occur in a warmed world (Figure 4), with no consensus.

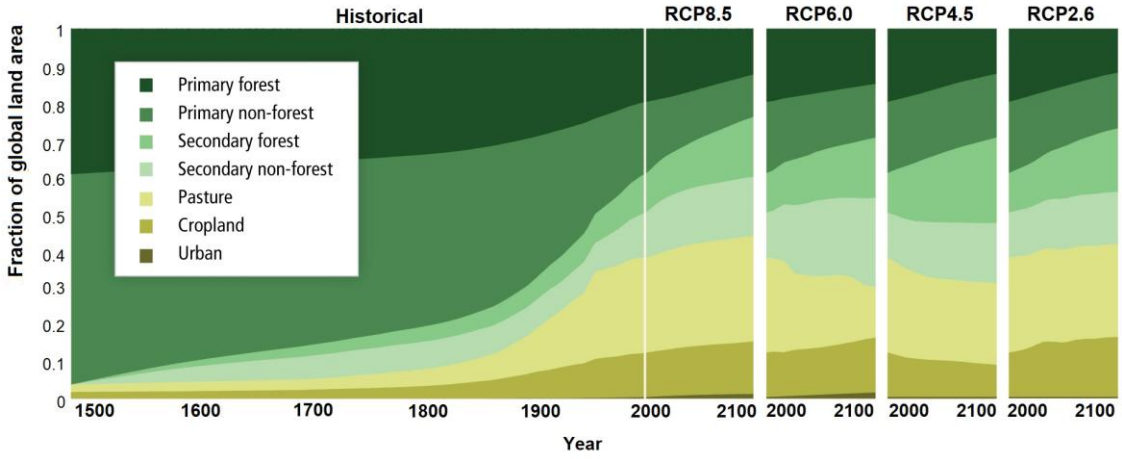

Figure 3: Fraction of past global land area and future projections for the 21st-century under different CO_2 emissions scenarios. The representative concentration pathway (RCP) oscillates between 2.6 and 8.5. All models' simulations point out to reduce Primary forest (rainforest) coverage (IPCC, AR-5).

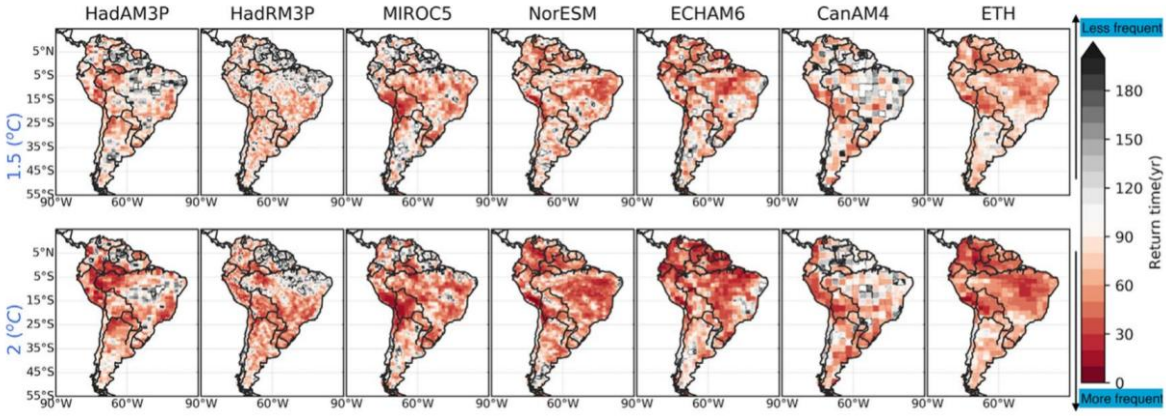

Figure 4: Distinct models show dangerous extreme precipitation events have shorter return times, i.e., they happen more frequently with the additional 0.5°C warming. The models disagree over Northern and Northeastern. For the Northern region, HadAM3P, HadRM3P, MIROC5, and CanAM4 show the less frequent occurrence of vigorous precipitation under both warming levels, whereas the other models show more regular occurrence. For the Northeastern region, HadAM3P, HadRM3P show less frequent occurrence of dangerous extreme precipitation, and CanAM4 shows less frequent occurrence over most of the Northeastern region. In contrast, the other models mostly show more frequent occurrence (Li *et al.,* 2020).

In constant development, climate models are increasing the variables to get closer to the reality of the natural world and to enhance accuracy. Recently, the Paleoclimate Modelling Intercomparison Project (PMIP) has incorporated paleo data to evaluate the capability of numerical models to reproduce different climates´ backgrounds (e.g., specific orbital

conditions and greenhouse gasses concentration). Regional paleoclimatic reconstructions represent a unique opportunity to understand patterns of climate variability and the environment response as well. Northern and Northeastern Brazil are the focus of interest in paleoclimate studies as climatic oscillations in these regions have the potential to track variations in ocean circulation and past shifts in the meridional position of the tropical rain belt. Still, northeastern Brazil seasonality leads to more transitional features susceptible to changes in the landscape. The presence of ecotone areas enables to investigate past shifts of the ITCZ, with subsequent oscillations in vegetation distribution inland.

In this context, this doctoral thesis presents a palynological approach (dinoflagellate cysts, pollen grains, and spores) applied on a marine core (GL-1248) retrieved from the slope in Northeastern Brazil and under the influence of the Parnaíba hydrographic basin. The current work investigates continental and ocean dynamics, interconnected by the Parnaiba river discharge and modulated by the precipitation pattern in Northeastern Brazil. The GL-1248 marine core has a span time of 130 thousand years, which allows us to address the variations in vegetation cover in the PHB over the last interglacial period (MIS 5e). The main motivations are to develop a better understanding of vegetation coverage response to different climate backgrounds and its main driving forces. Understanding the gaps of palynological information in the western equatorial Atlantic ocean, we increased the resolution of the samples along the last glacial period to observe the phytoplankton responses to different events on a millennial-scale. We integrated the responses of palynomorphs on land and over the ocean that occurred under the same climate backgrounds. This doctoral thesis intends to cooperate with the observational data acquirement and, if possible, assist the scientific community in improving the predictability of climate models.

1.2 Research objectives

The present study has the palynological perspective in a marine sediment core retrieved on the western equatorial Atlantic slope. We aim to reconstruct the vegetation dynamics in the vicinity of Parnaíba Hydrographic Basin, as the paleoproductivity and hydrography in the adjacent ocean over the last ~130 kyr. Additionally, the following themes will be explored:

- The driving forces of neotropical vegetation shifts in northeastern Brazil.
- The ocean and atmospheric interactions on the sea surface led to paleoproductivity changes, in the oligotrophic western equatorial Atlantic ocean.

1.3 The layout of the thesis:

This thesis has been divided as follows:

2 Climate changes leading intermittent connections of neotropical vegetation: Provides the continental perspective, base on the pollen records from a marine sediment core, to reconstruct environmental changes since the last interglacial maximum (~130 cal kyrs). The Parnaíba Hydrographic Basin is a region of transitional vegetation, with several ecotone areas. We will discuss the adjustment of vegetation in response to past precipitation events, and the subsequent changes provoked inland by the expansion and contraction of biomes. We will discuss the periodicity of vegetation response over the climatic fluctuations, in an attempt to identify the main conditioning factors.

3 Changes in sea surface hydrography and productivity in the western equatorial Atlantic since the last interglacial: The discussion will permeate the paleoproductivity over the last ~130 kyr using a dinoflagellate cyst (dinocysts) record located in the western equatorial Atlantic Ocean. Past ocean parameters (e.g., productivity, sea surface temperature, and salinity) and dynamics of ocean current (North Brazilian Current and North Brazilian Undercurrent) have been reconstructed throughout dinocysts assemblages. We will discuss the glacial-interglacial patter of hydrographic mechanisms that favor assemblages of dinocysts with optimized absorption of atmospheric CO_2.

4 Conclusions and future challenges: Bullet conclusions for each chapter and the open questions.

5 Supplementary material: Tables, figures, and graphs with additional information.

2 CLIMATE CHANGES LEADING INTERMITTENT CONNECTIONS OF NEOTROPICAL VEGETATION

The territorial extension of Brazil covers several latitudes, contemplates six different biomes, and has the most complex ecological systems on the planet (IBGE, 2004). The emergence of vast Neotropical diversity and the several processes that lead to the actual standards have attracted scientists' attention for centuries. Different hypotheses about the distribution of plant diversity rise attributing distinct relevance to biotic and abiotic factors (Antonelli *et al*., 2011). Ecologists and paleoclimatologists debate the expansion and contraction response of vegetation types in the face of glacial-interglacial climate changes, as one of the environmental mechanisms that enabled the species richness of Neotropical biology (Van Der Hammen, 1974; Behling, 2000; Pessenda *et al.,* 2010; Maslin *et al.,* 2011). Ecotonal regions proved to be fundamental to assist the emergence of biodiversity, connecting ecosystems. The interface of different vegetation types gives rise to diverse vegetation, creating a heterogenic environment and an initial center of biological diversification (Primack, 1993; Risser, 1995). The Parnaiba hydrographic basin (PHB) is in the vicinity of the Amazon forest and has a mosaic of ecotone areas, as the interface of the three main biomes in the region: caatinga, cerrado, and rainforest (Figure 5). The caatinga and rainforest biomes are known for their high contrast of water requirements, and the dispositions of biomes over the PHB imprint the east-west decrease in topography, promoting uneven hydrological delivery. The synoptic atmospheric features also control water availability over northeastern Brazil (NEB). Still, the Intertropical Convergence Zone (ITCZ) is the leading carrier of moisture over the continent (Hastenrath, 2012), and its displacement modulates ecological patterns.

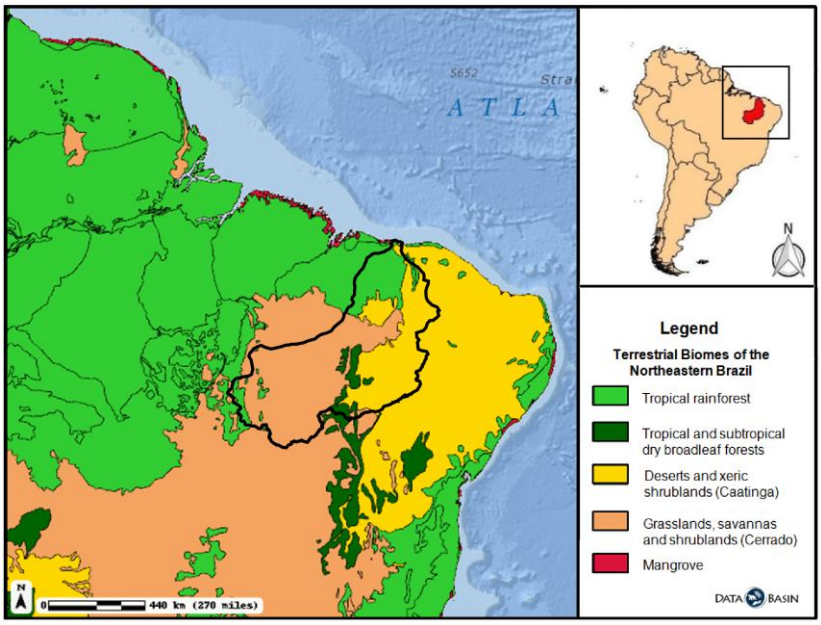

Figure 5: Map presenting the disposition of the main terrestrial biomes of Northeastern Brazil, according to Olson *et al.* (2001). The contour of the Parnaiba Hydrographic basin is highlighted in black.

During the last glacial period, millennial time scales shifts of ITCZ over NEB occurred in synchronicity with abrupt and extensive freshwater intrusion into the North Atlantic Ocean, known as Heinrich Stadials (HS) (Wang *et al.,* 2004; Strickis *et al.,* 2018). The weakened Atlantic meridional overturning circulation (AMOC) accentuated meridional sea surface temperature (SST) gradients, heating the sea surface of South Atlantic. Warmer tropical South Atlantic drove the southward displacement of ITCZ and subsequent wet periods in NEB (Mulitza *et al.*, 2017; Utida *et al*., 2019). Jennerjahn *et al.* (2004) and Sifeddine *et al.* (2003) found the increase in the number of pollen grains in NEB post-HS wet periods, and both studies suggested rapid reforestation as a consequence of prolonged precipitation events. The records of the transition between more open vegetation and the rainforest response have the potential to assist the understanding of past ITCZ displacements. More recent studies of past vegetation at NEB have highlighted the plasticity of the rainforest vegetation. The occurrence of pollens, spores, and macrophytofossils from the Atlantic and tropical rainforest in the current semi-arid NEB gave sustainability to the hypothesis that natural ecological corridors formed after large wet intervals. Shreds of evidence that the rainforest enhancement connected distant regions, spreading biodiversity according to precipitation fluctuations during the late glacial period (HS1) and Younger Dryas (Cristalli *et al*., 2006; Dupont *et al.,* 2010; Bouimetahan *et al.,* 2018; Pinaya *et al.,* 2019).

Ecological models use palynological data to evaluate past biogeographical scenarios, and to understand the processes inherent in the radiation of Neotropical biodiversity (Prentice *et al.,* 1992; Carnaval and Moritz 2008; Ledo and Colli, 2017; Silveira *et al.,* 2019). However, the majority of paleoclimatic studies over the NEB covers a time span restricted to

the late glacial period, with a detailed description of vegetation response over HS1. Few studies focus on the comparison of vegetation response over different wet periods to support that the expansion of rainforest occurred equally through time. The time range of palynological reconstructions at NEB also prevents comparisons with other interglacial periods beyond the Holocene. Besides the natural climatic disturbances, the planet earth faces an interglacial period under anthropogenic effects, with a substantial emission of greenhouse gas to the atmosphere.

The Fifth Assessment Report of the Intergovernmental Panel on Climate Change (IPCC-AR-5) consistently emphasized global warming and the subsequent effects on the frequency of extreme climatic events for the next decades. More severe and persistent climatic events may generate a sharp contrast in water availability over different regions of the world, and the scientific community still not sure about the hydrological projections for NEB. Despite that, some studies suggest that prolonged droughts may create the impact of resource bottlenecks, inducing biodiversity loss, and triggering the expansion of more open vegetation, as the Caatinga biome (Kirtman *et al.,* 2013; Maron *et al.,* 2015). The occurrence of sparse vegetation implies structural changes that generate robust sensible heat flux, reducing the regional moisture. In addition, threats to rainforest distributions could cause a severe reduction in CO_2 uptake, creating a positive feedback loop that accelerates global warming (Cox *et al*., 2000). The absence of palynological data over different warm periods enhances the uncertainties about the tendency of biological response, as the identification of cryptic species able to prevail in these boundaries conditions. The development of botanical knowledge may also assist in the maturing of more effective conservation measures.

In this context, we will address the reconstruction of the ecotonal vegetation present in the PHB over the last ~130 kyr. The present study derived from the GL-1248 marine core, 280 km distance from the mouth of Parnaíba River. Alongside the X-ray fluorescence (XRF) Ti/Ca ratio used as a continental proxy to support interpretation on the hydrological conditions at the study area. We will discuss the impacts of different driving factors that might lead to vegetation response. To investigate the transitions of vegetation, we implement the use of delta coverage handling the anomalies of dense (rainforest) and sparse vegetation. The delta coverage also assists in identifying wet and dry fluctuations. Our results have important implications for biogeography and diversity spread in South America. Comprehend the patterns of biodiversity response to different climate backgrounds is crucial to mitigate anthropogenic impacts and preserve the rainforest vegetation through political management.

2.1 Current climate and vegetation distribution of Parnaíba Hydrographic Basin

The marine sediment core GL-1248 (0° 55.2'S, 43° 24.1'W) was retrieved from the continental slope (2.264 meters depth) of the northeastern region of Brazil, located at about

160 km distance from the modern coastline (Figure 6), and 280 km distance from the Parnaiba River fan. The Parnaíba Hydrographic Basin (PHB) has 344.112 km^2, and presents a rainfall contrast between dry and wet seasons controlled by the intermittent presence of The Upper Tropospheric Cyclonic Vortices (UTCV) and seasonal displacement of ITCZ. The formation of the UTCV occurs during the pre-wet season. It creates a gradient of precipitation, with semi-arid conditions at its center and heavy rainfall at its borders (Kousky and Gandu, 1981). During the Austral summer, the southern displacement of ITCZ (2°S) marks the beginning of the wet season, enhancing the moisture into the continent (Hastenrath, 2012). The seasonal rainfall regulates the vegetation distribution along the Parnaíba Hydrographic Basin and allows the coexistence of different vegetation types. Three types stand out due to the divergence of water requirements: caatinga, cerrado, and rainforest.

The caatinga is an exclusive Brazilian biome, and from a broad perspective, it occurs in areas of the semi-arid climate, with precipitation up to 700 mm per year (CODEVASF, 2005). The vegetation structure has small trees with xerophytic characteristics and with a small or medium size (3 to 7 meters high), spiny trees, shrubs with deciduous foliage during the dry season, and drought-tolerant grasses (Ab'Saber, 1974; Kuhlmann, 1977). Despite that, thirteen types of caatinga vegetation were established and set according to location, physiognomy, and ecology. In less semi-arid parts of the caatinga, forest fragments and floodplain forests occur along rivers. The fringe forest is frequent at the low PHB and in alluvial soils. The vegetation is marked by the presence of *Copemicia cerifera* (Arecaceae), *Licania rigida* (Chrysobalanaceae), *Geoffroea striata* (Fabaceae), *Sideroxylon obtusifolium* (Sapotaceae), *Erythrina velutina* (Fabaceae), *Ziziphus joazeiro* (Rhamnaceae), *Capparis yco (*Capparaceae*).* However, we must highlight that *Copernicia prunifera, Licania rigida,* and *Capparis yco* are not endemic to the caatinga vegetation (Andrade-Lima, 1981 *apud* Leal *et al.,* 2003).

Fragments of cerrado vegetation may occur in caatinga's domain. These habitats refuges may present less taxon diversity than in the cerrado domain and are established by species of wide geographical distribution (Figueiredo, 1997). However, the caatinga is regularly found in diabase rocks and more fertile soils, while the cerrado appears to be restricted to a mineral-rich substratum. In Brazil, the cerrado domain is recognized as the "dry diagonal," a region with soils rich in minerals, low pH, and a natural barrier for biotic exchange (Prado and Gibbs, 1993; Anhuf *et al.,* 2006; Werneck, 2011). Similar to the caatinga biome, cerrado has diverse vegetation. In the Piauí state, Ribeiro & Tabarelli (2002) mentioned four structural types of vegetation, classified by the density of the woody plant species. The vegetation density gradient and the species diversity seem to operate

coordinately (Eiten, 1994), changing the landscape and conducting transitional features between the caatinga and the Amazonian deciduous forest.

The seasonal deciduous and semi-deciduous forest, and open ombrophilous forest (rainforest), are denser than the cerrado and caatinga vegetation and prevails in wetter conditions (> 1.300 mm per year). Richier and diverse vegetation occur in the northwest of PHB, as in the "Serra da Ibiapaba" (CODEVASF, 2005). Muniz (2011, 2006) pointed out some similarities between the vegetation at the northwest part of PHB to the Amazon rainforest and highlighted the following families: Leguminosae, Sapotaceae, Moraceae, Burseraceae, Sapindaceae, Euphorbiaceae, Apocynaceae, Annonaceae, Lecythidaceae, Rubiaceae, Lauraceae, Bignoniaceae, Meliaceae, and Rutaceae.

Predominantly carried by the river outflow, the variability of pollen grains on GL-1248 reaches the seabed as a continental source. The Parnaíba river plume flows northward at the sea surface transported the Nort Brasilian Current (NBC). The NBC forms at the 10°S with the increment of the South Equatorial Current (SEC) carrying warm Tropical Water to the Northern Hemisphere. The strengthened NBC transport during the Austral winter is favored by the northern displacement of ITCZ and more vigorous tradewinds (Stramma *et al.,* 1995; Johns *et al.,* 1998). NBC's strength oscillated over the past geological time and was reduced during the glacial maximum. Despite the proximity of the Amazon River, the most copious river discharge in the world, the marine sediment core GeoB16206-1 is located further south than GL-1248 and did not present any remnant vestige from the Amazon river plume during the Heinrich Stadial 1 (Zhang *et al.,* 2015). For this reason, we disregard an imprint of the Amazon River plume in our study area and maintain the Parnaiba River as the primary source of continental material on GL-1248. The variability of pollen grains must have reflected changes on the continent at the vicinities of PHB.

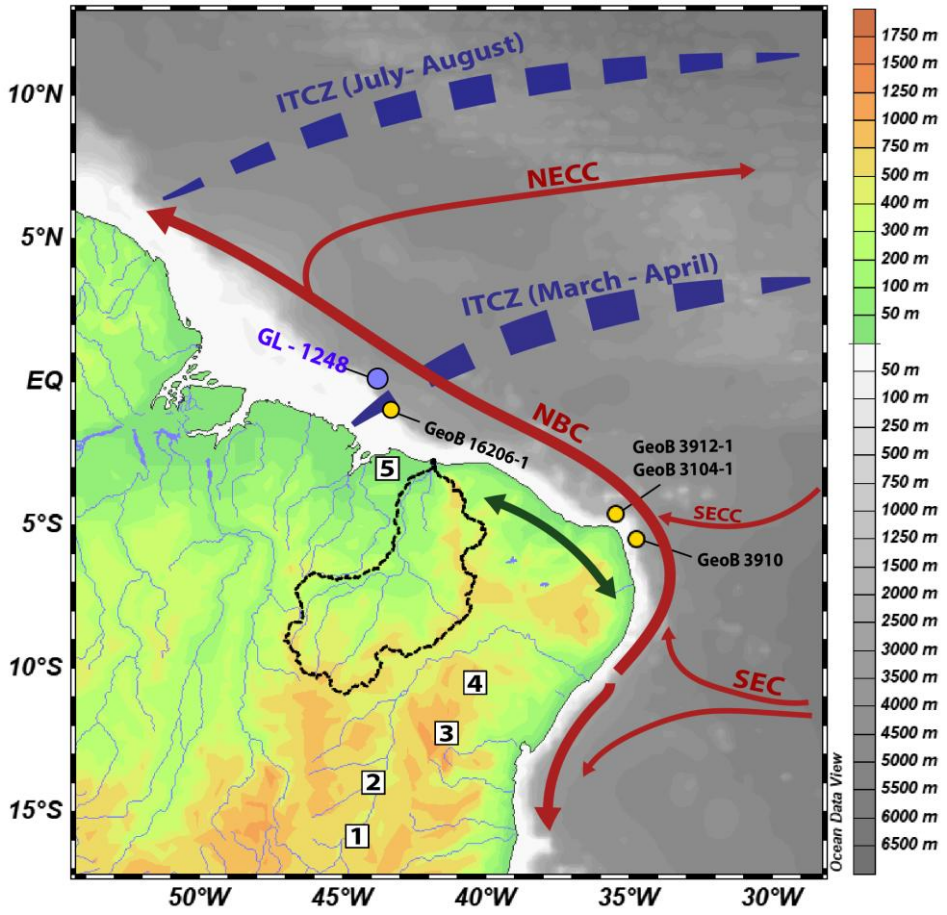

Figure 6: Topographic map of the study area in NEB and the location (Blue dot) of core GL-1248 (0° 55.2'S, 43° 24.1'W). White squares are related to inland records, are they: 1- Lapa Sem Fim (LSF) (16°09'S, 44°36'W) (Strikis *et al.,* 2018), 2- Lapa Grande (LG) (14°22'S, 44°17'W) (Strikis *et al.,* 2018), 3- Marota cave (MAG) (12°35'S, 41°02'W) (Strikis *et al.,* 2018), 4- Toca da Boa Vista (TBV) (10º10'S, 40º50'W) (Wang *et al.,* 2004), 5- Caço Lake (CL) (2° 58'S, 43° 25'W)(Sifeddine *et al.,* 2003). The map also shows the area of the hydrography basin of the Parnaíba. The dashed blue line displays the southmost position of the Intertropical Convergence Zone (ITCZ) during the end of Austral summer (March-April) and the Austral winter. The green both sides arrow indicate the tendency to form forest corridors connecting Amazon and the Atlantic rainforest. The marine sediment cores Geob 16206-1 (Zhang *et al.,* 2015), Geob 3912-1/Geob304-1 (Jennerjahn *et al.,* 2004), and Geob3910 (Dupont *et al.,* 2010) are also represented.

2.2 Material and methods

2.2.1 Depth-age model

We studied marine sediment core GL - 1248 (0°55.20S, 43°24.1 0W; 2,264-m water depth), retrieved off the Parnaíba River mouth in the western equatorial Atlantic Ocean. The recovered sediment column was marked by silty-clay greenish sediments, with some carbonate-rich layers, represented by more reddish-brown and whitish clays (Venancio *et al.,* 2018). The age model for core GL-1248 is based on 12 AMS 14C measurements. The radiocarbon samples contained tests of two planktonic foraminifera types, *G. ruber and T. sacculifer* (>150 mm) performed at the Beta Analytic Radiocarbon Dating Laboratory, USA. Downcore ages and the radiocarbon ages were calibrated with the IntCal13 calibration curve

(Reimer *et al.,* 2013) with a reservoir age of 400 ± 200 years (2σ) and no additional local reservoir effect (ΔR = 0; Mulitza *et al.,* 2017), but downcore ages were modeled using the software clam 2.2 (Blaauw, 2010) (see all details regarding the age model in the Venancio *et al.* (2018)). The core is ~19.0 m long and spans the interval between ~130 and 2 kyr BP.

2.2.2 Palynological preparation

A total of 139 samples were prepared for pollen and spores' identification. We used standard laboratory procedures (Faegri and Iversen, 1989), but excluded the acetolysis step to preserve other palynological proxies. About 4-6 g (wet weight) samples were prepared for palynological analyses. At first, the sediment samples were sieved with a 150 µm mesh to remove the larger particles, such as shells and stones. After that, one tablet of exotic *Lycopodium clavatum* spores was added to each sample to estimate the concentration (grains/cm^3) and influx (grains/cm^2/yr) values (Stockmarr *et al.,* 1971). Then, the samples were treated with hydrochloric acid (HCl, ca. 35%) for decalcification and cold hydrofluoric acid (HF, 40%) for siliceous content removal. After the chemical treatment, aided an ultrasonic bath (maximum 30 seconds) for organic matter disaggregation. The samples were sieved with a 1 µm nylon mesh, but particles up to 5 µm may still pass through. The samples were processed at the Department of Palynology and Climate Dynamics, Georg-August-University Göttingen (Germany).

2.2.3 Palynological analysis

The identification of the pollen and spores is based on the reference collections at the Department of Palynology and Climate Dynamics of the University of Göttingen and literature (Behling, 2000). Permanent microscope slides were made, and due to the shallow content, one to four slides per sample were counted. Pollen and spores' samples were counted to a minimum of 100 pollen grains and spores in the case of samples with a relatively low concentration (mostly interglacial samples), and an average of ~180 grains was counted per sample. The most frequent taxa are presented in relative abundance and grouped based on their ecological affinities. The pollen and spore's influx (grains/cm^2/yr) was calculated multiplying the concentration with the sedimentation rate, and the concentration was calculated for each sample following the equation of Benninghoff (1962).

The identified pollen and spore taxa were grouped according to their structure (tree and shrubs, and herbs) and group types. Due to the similarities between both the groups, we opted for the vegetation groups approach. The complete list with the pollen and spore types identification is in the supplementary material (Tables S1) The pollen taxa were designated as open vegetation, rainforest lowland, mountain vegetation, mangrove, wetland, exotic, and unknown. The wetland pollen grains and a few aquatic taxa are included in the pollen sum,

as wetland taxa (e.g., *Cyperaceae*) also occur in the grassland. The spore's taxa were designated as monolete, trilete, Cyatheacea*e* spp*, Selaginella*, wetland spores sum, tree fern, Cyatheaceae (*Hemitelia* type) and reworked trilete. We use the term "other" for pollen types that belong to a family, but could not be identified to the genus level. The diversity index was calculated by using the Past3 software (Hammer *et al.,* 2001).

2.2.4 Time series analysis

We used the REDFIT algorithm (Schulz & Mudelsee, 2002) to test for the presence of periodicities in our data. For this analysis, the data were linearly detrended with the software PAST (Hammer *et al.,* 2001) with segment set to one and the oversampling set to three, tapered with a Welch spectral window.

2.2.5 Delta coverage analysis

The index was calculated based on the difference between the normalized time series. The normalizations were calculated using the following equation:

$$\text{Normalized data} = (x - \bar{x})/\sigma \quad (1)$$

Where:
x: is a punctual percentage value from vegetation type assemblage.
$\bar{x}$: is the average percentual from vegetation type assemblage.
σ: is the standard deviation of the vegetation type assemblage data set.
Equation 1: vegetation type normalized data

The difference between the normalized time series composes the delta coverage (equation 2). The positive values are related to the improvement of rainforest and negative values to the expansion of the sparse vegetation.

$$\Delta\text{vegetation type} = \text{vegetation1 normalized data} - \text{vegetation2 normalized data} \quad (2)$$

Equation 2 – Delta coverage

2.3 Results

2.3.1 Sedimentation rate, pollen and spore concentrations, and influx

The pollen concentration was generally low in GL-1248 and varied down-core from ~0.8 to 22x10^{2}grains/cm³ (average 5.7x10^2 grains/cm³), and the influx values oscillated from 5.5 to 1470x10^2 grains/cm^2/yr (average. 161 grains/cm^2/yr) (Figure 7C and 7D). The spores also appeared with low concentration in GL-1248, and varied down-core from ~0.9 to 15x10^{2}grains/cm³ (average 3.8x10^2 grains/cm³), and the influx values oscillated from ~7.5 to 826x10^2 grains/cm^2/yr (average 117 grains/cm^2/yr) (Figure 7F and 7G). The palynological content of the studied core was not sufficient for appropriate analysis for the section between ~90 and 100 kyr (1.392 and 1.486 cm). The content was reduced in pollen and spores for proper investigation and was excluded from the interpretation. The Hiatus present in the

marine core GL-1248 did not allow the reconstruction of vegetation during the Last Glacial Maximum (LGM).

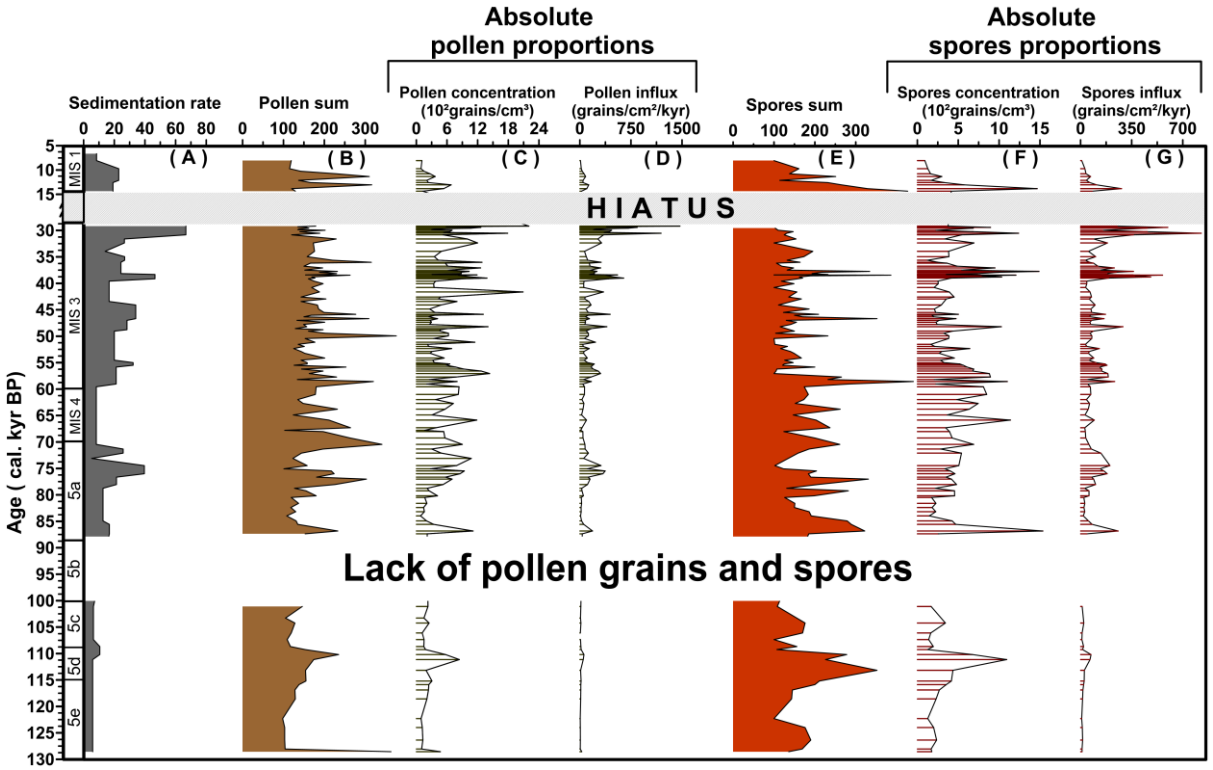

Figure 7: A) Sedimentation rate; B) Sum of counted pollen grains; C) Concentration; D) Influx of pollen; E) Sum of counted spores; F) Concentration, G) Influx of spores data for GL-1248. The dashed line in red is delimiting the median concentration values.

2.3.2 Pollen and spore grains relative abundances

A total of 102 pollen taxa were identified and grouped according to their respective vegetation, and the 13 spores' types identified were grouped according to their ecology or morphology (Tables S1, supplementary material). In the following, we shortly describe the main features of pollen and spore content of the GL-1248 marine sediment core. The ten types of pollen grains with the highest percentage were *Cyperaceae* (38%), *Poaceae* (28,8%), *Polygalaceae Polygala* (17,2%), *Malpighiaceae* (17%), *Rubiaceae* (14%), *Arecaceae* (12.9%), *Chloranthaceae Hedyosmum* (11%), Asteraceae (11%), *Apocynaceae* (8,15%), *Rubiaceae Borreria* (7,75%) (Figure 8). The spore percentages of Monolete reach 67%, and general Trilete reaches 62.6%. Cyatheaceae spp. sum (*Cyathea horrida, Cyathea schanschin-type,* Cyatheaceae spp.) reached 38.2%, *Selaginella* 19.35%, wetland spores sum (*Isoetaceae Isoetes, of Lycopodium cerrum, Pseudoschizaea rubina, Salvina type*) reached 14.3%, *Cyathea* Hemitelia reaches 13.7%, Tree fern reached 8.1%, and Trilete reworked reached 3% (Figure 9). We must highlight the Cyperaceae maxima during the MIS4 (61 to 71.5 kyr, or 1.022 to 1.132cm), and the wetland spore maxima occurred during early MIS 4 (64.9 to 70.5 kyr, or 1.054 to 1.100cm) (Figure 5 and 6).

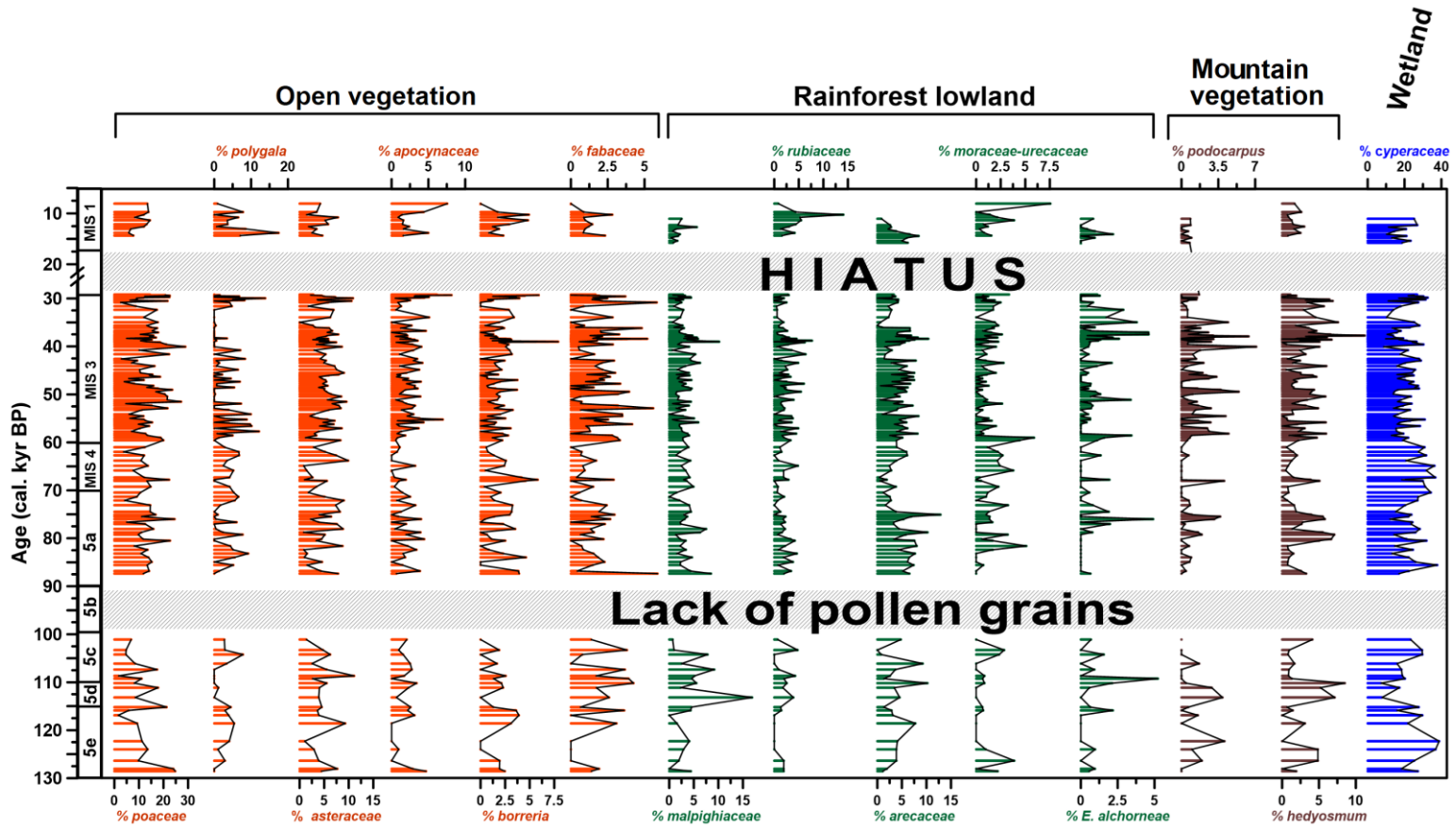

Figure 8: Chart of the 15 pollen types that appear in the highest percentage over ~ 130 kyr down the marine core GL-1248. The groupings were established according to the local ecology of each pollen type and defined as open vegetation, rainforest lowland, mountain vegetation, and wetland pollen. Due to the low percentage of representative pollen types, the other groupings are present only in table S1 that contains all information.

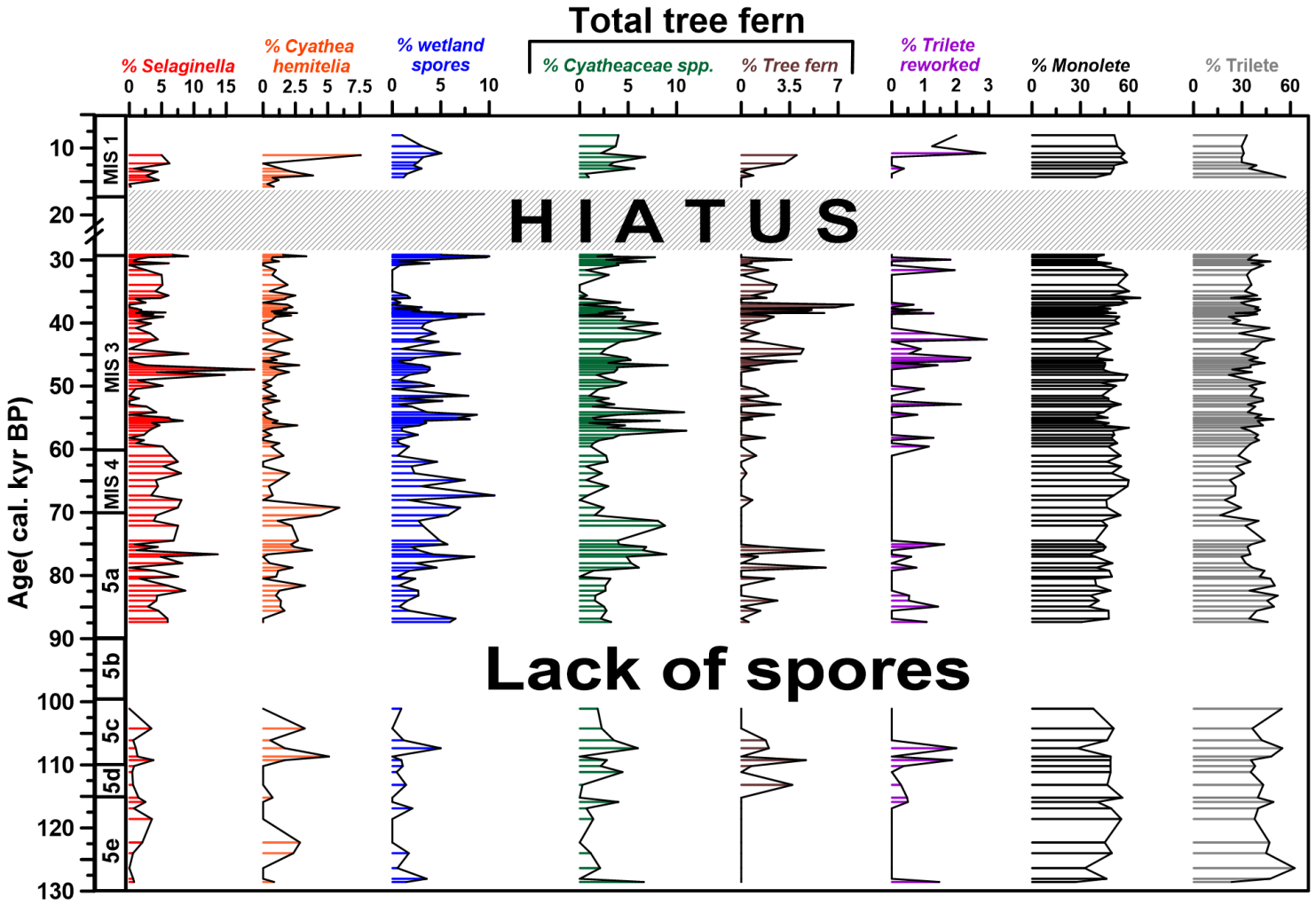

Figure 9: Chart of the spore types over ~ 130 kyr down the marine core GL-1248. Detailed information regarding the types of spores is present in table S2.

2.3.3 Spectral analysis

Among the pollen groups that stood out, wetland and rainforest lowland (Figure 10A and 10C) revealed the presence of short and long-term periodicities with high spectral power was above the Chi2 false-alarm level (Thomson, 1990). Short-term frequencies were oscillated throughout the pollen groups, achieving Chi2 with wetland pollen group, and 95% false-alarm level with rainforest lowland. The open vegetation denotes short-term periodicities in high spectral power, reaching a 99% false-alarm level. Instead, the long-term periodicities presented a 95% false-alarm level (Figure 10B). All pollen groups showed millennial frequency, but only the rainforest lowland and wetland groups showed relevance superior to Chi2 in the obliquity orbital-scale. The rainforest lowland also showed significance representativity in the precession orbital-scale.

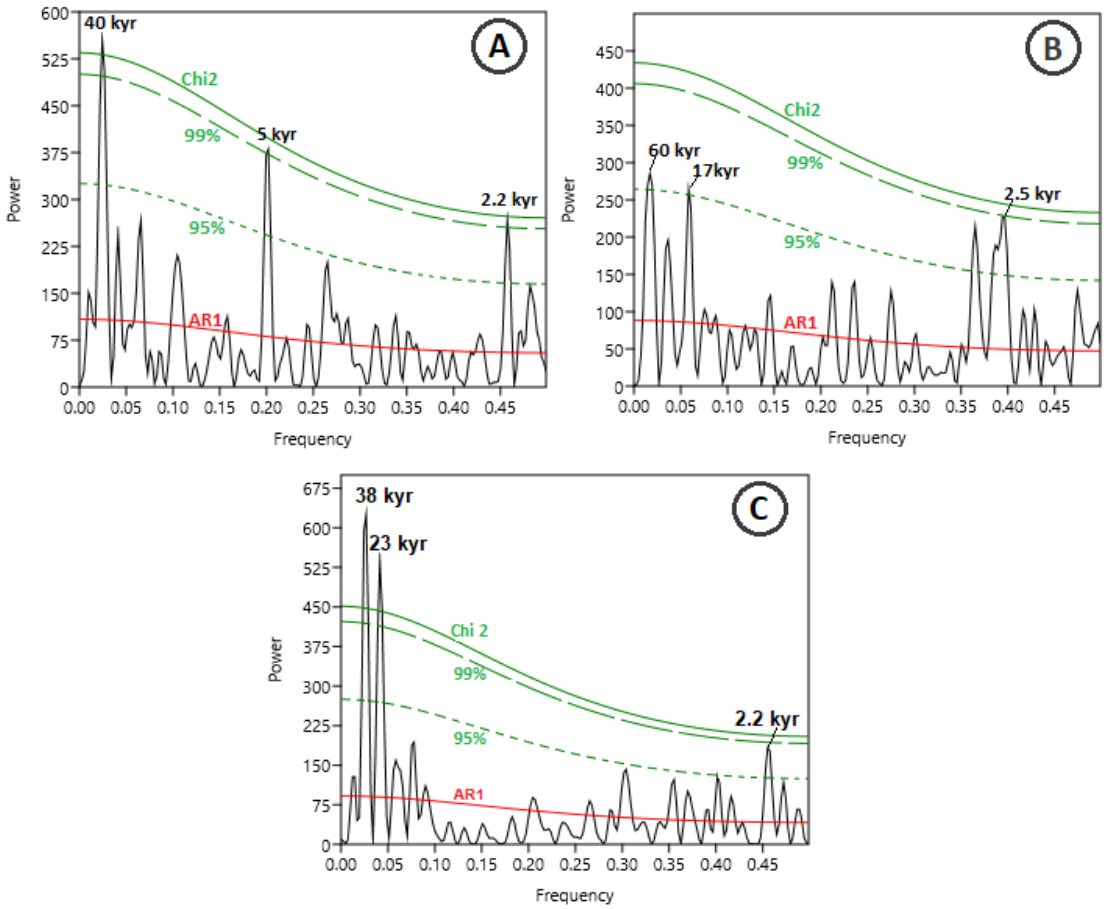

Figure 10: Spectral analysis with the REDFIT algorithm (Schulz & Mudelsee, 2002), performed among the groups that stood out A) Wetland pollen group, B) Open vegetation pollen group, and C) Rainforest lowland pollen group. The red line represents the red-noise spectrum, and the green lines show the false-alarm levels at 99% (dashed line), Chi2% (line). Labels above spectral peaks indicate the periodicities in a thousand years (kyr).

2.3.4 Delta coverage

The positive values of the delta coverage point to a predominance of rainforest vegetation, and the negative values are related to the development of sparse vegetation.

2.3.5 Diversity index

The diversity index oscillated from 3.35 to 2.10 and represents a maximum of 51 taxa of pollen grains and a minimum of 16 taxa of pollen grains. The average was 2.80, an equivalent of 33 taxa of pollen grains. Values higher than three were highlighted in red to identify when biodiversity was greater than 70%.

2.4 Discussion

2.4.1 Vegetation response to Heinrich Stadials precipitation events

As described in the age model of the GL-1248, it was derived from the alignment of the Ti/Ca ratio with ice cores $\delta^{18}O$ isotopes from NGRIP (Venancio *et al.,* 2018). The concept is supported by the interconnection of global climate oscillations, where Greenland stadials are related to precipitation anomalies over NEB, with subsequent increase of the Parnaíba river outflow and continental loading in the adjacent ocean (Wang *et al.,* 2004; Govin *et al.,* 2012; Nace *et al.,* 2014). The synchronicity of Ti/Ca peaks with ice-rafted debris (IRD) records from the MD95-2040 marine core (de Abreu *et al.,* 2003) also endorse the thermal unbalance events along the Atlantic Ocean during the glacial period, named Heirinch Stadials (HS). However, we observed discrepancies among the maximum and minimum values of Ti/Ca and IRD proxies (Figure 11A and 11G). Possibly the regional conditions modulated the magnitude of Ti/Ca and IRD transportation during HS. To better understand the local climatic dynamics of NEB and the impacts on the vegetation, we investigate the pollen and spores' content in the GL-1248 core. Three pollen groups showed interesting variabilities in terms of their relative abundance: wetland, open vegetation, and rainforest lowland. Aligned with that, we used the *Selaginella* spores and Cyatheaceae spp. fern spores to evaluate the vegetation succession.

The Cyperaceae is the most representative type of pollen grains in the wetland pollen group, guiding the general trend. However, the Cyperaceae is anemophilous with a high pollen production and might be overrepresented when compared to zoophilous tropical trees (Subba Reddi & Reddi, 1986). Despite this, Cyperaceae is also an aquatic plant with ecological requirements that enable its predominance in riparian vegetation, swamps, and open areas with a high presence of herbs and

grasses (Behling *et al.,* 2004; Oliveira *et al.,* 2013). The Cyperaceae pollen type reached values above 30% during MIS 4 (70 - 60 kyr) and along other wet periods as HS (Figure 11B). The increase in the relative abundance of Cyperaceae, emphasizes the removal of riparian vegetation due to increased river outflow. We suggest that the rise of the Cyperaceae percentage might indicate increases in Parnaiba River discharge (Figure 11A and 11B). Despite the high relative abundance of the wetland pollen group, it does not reflect vegetation oscillations.

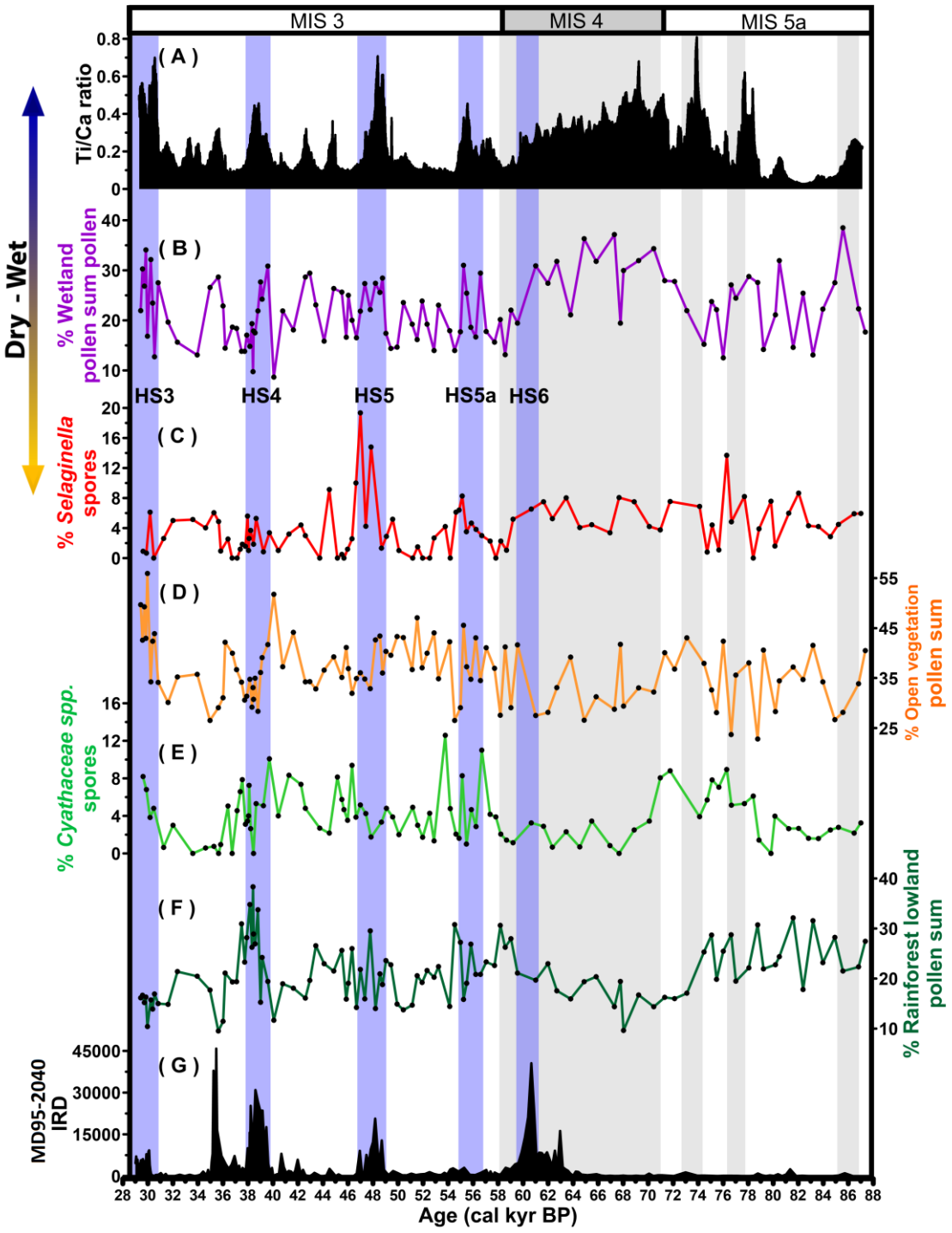

Figure 11: Pollen groups percentage and spores' types percentage between ~30 to 90 kyr. (A) GL-1248 XRF Ti/Ca ratio (Venancio *et al*., 2018); (B) Wetland pollen group, (C) *Selaginella* spores; (D) Open vegetation pollen group; (E) Cyatheaceae spp. Spores; (F) Rainforest lowland pollen group; (G) MD95-2040 IRD (Ice-Rafted Debris). The Heinrich Stadials (HS), are marked in blue. The MIS 4, and other wet periods are highlighted in gray. The arrow with the gradient transition from dry to wet is related to Ti/Ca ratio, Wetland pollen group, and *Selaginella* spores.

The fern and the spores occurred with more frequency during the glacial period, in agreement with other palynological inferences in South America and with

phylogeographic data that suggest the tree fern expansion to the lowlands during glacial cycles (Van Der Hammen and Hooghiemstra, 2000; Ramírez-Barahona & Eguiarte, 2014). According to Behling (2000), *Selaginella* spore grows on moist soil, and are used as a proxy of erosion during intense precipitation events. The *Selaginella* spore rises over HS events or wet periods as the MIS4. Still, *Selaginella* spore denoted a singular increase during the HS5 precipitation event (Figure 11C). Extended dry climatic conditions lead to the development of the sparse vegetation, amplifying the space between trees, and reducing the presence of roots in the soil (Prado, 2003). The reduced stability along a prolonged dry period favored high erosion rates over the HS5, imprinted in the disproportionate increase of *Selaginella* spore relative abundance. This panorama is consistent with the persistence of high values (>40%) of open vegetation vegetation between ~60 and 50 kyrs (Figure 11D), and the high peak of Ti/Ca during HS5. In contrast, the wetland pollen grains and S*elaginella* spores' decay to low values in HS4 and during late MIS 4.

The transition between the moss to fern spores was previously used in NEB as an indicator of a succession of vegetation, improving the soil stability and forest development (Jennerjahn *et al.,* 2004; Dupont *et al.,* 2010; Bouimetarhan *et al.,* 2018). The Cyatheaceae spp. fern spores exhibited a consistent rise in its percentage after significant precipitation events, indicating the natural trend of the succession in local vegetation (Figure 11E). Synchronous increase in the relative abundance trend of Cyatheaceae spp*.* spores and rainforest lowland pollen group over 78-74 kyr, post-MIS4, and HS4 are indicatives of robust tropical forest development (Figures 11E and 11F). The presence of more trees and roots possibly turn the soil more stable, and reduced continental loading, consequently decreasing the Ti/Ca ratio.

2.4.2 The continental loading hindered by vegetation development

The disparity of hydrological requirements between the rainforest lowland and open vegetation and the oscillations in the prevalence of occurrence throughout the time reinforces past changes in pluvial conditions over the PHB region. The interchange between both vegetation also encompasses other environmental implications, as the plant coverage and soil stability. Thus, prolonged periods of rainfall do not necessarily produce considerable soil erosion if it occurs in a well-established forest (Gyssels *et al.,* 2005). Still, the wetland pollen group stood out over wet periods, with a unique imprint over the MIS 4, possibly overlaying more considerable variations of the other pollen groups. To evaluate the effects of a prolonged wet period on the process of vegetation expansion and contraction, we performed the delta coverage

based on rainforest lowland and open vegetation normalized data (Figure 12A), attenuating the influence of wetland pollen group.

Aiming to understand the effect of runoff interferences on the GL-1248, we plotted the Ti/Ca ratio against speleothems from local caves. Periods of maxima insolation during austral autumn (March to May) were related to the latitudinal gradient of precipitation, which generates high thermal contrast between land and sea. The maxima insolation is marked by seasonal tropical rainfall and reduce inequalities in the distribution pattern of continental moisture (Hastenrath, 1991), intensifying the precipitation events over NEB (Figure12B). The speleothems from Lapa Grande cave (LG) (14°22'S, 44°17'W) marked the wet period through the transition from MIS4 to MIS3, HS5, and precipitation events between HS5 and HS4. The speleothems growth phases from Toca da Boa Vista cave (TBV) (10°11'S, 40° 58'W) occurred during the pluvial periods as HS4, HS5, and HS6 (Figure 12C and 12D). Both sites have shown an increase in tropical rainfall during the HS6 enduring humid conditions after the event, as the MIS4 (Wang *et al*., 2004; Strikis *et al.,* 2018).

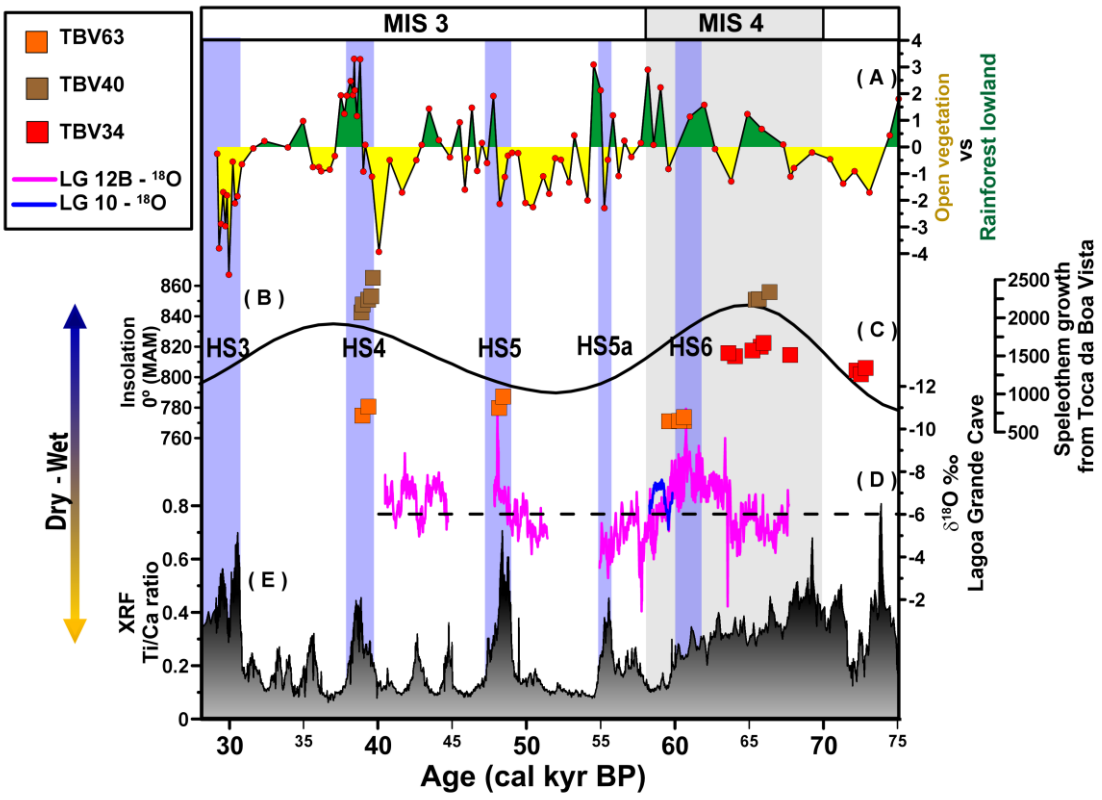

Figure 12: (A) Delta coverage, positive values indicate an increase in rainforest lowland (filled in green) and negative values indicate an increase in open vegetation (filled in yellow); (B) Insolation 0˚(March to May); (C) Speleothems grow phases from Toca da Boa Vista (TBV) (Wang *et al.,* 2004); (D) Two speleothems from Lapa Grange cave, central west of Brazil, LG - 12B (in pink) and LG - 10 (in blue) (Strikis *et al.,* 2018); (E) GL-1248 XRF Ti/Ca ratio (Venancio *et al*., 2018). The Heinrich Stadials (HS), are marked in blue, and the MIS 4 is highlighted in gray.

During the late MIS4, the rainforest vegetation shows gradual gains, reaching higher values after the HS6 event. The growth of rainforest lowland follows the rainfall pattern inferred from the speleothem of LG and TBV caves for the period. However, the same trend was not found in the Ti/Ca ratio (Figure 12E). The Ti/Ca displayed an anti-phase with rainforest vegetation, with decreasing values by the late MIS 4. A similar pattern was recurrent in other HS events. The Ti/Ca ratio showed reduced peaks (0.4) in periods when the rainforest lowland appeared with a high relative abundance as also occurred during the HS4. Higher peaks of the Ti/Ca ratio (0.7) occurred when the vegetation was sparse or not well established, as inferred by the open vegetation expansion that preceded the HS5. The trend indicates that Ti/Ca ratio works as a pointer of the precipitation events but does not reflect the dimension of them. A consolidated soil by the increased presence of roots possibly retained more sediments on the continent.

Over the interglacials, the sea level rise hindered the continental inflow to the ocean, increasing the distance between the coastline and the GL-1248 marine sediment core. Still, the local speleothems and rainforest vegetation were coordinated and respond positively to the increase of moisture (Figure S11). The retention of the continental load to the ocean is evident, as the higher sea level and the improvement of rainforest vegetation operated combined. The result is imprinted the maximum values of the Ti/Ca ratio along the Younger Dryas and the precipitation events between 115 and 110 kyrs.

2.4.3 The response of neotropical vegetation to orbital variations

The Earth's climate is a system regulated by the uneven distribution of solar heat, and the equatorial region receives solar irradiation readily, almost unchanged throughout the year. The warm and humid conditions create an ideal environment for the development of rainforest. The equatorial region is an abundant source of heat, and the tropical rain belt has a significant influence on rainforest formation. Shifts in the ITCZ position regulates the prevalence between open vegetation and rainforest at PHB. The REDFIT spectral analysis has shown that both vegetations were periodically guided under the millennial time-scale variability (~2.5 kyrs). Still, open vegetation was more prone to change in response to the climatic anomaly than the rainforest lowland. Jennerjahn *et al.* (2004) found a rhythmic delay in the successional pattern of vegetation post precipitation events (1000 to 2000 years), based on *Sellaginela* and Cyatheaceae spp. spores. We suggest that the succession of vegetations found in our data occurred in response to the millennial time-scale pluvial events, altering open design first, forming more dense vegetation until the establishment of the rainforest.

Other studies at NEB presented a similar pattern of tropical forest development after prolonged precipitation events (Dupont *et al.,* 2010; Bouimetahan *et al.,* 2018). However, our data indicated that the vegetation response to different HS wet periods is not uniform, denoting that other factors overlap (Figure 13A).

The $\delta^{18}O$ of calcite in speleothems of NEB imprinted precipitation oscillations on the orbital frequency, and the tropical insolation force played a vital role in the South American climate (Hastenrath, 1991; Wang *et al.,* 2004; Cruz *et al*., 2005; Cheng *et al*., 2013). Precessional forcing alters the incidence of heat received by the sun in the tropics during a restricted season, modulating the humidity circulation from ocean to land. The southern hemisphere is more susceptible to vigorous precipitations during a period of minimal precession (Wang *et al*., 2004; Clement *et al*., 2004; Bischoff *et al*., 2017). Throughout the geological time, the maximal insolation during the austral autumn (MAM) and minimal precession acted relatively paired in the NEB, generating a clear sign of precipitation in the speleothems of the region. Our spectral analysis of the rainforest lowland vegetation data highlighted more relevance to orbital time-scale periodicities than to millennial timescales, with 38 kyrs and 23 kyrs exciding the Chi2% false-alarm level (Figure 10C). The data is consistent with forcing by insolation maxima and minimal precession influences and a more significative response of the rainforest lowland relative abundance (Figure 13A, 13B, and 13C). However, the periodicity of 38 kyrs reflects the influence of the obliquity orbit (41kyrs). The obliquity alters the tilt on earth with severe impacts on ice caps of the Northern Hemisphere and sea-ice, changing atmospheric circulations, and the trajectories of moisture (de Menoccal, 1995; Tuenter *et al.,* 2005). Despite weak changes in the solar radiation received at low latitudes, the obliquity signal was observed over palaeoclimate data and model studies, and those suggest changes on the strength of monsoon systems (Bosman *et al*., 2015). Thus, when minimal obliquity is aligned with minimal precession, it may cause an even more disruptive rainfall event over NEB (Figure 13E). Along the time span of our pollen record, three peaks of minimal obliquity occurred. One incident occurred during the interglacial MIS 5d, which despite the high sea level, the pollen concentration was high in comparison with other samples of MIS 5. The other two separate peaks of minimal obliquity occurred during the glacial period, one during the MIS4 with the highest delivery of exotic spores and pollen grains, and the other one occurred in synchronicity with the hiatus of the marine core. As much as it is redundant, we must say that the opposite effect is also expected for maximal obliquity. Some studies point to the relevance of obliquity-induced changes in climate models, as they may present qualitative similarities to the reality of global warming (Mohtadi *et al.,* 2016).

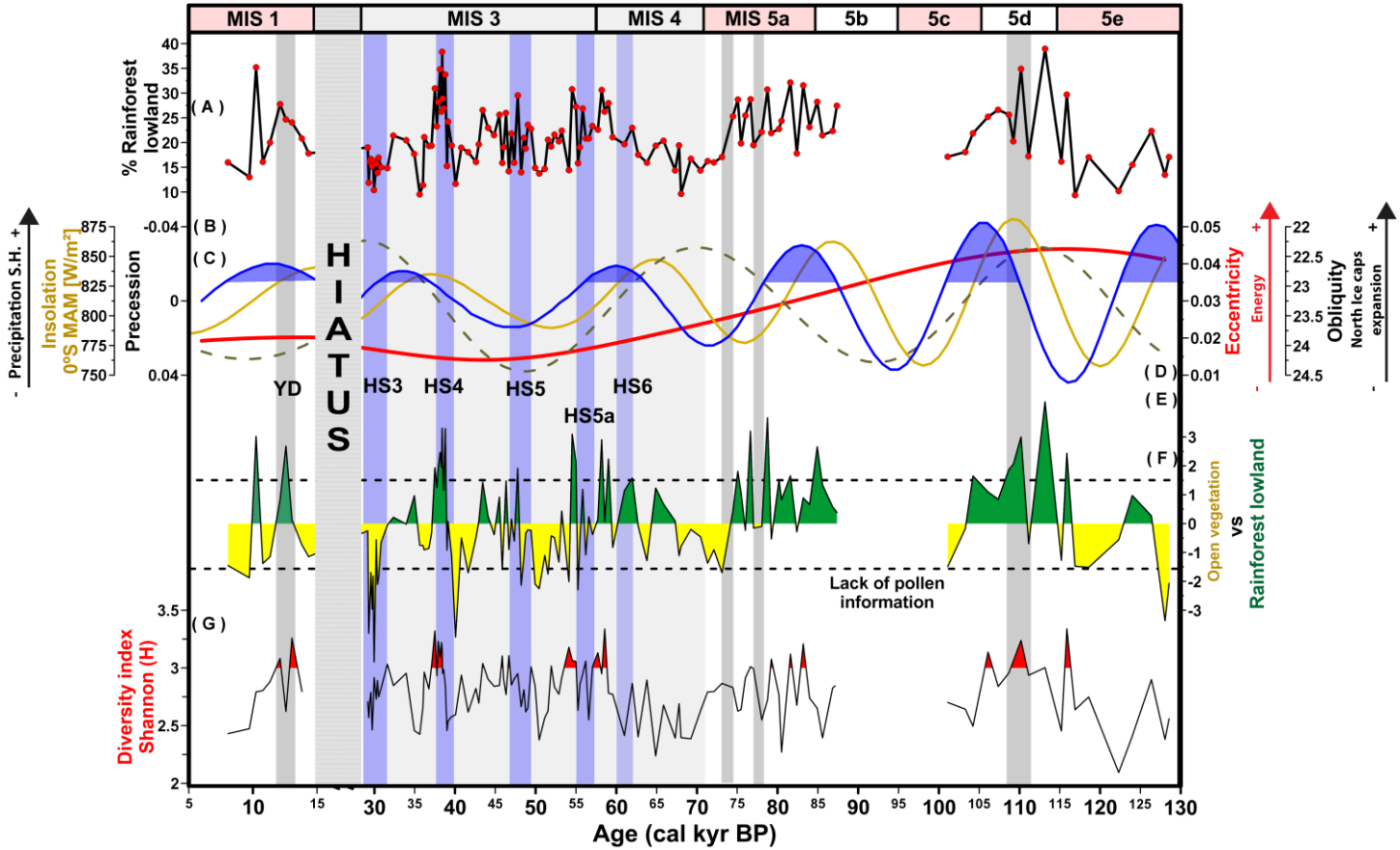

Figure 13: (A) Rainforest lowland relative abundance; (B) Insolation 0° de March to May (MAM) (Berger and Loutre, 1999); (C) Precession orbit, blue line with the minimum values, highlighted in blue (Berger and Loutre, 1999); (D) Obliquity orbit, dotted line; (E) Eccentricity orbit, red line; (F) Delta coverage, positive values indicate an increase in rainforest lowland (filled in green) and negative values indicate an increase in open vegetation (filled in yellow); (G) Diversity index, with values higher than 3 (~70%) highlighted in red. The dotted lines in black are guidelines of the average values. Heinrich Stadials (HS) are marked in blue. The MIS 4 and MIS 3 are represented in light blue to highlight the glacial period. Vigorous precipitation events during the interglacials are marked in light red.

A counterpoint must be emphasized for the interglacials periods. The relative abundance of rainforest throughout the mid-MIS5 drew the attention. Over the interglacials, the ITCZ'S average position is to the north of the equator (Philander *et al.,* 1996). Transitory oscillations in the meridian temperature gradient altered the ITCZ position, which shifted to the southern hemisphere. Within the context of the South American Dipole (SAD), the rainfall variability NEB occurs out of phase with the western Amazon, and southeastern Brazil (Cruz *et al*., 2009; Cheng *et* al., 2013). A continuous lake-peat sediment record (180 kyrs B.P.) from the Colônia basin, southeastern Brazil, was in general agreement with the SAD and described the opposite tendency of rainforest pollen grains found in GL-1258. However, Rodriguez-Zorro *et al*., (2020) noticed a singular increase of tropical rainforest pollen grains during MIS 5 d, with a peak at 110 kyrs, and validated by a speleothem near the region St8 (Cruz *et al.*, 2006). Both studies explain the anomalous precipitation as a consequence of summer insolation and decrease of Northern Hemisphere temperatures, leading the ITCZ southward during the transition from MIS 5e to 5d. We suggest that the amplitude of the orbital cycles and the discrepancies in eccentricity led to different energy budgets between the interglacials (Figure 13D), enhancing the ITCZ transitions over MIS5 and possibly impacting the rainforest performance.

The positive values of delta coverage indicate the increase of rainforest lowland vegetation in periods of the southernmost position of the ITCZ. Positive values of delta coverage that exceed the average line correlate with high values (>70%) of biodiversity index (Figure 13F and 13G). In contrast, periods of open vegetation expansion are mostly related to low values in the diversity index. The rainfall periodicity enables the development of the rainforest and the subsequent biodiversity of plants. Our data corroborate with previous palynology works carried out in NEB, which evidenced the rapid reforestation post-precipitation events (Jennerjahn *et al.,* 2004; Dupont *et al.,* 2010; Bouimetahan *et al.,* 2018). However, millennial time-scale precipitation events imprinted a more robust response over NEB on rainforest vegetation when orbital forcing acted simultaneously (e.g., minimum precession and maximum insolation). Other pollen records in South America operated gains in the local Arboreal Pollen (AP%) in different variability than in the NEB (Figure S12, S13, and S14). The comparison with those studies highlighted the vegetation response to various sources of moisture into the continent, as the SASM and latitudinal shift of the ITCZ during the Pleistocene (Paduano *et al.,* 2003; van der Hammen and Hooghiemstra, 2003; Hanselman *et al.,* 2011; Rodriguez-Zorro *et al*., 2020). The heterogeneity in the landscape and prolonged clusters of forest vegetation possibly promoted effective migration routes of animals and plants during extended precipitations events and

guided the neotropical biodiversity. Thus, our reconstructed vegetation data support the hypothesis of evolutionary radiation in response to environmental change (Gentry,1982). Despite the differences between the millennial time-scale pluvial events over NEB, the improvement of rainforest vegetation could potentially be considered as evidence of the intermittent forest corridors formation. The enhanced connectivity between distant regions promoted periodic genetic exchange among them (Silveira *et al.,* 2019; Ledo and Colli, 2017; Carnaval and Mortiz 2008).

2.5 Conclusion

The marine sediment core GL-1248 was used to reconstruct de vegetation of PHB over the last ~130 kyr. We investigated three pollen groups and their relative abundance: wetland, open vegetation, and rainforest lowland. The open vegetation and the rainforest lowland vegetation have different environmental requirements, and oscillations in the ITCZ modulated the response of plants in ecotone areas of PHB. The rise of the relative abundance of the wetland pollen group was related to the most representative component of the wetland pollen group (Cyperaceae) and reflected the Parnaiba River discharge. The ferns and the spores gave excellent indicatives of the succession of vegetation and the soil stability over HS events or wet periods. The rainforest vegetation shows gradual gains during MIS4, in anti-phase with the XRF Ti/Ca ratio. We suggested that a consolidated soil by the increased presence of roots may have retained more sediments on the continent, with subsequent impact in the Ti/Ca ratio.

As previously discussed in the literature of palynological studies in NEB, the reconstructed rainforest lowland responded positively to precipitations events on the millennial-scale. However, the expansion and retraction of tropical forest boundaries over NEB resulted from rain pulses, but robust gains in rainforest vegetation were mainly orchestrated by orbital cycles. Intermittent formations of ecological corridors improved connectivity between different regions, amplifying the dynamics in neotropical genetic flow. The Neotropical biodiversity is a consequence of a wide broad range of distinct evolutionary processes. Comprehend the vegetation development in NEB has implications to the biodiversity, and still a current discussion.

2.6 REFERENCES:

AB'SABER, A. N. O domínio morfoclimático semi-árido das caatingas brasileiras. ***Geomorfologia***, São Paulo, n. 43, p. 1-39, 1974.

ANHUF, D., LEDRU, M.-P., BEHLING, H., DA CRUZ JR, FW, CORDEIRO, RC, HAMMEN, VAN DER, KARMANN, I., MARENGO, JA, DE OLIVEIRA, PE, PESSENDA, L., SIFEDDINE, A., ALBUQUERQUE, AL, DA SILVA DIAS, P.L. Paleo-environmental change in Amazonian and African Rainforest Turing the LGM. **Palaeogeography, Palaeoclimatology, Palaeoecology** 239, 510–527. 2006.

ANTONELLI, A. & SANMARTÍN, I. Why are there so many plant species in the Neotropics? **Taxon**, 60, 403–414. 2011.

BEHLING, H., ARZ, HW, PÄTZOLD, J., WEFER, G. Late Quaternary vegetational and climate dynamics in northeastern Brazil, inferences from marine core GeoB 3104-1. **Quaternary Science Reviews**, 19 (10), 981-994. 2000.

BEHLING, H., COHEN, M. C. L, AND R. J. LARA, RJ Late Holocene mangrove dynamics of the Marajó Island in Amazonia, northern Brazil. **Vegetation History and Archaeobotany**, 13, 73-80. 2004.

BERGER, A., LOUTRE, M-F. Insolation values for the climate of the last 10 million of years. **Quaternary Science Reviews**, 10 (4), 297-317, 1991.

BENNINGHOFF, W. S. Calculation of pollen and spores density in sediments by the addition of exotic pollen in known quantities. **Pollen et Spores**, 4 (2), 332-333. 1962.

BERGER, A., LOUTRE, M.F. Parameters of the Earths orbit for the last 5 million years in 1 kyr resolution, **PANGAEA**. 1999.

BISCHOFF, T. *Dynamics of the Intertropical Convergence Zone.* Dissertation (Ph.D.), California Institute of Technology. 2017.

BLAAUW, M. Methods and code for 'classical' age-modeling of radiocarbon sequences. **Quaternary Geochronology**, 5 (5), 12-518. 2010.

BOUIMETARHAN, I., CHIESSI, C. M., GONZALEZ-ARANGO, C., DUPONT, L., VOIGT, I., PRANGE, M., ZONNEVELD, K. Intermittent development of forest corridors in northeastern Brazil during the last deglaciation: Climatic and ecologic evidence. **Quaternary Science Reviews**, 192, 86-96, 2018.

BOSMANS, J. H. C., HILGEN, F. J., TUENTER, E., LOURENS, L. J. Obliquity forcing of low-latitude climate**. Clim. Past** 11, 1335–1346. 2015.

CARNAVAL, A. C., MORITZ, C. Historical climate modelling predicts patterns of current biodiversity in the Brazilian Atlantic forest. **Journal of Biogeography**. 35,

1187-1201. 2008.

CHENG, H., SINHA, A., CRUZ, F. W., XIANFENG, W., EDWARDS, R.L., D'HORTA, F. M., RIBAS, C. C., VUILLE, M., STOTT, L. D., AULER, A. S. Climate change patterns in Amazonia and biodiversity. Nat Commun 4:1411. to distant climate anomalies. Nature, 432:740–743. 2013.

CODEVASF. Companhia de Desenvolvimento dos Vales do São Francisco e do Parnaíba, 2005. Disponível em: <www.codevasf.gov.br>. Acesso em: 6 março de 2020.

CLEMENT, A. C., HALL, A., BROCCOLI, A. J. The importance of precessional signals in the tropical climate. **Climate Dynamics**, 22, 327–341. 2004.

COLINVAUX, P. A., DE OLIVEIRA, P. E., MORENO, J. E., MILLER, M. C., BUSH, M. B. A long pollen record from lowland Amazonia forest and cooling in glacial times. **Science**, 274, 85–88. 1996a.

COX, CB & MOORE, PD **Biogeography: an ecological and evolutionary approach**. Fifth Edition. London, Blackwell Scientific Publications. 1993.

CRISTALLI, P. S. Macrofitofósseis em tufos calcários quaternários do norte da Bahia como indicadores paleoclimáticos. 2006. 195p. (Tese de Doutorado) - Instituto de Geociências da Universidade de São Paulo, São Paulo, 2006.

CRUZ, F.W., BURNS, S.J., KARMANN, I., SHARP, W.D., VUILLE, M., CARDOSO, A. O., FERRARI, J. A., SILVA DIAS, P. L., VIANA JR., O. Insolation- driven changes in atmospheric circulation over the past 116,000 years in subtropical Brazil. **Nature** 434, 63–66. 2005.

CRUZ FW, BURNS SJ, KARMANN, I. Reconstruction of regional atmosphere circulation features during the late Pleistocene in subtropical Brazil from oxygen isotope composition of speleothems. **Earth Planet Science Letter** 248:494–506. 2006.

CRUZ, F.W., VUILLE, M., BURNS, S. J., WANG, X., CHENG, H., WERNER, M. EDWARDS, L., KARMANN, I., AULER, A. S., NGUYEN, H. Orbitally driven east–west antiphasing of South American precipitation. **Nature Geoscience**. 2, 210–214. 2009.

DE ABREU, L. SHACKLETON, N. J., SCHÖNFELD J., HALL, M. A., CHAPMAN, M. R. Millenial-scale oceanic climate variability off the Western Iberian margin during the last two glacial periods. **Marine Geology**. 196(1-2), 1-20. 2003.

DUPONT, L. M., SCHLÜTZ, F., EWAH, C. T., JENNERJAHN, T. C., PAUL, A. AND BEHLING, H. Two-step vegetation response to enhanced precipitation in Northeast Brazil during Heinrich Event 1. **Global Change Biology**. 16, 1647-1660. 2010.

EITEN, G. Vegetação. In Cerrado: caracterização, ocupação e perspectivas, 2ª ed. (M.N. Pinto, org.). **Editora Universidade de Brasília**, Brasília, p.17-74. 1994.

FAEGRI K., IVERSEN J. **Textbook of Pollen Analysis**, 4th ed. (revised by K Faegri, PE Kaland, K Krzywinski), John Wiley and Sons, Chichester, 328. 1989.

FIGUEIREDO, M.A. **Unidades Fitoecológicas**. In: Atlas do Ceará, Fortaleza, Ed. **IPLANCE**. 1997.

GENTRY, A.H. Neotropical floristic diversity: phytogeographical connections between Central and South America, pleistocene climatic fluctuations, or an accident of the andean orogeny? Ann. Missouri. **Bot. Gard**. 69:557-593. 1982.

GOVIN, A., HOLZWARTH, U., HESLOP, D., FORD KEELING, L., ZABEL, M., MULITZA, S., COLLINS, JA, CHIESSI, CM, Distribution of major elements in Atlantic surface sediments (36°N-49°S): Imprint of terrigenous input and continental weathering. **Geochemistry, Geophysics, Geosystems.** 13, 1–23. 2012.

GYSSELS, G., POESEN, J., BOCHET, E., LI, Y. Impact of plant roots on the resistance of. soils to erosion by water: a review. Prog. **Phys. Geogr**. 29, 189–217. 2005.

HAMMER, Ø., HARPER, D. A. T., AND RYAN, P. D. PAST: Paleontological Statistics Software Package for Education and Data Analysis. **Palaeontologia Electronica** 4 (1): 9pp. 2001.

HANSELMAN, J.A., BUSH, M.B., GOSLING, W.D., COLLINS, A., KNOX, C., BAKER, P.A., FRITZ, S.C. A 370,000-year record of vegetation and fire history around Lake Titicaca (Bolivia/Peru). Paleogeog. Palaeoclim.,Palaeoecol. 305, 201 - 214. 2011.

HASTENRATH, S. **Climate Dynamics of tropics**. Kluwer, Dordrecht. 488 p. 1991.

HASTENRATH, S. Exploring the climate problems of Brazil's Nordeste: A review. **Climatic Change.** 112, 243–251. 2012.

IBGE, INSTITUTO BRASILEIRO DE GEOGRAFIA E ESTATÍSTICA. **Mapa de Biomas e de Vegetação do Brasil**. Disponível em: <http://www.ibge.org.br/>. 2004.

JENNERJAHN, T. C., ITTEKKOT, V., ARZ, H. W., BEHLING, H., PÄTZOLD, J. AND WEFER, G. Asynchronous terrestrial and marine signals of climate change during Heinrich Events. **Science**, 306, 2236-2239. 2004.

JOHNS, W. E., LEE, T. N., BEARDSLEY, R. C., CANDELA, J., LIMEBURNER, R., CASTRO B. Annual cycle and variability of the North Brazil Current. **Journal of Physical Oceanography**, 28 (1), 103–128. 1998

KIRTMAN, B., POWER, SB, ADEDOYIN, JA, BOER, GJ, BOJARIU, R., CAMILLONI, I., DOBLAS-REYES, FJ, FIORE, A.M., KIMOTO, M., MEEHL, GA, PRATHER, M.,

SARR, A., SCHÄR, C., SUTTON, R., VAN OLDENBORGH, GJ, VECCHI G., AND WANG HJ Near-term Climate Change: Projections and Predictability. In: Climate Change 2013: The Physical Science Basis. Contribution of Working Group I to the Fifth Assessment Report of the Intergovernmental Panel on Climate Change. [STOCKER, TF, QIN, D., PLATTNER, G.-K., M. TIGNOR, ALLEN, SK, BOSCHUNG, J., NAUELS, A. XIA, Y. BEX, V. AND MIDGLEY, P.M. (eds.)]. **Cambridge University Press**, Cambridge, United Kingdom and New York, NY, USA. 2013.

KOUSKY, V. E., GANDU,M. A., Upper tropospheric cyclonic vortices in the Tropical South Atlantic. **Tellus**, 33, p. 538-551. 1981.

KUHLMANN, E. A vegetação. In: Geografia Do Brasil-região Nordeste, vol. 2. IBGE, Rio de Janeiro, pp. 85-110. 1977.

LEAL, I. R.; VICENTE, A.; TABARELLI, M. Herbivoria por caprinos na Caatinga da região de Xingó: uma análise preliminar. In: LEAL, I.R.; TABARELLI, M.; SILVA, J.M.C. (Orgs.). Ecologia e conservação da Caatinga. Recife: UFPE. p.695-716. 2003.

LEDO, R. M. D., AND COLLI, G. R. The historical connections between the Amazon and the Atlantic Forest revisited. **Journal of Biogeography**, 44, 2551–2563. 2017.

MASLIN, M. A., ETTWEIN, V. J., WILSON, K. E., GUILDERSON, T. P., BURNS, S. J., AND LENG, M. J.: Dynamic boundary-monsoon intensity hypothesis: evidence from the deglacial Amazon River discharge record, **Quaternary science review**, 30, 3823–3833, doi:10.1016/j.quascirev.2011.10.007, 2011.

DEMENOCAL, P. B.: Plio-Pleistocene African climate, **Science**, 270, 53–59, 1995.

MARON, M. Stop misuse of biodiversity offsets. **Nature**, 523, 401. 2015.

MULITZA, S., CHIESSI, C. M., SCHEFUß, E., LIPPOLD, J., WICHMANN, D., ANTZ, B., MACKENSEN, A., PAUL, A., PRANGE, M., REHFELD, K., WERNER, M., BICKERT, T., FRANK, N., KUHNERT, H., LYNCH-STIEGLITZ, J., PORTILHO-RAMOS, R. C., SAWAKUCHI, A. O., SCHULZ, M., SCHWENK, T., TIEDEMANN, R., VAHLENKAMP, M., ZHANG, Y. Synchronous and proportional deglacial changes in Atlantic meridional overturning and northeast Brazilian precipitation. **Paleoceanography**, 32, 622–633. 2017.

MUNIZ, F. H. A vegetação da região de transição entre a amazônia e o nordeste: diversidade e estrutura, p. 53-69. In: E.G. Moura (Ed.). Agroambientes de transição. Entre o trópico úmido e o semi-árido. Atributos; alterações; uso na produção familiar. São Luís, **UEMA**. 2006.

MUNIZ, F. H. Efeito do manejo florestal sobre a composição florística e fitossociologia da floresta na Amazônia maranhense. In: Marlúcia Bonifácio Martins e Tadeu Gomes de Oliveira (Org.). **Amazônia Maranhense: Diversidade e Conservação. Belém**: MPEG, p.118-140. 2011.

NACE, T. E., BAKER, P. A., DWYER, G. S., SILVA, C. G., RIGSBY, C. A., BURNS, S. J., GIOSAN, L., OTTO-BLIESNER, B., LIU, Z., ZHU, J. The role of North Brazil Current transport in the paleoclimate of the Brazilian Nordeste margin and paleoceanography of the western tropical Atlantic during the late Quaternary. **Palaeogeography Palaeoclimatology Palaeoecology,** 415, 3–13. 2014.

OLIVEIRA, R., SILVA, A., RIBEIRO, A., ARAÚJO, J., OLIVEIRA, O., AND CAMACHO, R. List of angiosperm species of the riparian vegetation of the Apodi-Mossoró River, Rio Grande do Norte, Brazil. **Check List***, 9* (4), 740-751. 2013.

PADUANO, G. M., BUSH, M. B., BAKER, P. A., FRITZ, S. C., AND SELTZER, G. O. A Vegetation and Fire History of Lake Titicaca since the Last Glacial Maximum, **Palaeogeogr. Palaeocl**., 194, 259–279, 2003.

PESSENDA, L. C. R.; GOUVEIA, S. E. M.; RIBEIRO, A. de S.; DE OLIVEIRA, P. E., ARAVENA, R. Late Pleistocene and Holocene vegetation changes in northeastern Brazil determined from carbono isotopes and charcoal records in soils. **Palaeogeography, Palaeoclimatology, Palaeoecology**, Amsterdam, v. 297, p. 597-608, 2010.

PINAYA, J. L. D., CRUZ F. W., CECCANTINI, G. C. T., PEDRO L. P. CORRÊA, PITMAN, N. VEMADO, F., LOPEZ, S. M. A., PEREIRA FILHO, A. J., GROHMANN, C. H., CHIESSI, C. M., STRÍKIS, N. M., HORÁK-TERRA, I., PINAYA, W. H. L., DE MEDEIROS, V. B., SANTOS, R.DE A., AKABANE, T. K., SILVA, M. A.,CHEDDADI, R., BUSH, M., HENROT, J., FRANÇOIS, L., HAMBUCKERS, A., BOYER, F., CARRÉ, M., COISSAC, E., FICETOLA, F., HUANG, K., LÉZINE, A-M., NOURELBAIT, M., RHOUJJATI, A.,TABERLET, P., SARMIENTO, F., ABEL-SCHAAD, D., ALBA-SÁNCHEZ, F. ZHENG, Z. & DE OLIVEIRA, P. E. Brazilian montane rainforest expansion induced by Heinrich stadial 1 event. **Scientific Reports** 9. 2019.

PHILANDER, S. G. H., GU, D., HALPERN, D., LAMBERT, G., LAU, N. C., LI, T. AND PACANOWSKI, R. C. Why the ITCZ is mostly north of the equator. **Journal of Climate**, 9, 2958–2972. 1996.

PRADO, D.E. As caatingas da América do Sul. Pp. 3-73. In: I.R. Leal, M. Tabarelli & J.M.C. Silva (eds.). **Ecologia e conservação da Caatinga**. Recife, Editora Universitária, Universidade Federal de Pernambuco. 2003.

PRADO, D. E. AND GIBBS, P. E. Patterns of species distributions in the dry seasonal

forests of South America. **Annals of the Missouri Botanical Garden**, 80, 902-927. 1993.

PRENTICE, I., CRAMER, W., HARRISON, S. P., LEEMANS, R., MONSERUD, R. A., SOLOMON, A. M. A global biome model based on plant physiology and dominance, soil properties and climate. **Journal of Biogeography**, 19, 117–134. 1992.

PRIMACK, Richard B. **Essentials of Conservation Biology**. Sunderland, MA: Sinauer, 1993.

RAMIREZ-BARAHONA S., EGUIARTE L. E. Changes in the distribution of cloud forests during the last glacial predict the patterns of genetic diversity and demographic history of the tree fern Alsophila firma (Cyatheaceae). **Journal of Biogeography**, 41, 2396–2407. 2014.

REIMER, P. J., BARD, E., BAYLISS, A., BECK, J. W., BLACKWELL, P. G., RAMSEY, C. B., BUCK, CE, CHENG, H., EDWARDS, R. L., FRIEDRICH, M., GROOTES, P. M., GUILDERSON, T. P., HAFLIDASON, H., HAJDAS, I., HATTÉ, C., HEATON, T. J., HOFFMANN, D. L., HOGG, A. G., HUGHEN, K. A., KAISER, K. F., KROMER, B., MANNING, SW, NIU, M., REIMER, RW, RICHARDS, DA, SCOTT, EM SOUTHON, JR, STAFF, RA, TURNEY, C. S. M., VAN DER PLICHT, J. IntCal13 and Marine13 radiocarbon age calibration curves 0–50,000 years cal BP. **Radiocarbon.** 55m (04), 1869–1887. 2013.

RIBEIRO, L. F. & M. TABARELLI. A structural gradient in cerrado vegetation of Brazil: changes in woody plant density, species richness, life history and plant composition. **Journal Tropical Ecology**. 18: 775-794. 2002.

RISSER, P.G. Biodiversity and ecosystem function. **Conserv. Biol**. 9, 742– 746. 1995.

RODRÍGUEZ-ZORRO, P. A., LEDRU M. P., BARD, E, et al. Shut down of the South American summer monsoon during the penultimate glacial. **Scientific Reports** 10: 6275. 2020.

SCHULZ, M., & MUDELSEE, M. REDFIT: Estimating red-noise spectra directly from unevenly spaced paleoclimatic time series. **Computers and Geosciences**, 28(3), 421–426. 2002.

SIFEDDINE, A.; ALBUQUERQUE, A. L. S.; LEDRU, M.-P.; TURCQ, B.; KNOPPERS, B.; MARTIN, L.; MELLO, W. Z.; PASSENAU, H.; DOMINGUES, J. M. L.; CORDEIRO, R. C.; ABRÃO, J. J.; BITTENCOURT, A. C. S. P. A 21.000 cal years paleoclimatic record from Caçó Lake, northern Brazil: evidence from sedimentary and pollen analyses. **Palaeogeography, Palaeoclimatology, Palaeoecology**, 189: 25-34. 2003.

SILVEIRA, M. H. B., MASCARENHAS, R., CARDOSO, D. AND BATALHA-FILHO, H.

Pleistocene Climatic Instability Drove the Historical Distribution of Forest Islands in the Northeastern Brazilian Atlantic Forest. **Palaeogeography, Palaeoclimatology, Palaeoecology**, 527, 67-76. 2019.

STOCKMARR, J. Tablets with spores used in absolute pollen analysis. **Pollen et Spores** 13: 615-621. 1971.

STRAMMA, L., FISCHER, J., REPPIN, J. The North Brazil Undercurrent. **Deep-Sea Research I** 42, 773-795. 1995.

STRÍKIS, N. M., CRUZ, F. W., BARRETO, E. A. S., NAUGHTON, F., VUILLE, M., CHENG, H., VOELKER, A. H. L., ZHANG, H., KARMANN, I., EDWARDS, L., AULER, A. S., SANTOS, R. V., SALES, H. R., South American monsoon response to iceberg discharge in the North Atlantic. **The Proceedings of the National Academy of Sciences**. USA 115, 3788–3793. 2018.

SUBBA REDDI C.,REDDI N. S. Pollen production in some anemophilous angiosperms. **Grana**, 25: 55–61. 1986.

THOMSON, D. J. Time series analysis of Holocene climate data. Philosophical Transactions of the Royal Society A: Mathematical, **Physical and Engineering Sciences**, 330(1615), 601–616. 1990.

TUENTER, E., WEBER, S., HILGEN, F., LOURENS, L., GANOPOLSKI, A.: Simulation of climate phase lags in response to precession and obliquity forcing and the role of vegetation, **Climate Dynamics**, 24, 279–295. 2005.

UTIDA, G., CRUZ, F.W., ETOURNEAU, J., BOULOUBASSI, I., SCHEFUß, E., VUILLE, M., NOVELLO, V.F., PRADO, L.F., SIFEDDINE, A., KLEIN, V., ZULAR, A., JCC, V., TURCQ, B. Tropical South Atlantic influence on northeastern Brazil precipitation and ITCZ displacement during the past 2300 years. Scientific Reports, 9, 1698. 2009.

VAN DER HAMMEN, T. The Pleistocene changes of vegetation and climate in Tropical South America. **Journal of Biogeography**, 1, pp. 3-26 1974.

VAN DER HAMMEN, T.,HOOGHIEMSTRA, H. Neogene and Quaternary history of vegetation, climate, and plant diversity in Amazonia. **Quaternary Science Review.** 19, p. 725-42, 2000.

VAN DER HAMMEN, T., HOOGHIEMSTRA, H. Interglacial-glacial Fuquene-3 pollen record from Colombia: an Eemian to Holocene climate record. **Global and Planetary Change** 36, 181–199. 2003.

VENANCIO, I. M., MULITZA, S., GOVIN, A., SANTOS, T. P., LESSA, D. O., ALBUQUERQUE, A. L. S., CHIESSI, C. M., TIEDEMANN, R., VAHLENKAMP, M., BITCKET, T., SCHULZ, M., Millennial- to orbital-scale responses of western equatorial Atlantic thermocline depth to changes in the trade wind system since

the Last Interglacial. **Paleoceanography and Paleoclimatology.** 2018.

WANG, X., AULER, A. S., EDWARDS, R. L., CHENG, H., CRISTALLI, P. S., SMART, P. L., RICHARDS, D. A. AND C-C. SHEN. Wet periods in northeastern Brazilover the past 210 kyr linked todistant climate anomalies. **Nature**, 432 (7018), 740–743. 2004.

WERNECK, F. P. The diversification of eastern South American open vegetation biomes: Historical biogeography and perspectives. **Quaternary Science Review**, 30, 1630-1648. 2011.

ZHANG, Y., CHIESSI, C. M., MULITZA, S., ZABEL, M., TRINDADE, R. I. F., HOLLANDA, M. H. B. M., DANTAS, E. L., GOVIN, A., TIEDEMANN, R., WEFER, G. Origin of increased terrigenous supply to the NE South American continental margin during Heinrich Stadial 1 and the Younger Dryas. **Earth Planetary Science Letters**. 2015.

3 CHANGES IN SEA SURFACE HYDROGRAPHY AND PRODUCTIVITY IN THE WESTERN EQUATORIAL ATLANTIC SINCE THE LAST INTERGLACIAL

Despite the relevance of more productive areas for the global carbon budget, the world's oceans have large-scale oligotrophic conditions. The western equatorial Atlantic is characterized as a low productivity area, mainly due to the presence of the North Brazil Current (NBC) (Peterson and Stramma, 1991; Krauss, 1996). In this region, warm sea surface waters pile up and deepen the seasonal thermocline due to the modern dynamics of the trade winds (Hastenrath and Merle, 1987), denoting a nutrient-depleted surface layer considered a quasí-permanent feature of the tropical and subtropical Atlantic (Herbland and Voituriez, 1979). Strong southeast (SE) trade winds create a thermocline tilt between the western and eastern equatorial Atlantic, with implications of the nutrient availability at the sea surface, setting the productivity regimes in both areas (Molinari *et al.*, 1986).

Previous studies focusing on paleoceanographic reconstructions have shown that the transport of warm waters to the western equatorial Atlantic was reduced during the phase with weak SE trades winds, consequently attenuating the east-west thermocline tilt (Wolff *et al.,* 1999; Venancio *et al.,* 2018). Oscillations in the thermocline thickness possibly influenced past productivity by modulating the nutrients diffusion into the photic zone. Indeed, several studies indicate that glacial-interglacial changes in productivity occurred in the region, with higher productivity during interglacials compared to glacials (Rühlemann *et al.,* 1996; Bickert *et al.,* 1997; Mulitza *et al.,*1998; Kinkel *et al*., 2000; Vink *et al.,* 2002).

The last glacial period exhibits singular environment conditions with lower relative sea-level (RSL) than the present, expanding the shoreline, and delivering more continental material to the ocean areas. Another particular feature was the intensification of the meridional temperature gradient between the North and the Tropical Atlantic, generating the compression of climatic zones towards the equator and driving stronger trade winds (Parkin, 1974; Leroux, 1973). In addition, displacements of the Intertropical Convergence Zone (ITCZ) generated changes in trade winds' direction and strength. Nevertheless, the southward shift of the ITCZ was accompanied by periods with weak southeast (SE) trade winds and intense precipitations events in northeastern Brazil. Rivers that flow into the ocean increased their freshwater and nutrients contribution due to more severe runoff, modulating the biological productivity in the western equatorial Atlantic (Vink *et al.*, 2000).

Studies in different margins of the South Atlantic indicated that biological productivity could be reconstructed through organic-walled dinoflagellate cysts (dinocysts) (Gu *et al.*, 2017; Hardy *et al.*, 2016). In the western equatorial Atlantic,

Portilho-Ramos *et al.* (2017) showed changes in stratification during millennial-scale events, triggered by the direct effect of precipitation over the ocean linked to ITCZ shifts. However, the authors did not focus on the impact of such stratification changes over primary productivity. Based on that, we aimed to reconstruct over a longer period the influence of these changes in mixed layer depth in the productivity. Thus, an assessment of the impact of these distinct productivity-related processes during the past was still needed for this area. Oligotrophic regions comprise a vast portion of the oceans. In order to achieve greater accuracy in models that estimate the efficiency of primary productivity in the carbon cycle, it is important to understand the dynamics of primary productivity in oligotrophic regions. In this context, we aimed to evaluate the glacial-interglacial, millennial-scale changes in the sea surface hydrography and productivity, as well as the main processes linked to the observed variations at the western equatorial Atlantic over the last ~130 kyr.

3.1 Sediment core location and regional setting

The region is under the influence of different water masses, with the following vertical distribution: the North Atlantic Deep Water (NADW) in the range of 2.000–3.000 meters deep, the Antarctic Intermediate Water (AAIW) established between 800–1.500 meters deep, and the South Atlantic Central Water (SACW) which occupies the range of 200–500 meters deep. The SACW flows between the AAIW and the Tropical Water (TW) at the surface layer (Stramma and England, 1999) (Figure S15). Except for the southward flow of the NADW, the other water masses described (AAIW, SACW, TW) flow northward. At the surface layer, the NBC transports the TW, while the North Brazil Undercurrent (NBUC) flows at the sub-surface and within the thermocline layer, transporting the SACW (Stramma *et al.*, 1995; Schott *et al.*, 1995). The strength of NBC varies and is seasonally linked to the trade wind dynamics. During austral summer (December–March), the northeast (NE) trade winds gain strength and NBC transport reduces (Stramma *et al.*, 1995; Johns *et al.*, 1998). As a result of intensifying NE trade winds, ITCZ reaches its southernmost position (2°S), leading to enhanced precipitation in northeastern Brazil (Hastenrath, 2012).

The marine sediment core GL-1248 (0° 55.2’ 55.2’S, 43° 24.1’ 24.1’W) was retrieved by Petrobras with a length of 19.29 m at 2264 m water depth, located at the slope of the Barreirinhas Bight on northeastern Brazil. The Barreirinhas Bight had a shallow continental shelf, ~75 meters (m) below the sea surface (Krueger *et al.*, 2012; Mohriak, 2003), with a vertical gradient. The marine sediment core was about 160 km distance from the modern coastline (Figure 14). The GL-1248 core was collected 280 km from the Parnaiba River fan and approximately 740 km from the Amazon River fan

(Figure S16). These geographical features assigned a high dynamic abiotic system with significant seasonal contrasts between the surface and subsurface salinity and nutrient loading, which are regulator factors of primary production (Price *et al.*, 2016; Mallin *et al.*, 1993).

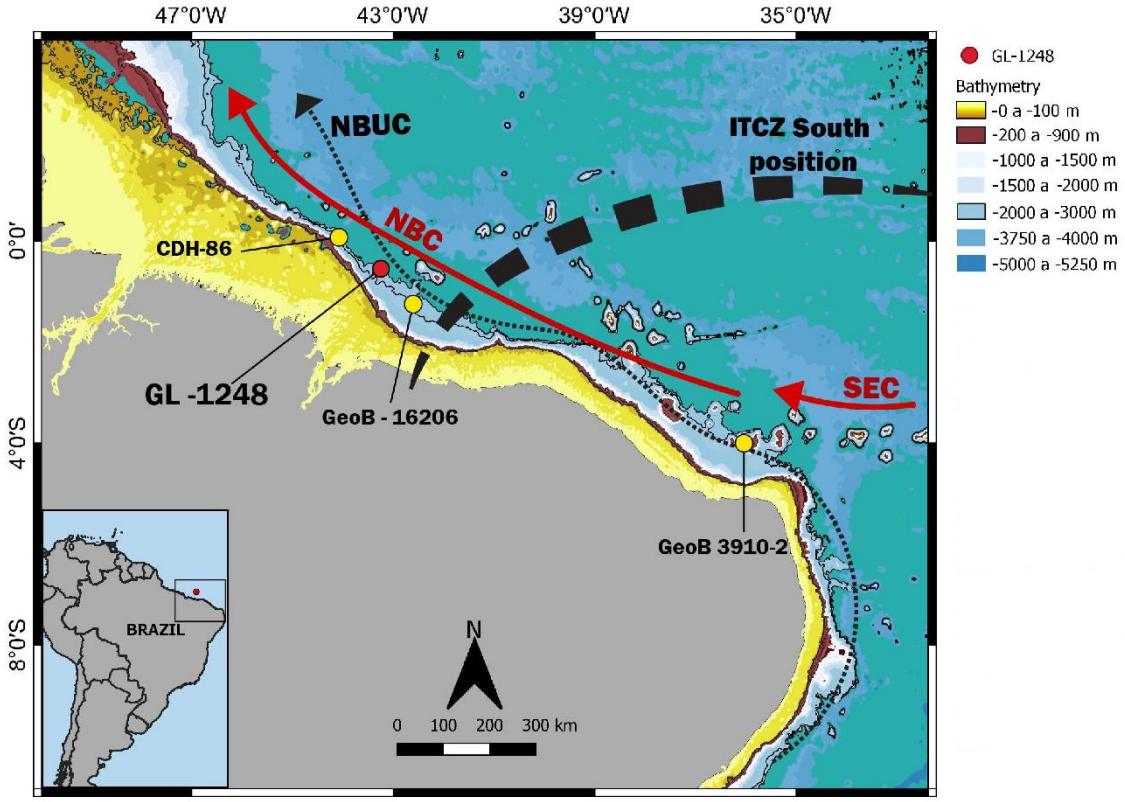

Figure 14: Bathymetric map of the study area in northeastern Brazil and the location (red dot) of core GL-1248 (0°55.2'S, 43°24.1'W). Yellow dots represent other cores discussed in the text namely: CDH-86 (00°20.00' N, 44°12.54' W) (Nace *et al.*, 2014), GeoB 16206 (1°34.75'S 43°01.42'W) (Zhang *et al.*, 2015), GeoB 3910-2 (4°15' S 36°21' W) (Dupont *et al.*, 2010). The map also shows relevant surface currents such as the South Equatorial Current (SEC) and the North Brazil Current (NBC) in red arrows and the subsurface North Brazil Undercurrent (NBUC) in black dotted arrows. The dashed black line displays the approximate southern position of the Intertropical Convergence Zone (ITCZ) during austral summer (December–March).

3.2 Material and Methods:

3.2.1 Age model

The age model was established based on 12 AMS radiocarbon dates and the alignment of X-Ray fluorescence (XRF) Ti/Ca values with reference curves. The radiocarbon analysis was performed on planktonic foraminifera species *Globigerinoides ruber* (white) and *Trilobatus sacculifer* (planktonic foraminifera). The radiocarbon ages were used to generate a chronology for the upper 6.30m of the core. The radiocarbon ages were calibrated with the IntCal13 calibration curve (Reimer *et al.*, 2013). The chronology for the lower part of core GL-1248 (from ~5 m to ~17 m) was

derived from tie points created between Ti/Ca alignment with the ice core $\delta^{18}O$ record from North Greenland Ice Core Project (Wolff *et al.,* 2010). The downcore ages were modeled on the linear interpolation using the package Clam 2.2 (Blaauw, 2010). Venancio *et al.* (2018) described the age model of the marine core GL-1248 in detail. The Marine Isotopic Stages (MIS) boundaries and sub-divisions were defined according to Lisiecki and Raymo (2005). They were established as MIS 1 (starts at 14 kyr before present), MIS 3 (29–57 kyr), MIS 4 (57–71 kyr), MIS 5a (peak at 82 kyr), MIS 5b (peak at 87 kyr), MIS 5c (peak at 96 kyr), MIS 5d (peak at 109 kyr), MIS 5e (peak at 123 kyr).

3.2.2 Palynological preparation

A total of 131 samples were prepared for palynological analysis using standard laboratory procedures (Faegri and Iversen, 1989), but excluding acetolysis to preserve the dinocysts. About 4–6 g (wet weight) samples were prepared for dinoflagellate cysts analyses. At first, the sediment samples were sieved with a 150 µm mesh to remove the larger particles, such as shells and stones. After that, one tablet of exotic *Lycopodium clavatum* spores (containing 20,848 ± 1546 spores) was added to each sample to estimate the concentration (cysts/cm³) and influx (cysts/cm²/kyr) values (Stockmarr, 1971). Then, the samples were treated with hydrochloric acid (HCl, ca. 35%) for decalcification and cold hydrofluoric acid (HF, 40%) for siliceous content removal. After the chemical treatment, the samples went through an ultrasonic bath (maximum 30 seconds) for organic matter disaggregation. The samples were sieved with a 1 µm nylon mesh, but particles up to 5 µm may still pass through. The samples were processed at the Department of Palynology and Climate Dynamics, Georg-August-University Göttingen (Germany). Permanent microscope slides were made, and due to the low content, one to four slides per sample were counted. An average of 130 cysts was counted per sample (min. 83, max. 367). In total, 38 dinoflagellate cyst types were identified according to Zonneveld and Pospelova (2015) morphological descriptions. Dinoflagellate cysts were grouped into autotrophic and heterotrophic taxa due to the different energy resources (Gaines and Elbrächter, 1987; Taylor, 1987; Taylor *et al.*, 2007). The most frequent taxa were presented in relative abundance and grouped based on their ecological affinities. The dinocysts influx (cysts/cm²/kyr) was calculated by multiplying the dinocysts concentration (cysts/cm³) with the sedimentation rate (cm/kyr), and the concentration was calculated for each sample following the Benninghoff (1962) equation.

3.2.3 Dinoflagellate cyst indexes

To evaluate the preservation condition of dinocysts in the marine environment, we calculated the degradation constant of sensitive cysts (k) and the reaction time (t). The kt index was obtained by the equation 1, with and X_f = final cyst concentration (cysts/cm³) and X_i = initial cyst concentration (cysts/cm³) (Zonneveld *et al.*, 2007; 2010). The sensible oxygen cysts were designated as S-Cysts. The kt index was used to evaluate the selective degradation of the S-cysts (supplementary material, Table S2) in the marine sediments to reconstruct deep-ocean ventilation and infer if the sedimentary signal was modified by oxygen degradation (Zonneveld *et al.*, 2007; 2010).

To indicate the heterotrophic and the autotrophic fluctuations through the last ~130 kyr, we used the ratio base on their relative abundances (H/A ratio) (equation 2). Values close to number 1 indicated a more significant proportion of heterotrophic dinocysts (Pospelova and Kim, 2010). The dominance index was calculated using the Simpson index in Past3 software (Hammer *et al.*, 2001).

Equation 1 – Kt equation

$$kt: \ln (X_i/X_f) \quad (1)$$

Equation 2 – H/A ratio equation.

$$H/A \text{ ratio} = H-cysts/ (H-cysts + A-cysts) \quad (2)$$

3.2.4 Foraminifera assemblages

We analyzed the planktonic foraminifera assemblages with 4 cm resolution for MIS 1 to 5e sections due to a low sedimentation rate and 10 cm for the other sections. The 10 cm^3 of sediment was washed through a 150 µm mesh sieve, and the residue material was dried at 50°C for 24h. The fraction larger than 150 µm was re-sieved, dried and then divided until 300–500 individuals remained for identification at the species level. Species were identified by following the Kennett and Srinivasan (1983) and Loeblich and Tappan (1988) definitions.

3.2.5 Statistical analysis

To characterize the ecological affinities of dinocysts assemblages, we performed a Correspondence Analysis (CA). The CA added to each species disposition through the Axis due to its similarities (Legendre and Gallagher, 2001). The CA is a statistical ordination analysis better recommended to species with unimodal responses if compared to PCA, which is preferred for data with a linear distribution (Jongman *et al.,* 1987; ter Braak and Prentice 1988). For a better statistical measurement, regarding the

samples with dinocyst taxa in low content, less than 5% were not taken into consideration. Unidentified species such as *Spiniferites spp.*, *Operculadinium spp.*, and *Impagidinium spp.* were also not considered, due to their controversial ecological affinities. Paleontological Statistics (Past3) software was used to perform CA statistical analysis (Hammer *et al.*, 2001).

3.3 Results

3.3.1 Sedimentation rate, dinocyst concentrations, and the influx

The core GL-1248 covered the last ~130 kyr (MIS 1–5), with the mean sedimentation rate of 21 cm/kyr, with higher values during Marine Isotopic Stage (MIS) 3 (67 cm/kyr), and lower values during the Interglacials (~10 cm/kyr) (Figure 15A). A total of 31 dinoflagellate cyst taxa were identified from 131 sediment samples. The dinocyst concentrations were generally low in GL-1248 (Figure 15B), variating down-core from ~64 to 911 cysts/cm³(averaging 249 cysts/cm³). The influx values oscillated from 4.5 to 315 10^2cysts/cm^2/kyr (avg. 57 10^2cysts/cm^2/kyr) (Figure 15C). Higher dinocysts concentration values were found during MIS 5 (~68 to 653 cysts/cm³, avg. 244 cysts/cm³), MIS 1 (~85 to 757 cysts/cm³, avg. 242 cysts/cm³), and during late MIS 3 (~64 to 911 cysts/cm³, avg. 259 cysts/cm³), periods of reduced sedimentation rate. The influx values during MIS 3 reached the highest values of the sediment core (~79.5 to 315 10^2cysts/cm^2/kyr, avg. 205 10^2 cysts/cm^2/kyr).

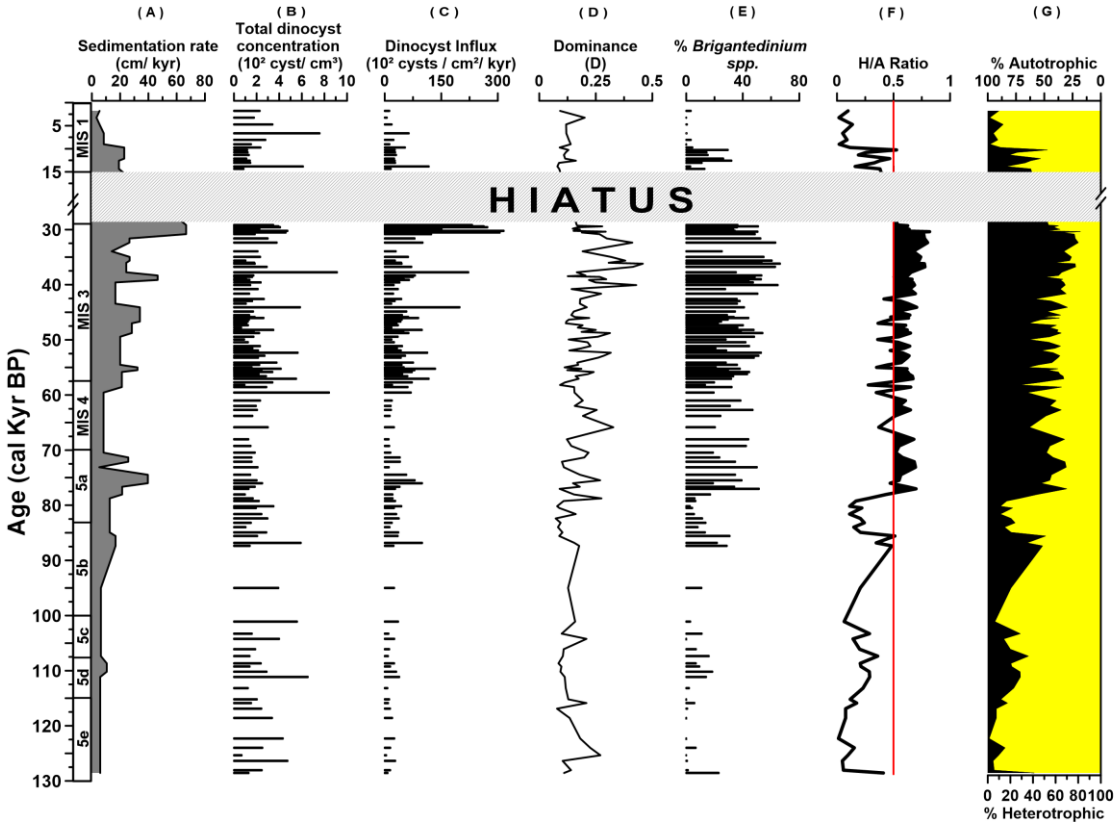

Figure 15: A) Sedimentation rate (cm/kyr); B) Total dinocysts concentration (10^2cysts/cm^3); C) Dinocysts influx (10^2cysts/cm^2/kyr); D) Dominance index; E) Relative abundance of *Brigantedinium spp.*; F) H/A Ratio; G) Percentage of heterotrophic and autotrophic dinocysts with autotroph highlighted in yellow.

3.3.2 Dinoflagellate cyst indexes

The kt index showed an asynchronous pattern to the sedimentation rate. Our result indicated a relatively low degradation during the glacial (kt <4, four is the critical value to evaluate the selective preservation in our record). The dominance index was weighted according to the abundance of the most common species (Figure 15D). The *Brigantedinium spp.* was pacing the dominance index and, as a consequence, was the most frequent heterotrophic dinocysts in the relative abundance (Figure 15D, 15E, and 15G).

The heterotrophic (H) and autotrophic (A) dinoflagellate cyst ratio (H/A) decreased during MIS 1 and 5e–5b and presents higher values over the MIS 5a, 4 and 3. Oscillations in the H/A ratio were observed during the early MIS 3 (Figure 15F).

3.3.3 Dinoflagellate cyst relative abundances

The autotrophic species (Figures 2G and S3) were the most dominant during the interglacials MIS 5 and MIS 1. The most representative species during both interglacials were *Spiniferites bentorii* (up to 33%), *Spiniferites mirabilis* (up to 33%),

Spiniferites spp. (up to 29%), *Spiniferites membranaceus* (up to 26%), and *Spiniferites pachydermus* (up to 26%). Other dominant autotrophic species were *Operculodinium centrocarpum* (up to 26%), *Tuberculodinium vancampoae* (up to 19%), *Pentapharsodinium dalei* (up to 18%) and *Impagidinium aculeatum* (up to 16%). The highest relative abundance of *Pentapharsodinium dalei* (~18–5%) occurred during MIS 5.

Leipokatium invisitatum is not common in the region and appears in a very low abundance. Despite that, *Leipokatium invisitatum* achieved values greater than 5% during the MIS 4 and was not excluded from the river outflow assemblage. The relative abundance of *Lingulodinium machaerophorum* reached a maximum of 31% during the early MIS 4. Cysts of heterotrophic taxa (Figure S17) were the most common during MIS 3, mainly represented by *Brigantedinium spp.* (up to 66%), *Echinidinium aculeatum* (up to 34%), *Selenopemphix nephroides* (up to 23%), *Protoperidinium americanum* (up to 14%), *Trinovantedinium applanatum* (up to 11%), and *Selenopemphix quanta* (up to 8%).

3.3.4 Foraminifera relative abundances

We calculated the relative abundances of planktonic foraminifera over the last ~130 kyr. We use three species of planktonic foraminifera to assist the understanding of local hydrography and productivity. They were *Globigerinoides ruber* (white, up to 47.5%), *Neogloboquadrina dutertrei* (up to 20%) and *Globigerinoides ruber* (pink, up to 11.8%) (Figure S19).

3.4 Discussion

3.4.1 Dinoflagellate cysts ecological affinities

The CA established the ecological clusters between different dinoflagellate cysts (Figure 16), which were in agreement with the literature. Arranged from values lower than -0.5 to the Axis 1 and higher than +0.5 values over the Axis 2, the following species were organized: *Polysphaeridium-zoharyi*, *Pentapharsodinium dalei*, *Operculodinium centrocarpum, Spiniferites bentorii, Spiniferites membranaceus, and Spiniferites pachydermus.* Those species are autotrophs and related to warm, oligotrophic, and more salinity waters (Vink *et al.*, 2000; Kim *et al.*, 2010; De Schepper *et al.*, 2011). Due to the similarity with NBC features, we defined them as open ocean assemblage.

The *Brigantedinium spp, Protoperidinium americanum, Selenopemphix nephroides,* and *Trinovantedinium applanatum* are related to low-salinity and considered turbidity-tolerant species (Marret and Zonneveld, 2003; Kim *et al.*, 2010). Both dinocysts

Selenopemphix nephroides and *Trinovantedinium applanatum* were previously observed in the local area, associated with the Amazon River plume and characteristic of low-salinity and light-limited environments (Vink *et al.*, 2000; Bouimetarhan *et al.*, 2009; Bouimetarhan *et al.*, 2018). The river outflow assemblage was highlighted by the positive values of the Axis 1, higher than 1, and established by the presence of *Brigantedinium spp, Leipokatium invisitatum, Protoperidinium americanum, Selenopemphix nephroides,* and *Trinovantedinium applanatum*.

In general, the species *Dalella chathamensis, Echinidinium aculeatum, Echinidinium granulatum, Echinidinium transparantum, Impagidinium patulum, Impagidinium sphaericum, Impagidinium velorum, Operculodinium israelianum, Pyxidinopsis reticulata, Spiniferites mirabilis, and Tuberculodinium vancampoae a*re related to well-ventilated water masses with higher nutrient availability as the South Atlantic Central Water (Gu *et al.*, 2017; Zonneveld *et al.*, 2013; Vink *et al.*, 2000). We designated the assemblage of these species as nutricline, and they were disposed in values lower than +0.5 over the Axis 1 and in negative values of the Axis 2.

The neritic species are identified by their tolerance to transient features, as mixed water masses (Dale, 1996; Zonneveld and Brummer, 2000; Marret and Zonneveld, 2003). The neritic assemblage was defined by positive values of Axis 2 and ranging from 0.5 to -0.5 in Axis 1. The neritic assemblage was set up by *Echinidinium delicatum, Impagidinium, Impagidinium paradoxum, Impagidinium strialatum, Lingulodinium machaerophorum, Nematosphaeropsis labyrinthus, Operculodinium centrocarpum* reduced processes*, and Selenopemphix quanta.* Low salinity attenuates the *Operculodinium centrocarpum* process length (Ellegaard, 2000; Verleye *et al.*, 2012), which corroborated with *Operculodinium centrocarpum* reduced processes included in the neritic assemblage. A complete list of species, ecological affinities, nutritional demands, selective preservation, and geographic distribution is shown in Table S2.

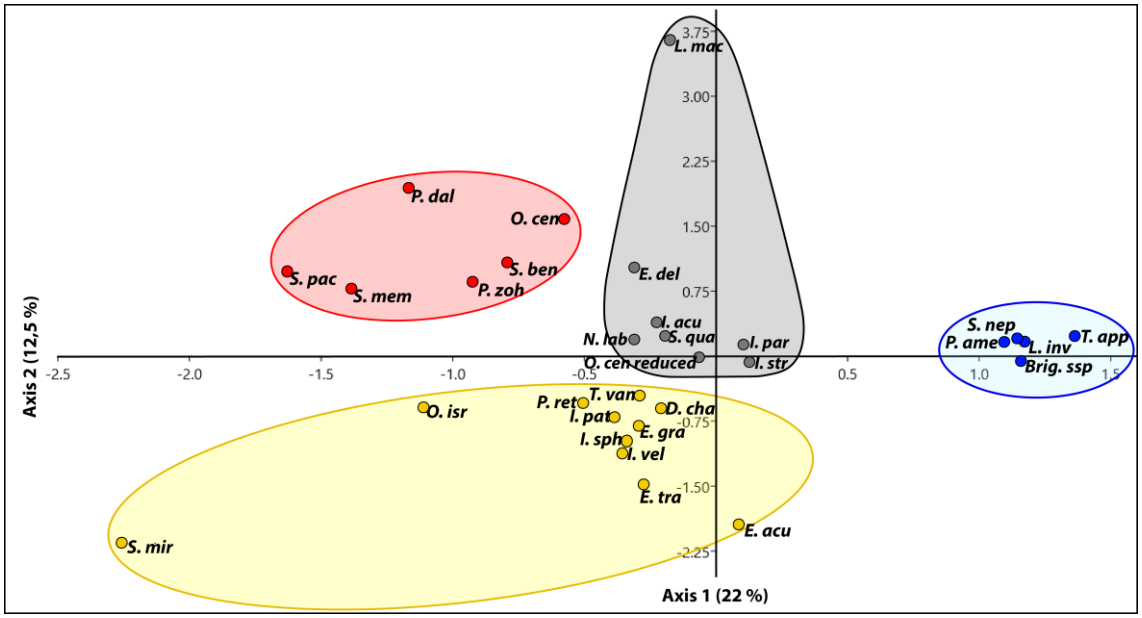

Figure 16: The dinocysts Correspondence Analysis (CA) from the GL-1248 marine core used to infer the ecological affinities. Four different assemblages were defined: 1- Open ocean assemblage was marked with red dots and composed by *Polysphaeridium-zoharyi* (*P. zoh*), *Pentapharsodinium dalei* (*P. dal*), *Operculodinium centrocarpum (O. cen), Spiniferites bentorii (S. ben), Spiniferites membranaceus (S. mem), Spiniferites pachydermus (S. pac);* 2- The neritic assemblage was marked with grey dots and established by *Echinidinium delicatum (E. del), Impagidinium aculeatum (I. acu), Impagidinium paradoxum (I. par), Impagidinium strialatum (I. str), Lingulodinium machaerophorum (L. mac), Nematosphaeropsis labyrinthus (N. lab), Operculodinium centrocarpum reduced processes (O. cen reduced), Selenopemphix quanta (S. qua);* 3- The river outflow assemblage was marked with blue dots and represented by *Brigantedinium spp (Brig. Spp), Leipokatium invisitatum (L. Inv), Protoperidinium americanum (P. ame), Selenopemphix nephroides (S. nep), Trinovantedinium applanatum (T. app);* 4- The nutricline assemblage was marked with yellow dots and defined by *Dalella chathamensis (D. cha), Echinidinium aculeatum (E. acu), Echinidinium granulatum (E. gra), Echinidinium transparantum (E. tra), Impagidinium patulum (I. pat), Impagidinium sphaericum (I. sph), Impagidinium velorum (I. vel), Operculodinium israelianum (O. isr), Pyxidinopsis reticulata (P. ret), Spiniferites mirabilis (S. mir), Tuberculodinium vancampoae (T. van).*

3.4.2 Glacial-Interglacial changes sea surface hydrography in the western equatorial Atlantic

Our results exhibited changes in the prevalence of dinocyst assemblages according to their nutritional requirements over the glacial and interglacial periods, as shown in Figure 4. The open ocean assemblage showed a synchronous variation with RSL changes, with improved relative abundance during the interglacials (Figure 17A and 17B). An opposite pattern was observed for the river outflow assemblage that increased in abundance during the entire glacial period when the RSL was lower compared to interglacials. We interpreted these patterns in the river outflow and open ocean assemblages as a consequence of glacial-interglacial changes in the RSL and

fluvial contribution to the adjacent ocean. The proximity of the coastline to our core site enhanced the contribution of fluvial material, elevating turbidity, and dissolved inorganic nutrients supply in surface waters. Those changes, aligned with the reduced sea surface salinity (SSS), had a significant impact on phytoplankton response (Figure 17B and 17C).

Another relevant aspect of the glacial period was the variability of precipitation over northeastern Brazil. High-latitude thermal changes with large intrusions of freshwater in the North Atlantic, known as Heinrich Stadials (HS), weakened the AMOC and reduced interhemispheric heat transport (Barker *et al*., 2009). The unbalanced distribution of sea surface temperatures over the Atlantic Ocean shifted the ITCZ toward the anomalously warm hemisphere (Broccoli *et al.,* 2006; Mulitza *et al*., 2017). Consequently, northeastern Brazil experienced several wet phases due to the millennial-scale presence of the ITCZ to the south (Wang *et al.*, 2004). The peaks in Ti/Ca ratio recorded in GL-1248 converge with the HS events and can be used as a tracer of fluvial discharge (Govin *et al.*, 2012; Nace *et al.*, 2014). The river outflow assemblage increased in abundance, due to their tolerance of low salinity waters and light limitation (Hardy *et al.*, 2016; Kim *et al.*, 2010; Marret and Zonneveld, 2003; Richerol *et al.*, 2008). The presence of *G. ruber* (*pink*) corroborated Ti/Ca fluctuations due to its affinity for low SSS and warm waters and imprints better response to the precipitation events than to the RSL changes or the increase of turbidity at the sea surface (Schmuker and Schiebel, 2002).

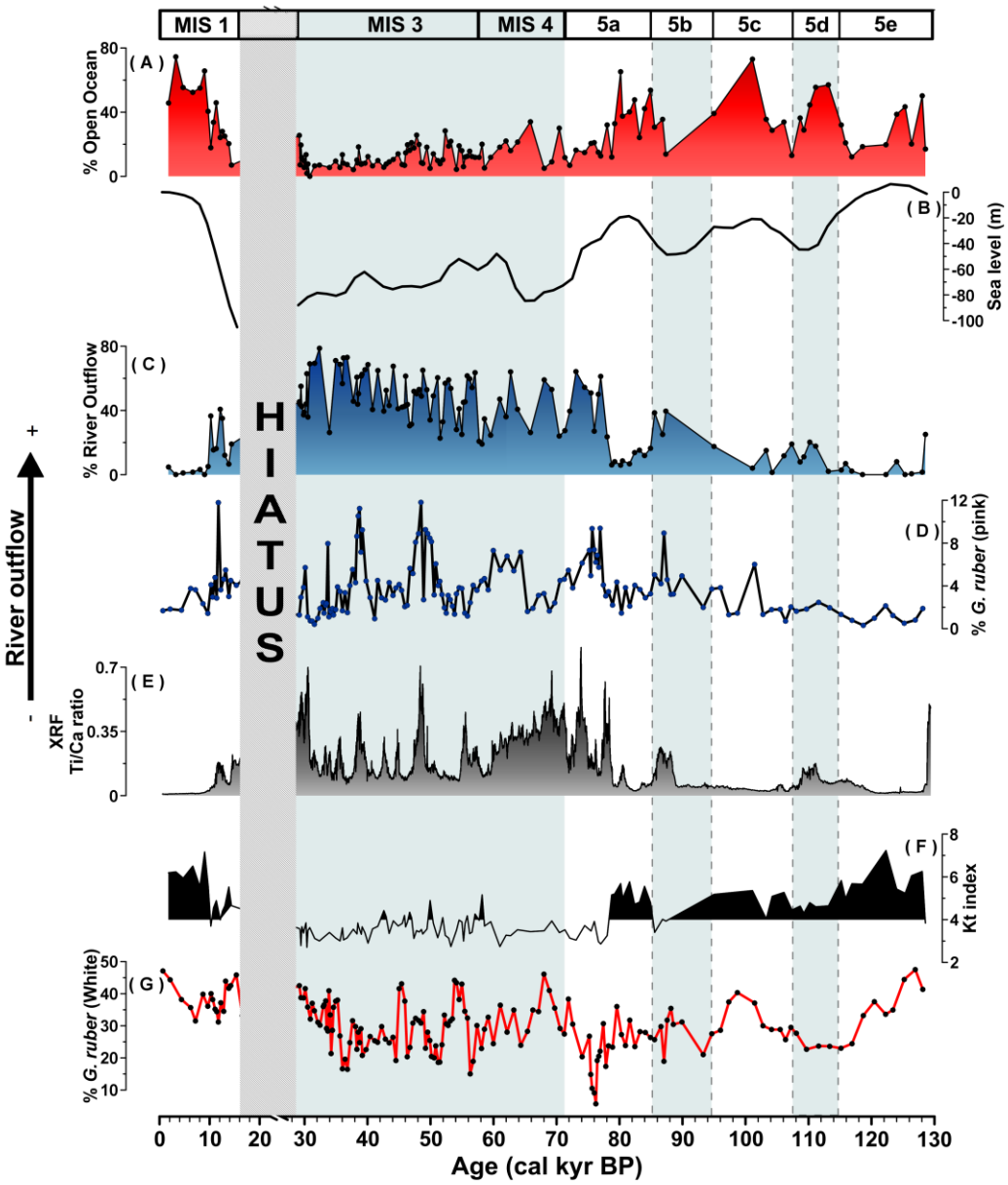

Figure 17: Glacial-interglacial dinocyst assemblages pattern along with the last ~130 kyr. A) Open ocean assemblage relative abundance; B) Relative sea-level curve (Waelbroeck *et al.*, 2002); C) River outflow assemblage relative abundance;D) *G. ruber* (pink) relative abundance; E) X-Ray fluorescence (XRF) Ti/Ca ratio (Venancio *et al.*, 2018); F) kt index – S-cysts degradation index, with values higher than 4 filled in black; G) *G. ruber* (white) relative abundance.

Although the glacial boundary conditions acted in favor of river outflow assemblage, we investigated the preservation of the dinocysts using the kt index (Zonnelveld *et al.*, 2010) (Figure 17F). The kt index exhibited values higher than 4 during interglacials, which suggested that the degradation of S-cysts needs to be taken into consideration due to more oxygenated waters at the surface sediments (Zonneveld *et al.*, 2010). Thus, the response of the river outflow assemblage may be underestimated during the interglacials, since almost half of the river outflow species (*Brigantedinium spp.* and the

P. americanum) are sensitive to oxidative waters as shown in Table 2. Notwithstanding, the low relative abundance of the river outflow assemblage (< 20%) was consistent with the decrease in river freshwater input during interglacials and was corroborated by reduced relative abundances of *G. ruber* (pink) (< 4%) and Ti/Ca ratio values (< 0.2) (Figure 17C, 17D, and 17E). Compared to the glacial period, the RLS was higher in interglacials and may have hampered the influence of fluvial waters on the GL-1248 sediment core-site.

Over the interglacial periods, the RSL was higher, and the coastal contribution was narrowed. The open ocean assemblage prevailed over the interglacial periods, and this assemblage is composed of autotrophs dinocysts with low demand for nutrients (Vink *et al.*, 2000; Bouimetarhan *et al.*, 2009). We also applied the *G.ruber* (white) relative abundance as an indicator of warm and oligotrophic conditions in the water column (Kucera, 2007). Changes in the *G.ruber* (white) values were consistent with the general trend of the open ocean assemblage over the interglacials. During the glacial period, both proxies didn't correlate, as the *G. ruber* (white) relative abundance didn't show a pattern similar to the oscillation of RSL (Figure 17G, 17A, and 17B), and probably varied according to changes in sea surface temperature (SST).

3.4.3 Oscillations of autotrophic assemblages over interglacials

The relative abundance of open ocean assemblage and *G. ruber* (white) transpassed 35% during the MIS 1 and over most of the warm intervals of MIS 5 (Figure 18A and 18B). Despite divergences over the MIS 5d, both proxies indicated the prevalence of warm, saline, and oligotrophic tropical waters at the sea surface during the interglacials. In contrast, the predominant assemblages of dinocysts presented an intermittent behavior and oscillated between open ocean and nutricline over the MIS5. Autotrophs dinocysts denoted the same nutritional strategy. Still, the nutricline and open ocean assemblages differed by their requirements of nutrient concentration (see Table S2). It is noteworthy that the nutricline assemblage improved its relative abundance (> 60%) during the warm substage MIS 5e (Figure 18C) with particular highlight to the specie *S. mirabilis* (Figure S17). The asynchrony between nutricline and the open ocean assemblage indicated oscillations in the concentration of the nutrients in the water column. The high RLS characteristic of interglacials followed by low Ti/Ca values (< 0.2), used as a proxy of the continental source (Figure 18D), led us to consider a different source of nutrients. Thus, these nutrients might come from more enriched water masses such as the SACW located below the thermocline. Other local studies also suggested more availability of nutrients during the warm substages of MIS 5 (Rühlemann *et al.*, 1996; Mulitza *et al.*, 1998; Vink *et al.*, 2002).

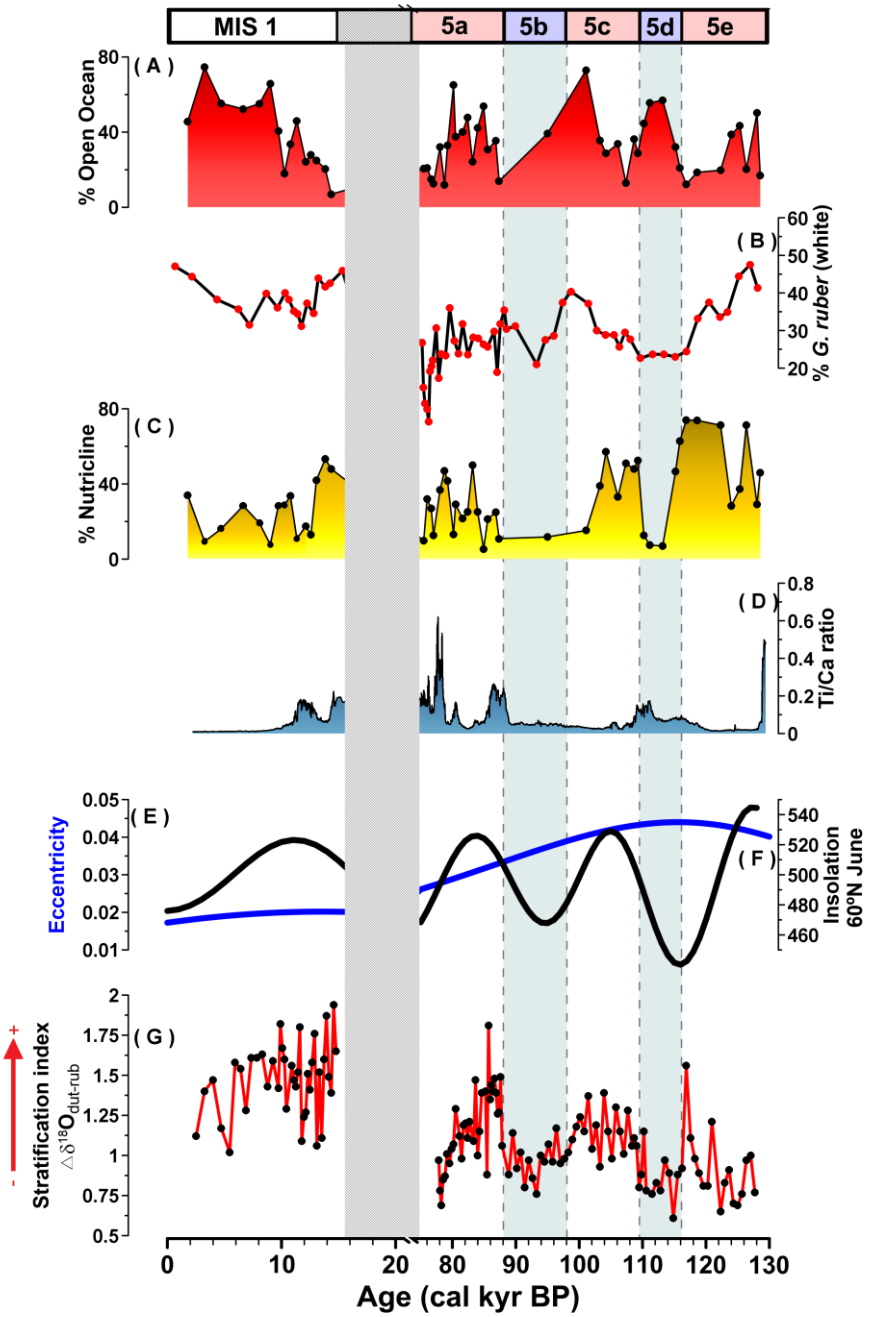

Figure 18: Comparisons between interglacials. A) The relative abundance of open ocean assemblage; B) The relative abundance of *G. ruber* (white); C) The relative abundance of nutricline assemblage; D) XRF Ti/Ca ratio (Venancio *et al.*, 2018); E) Orbital eccentricity oscillation; F) Insolation of June at 60˚N; G) Stratification index $\Delta\delta^{18}O_{dut\text{-}rub}$ (Venancio *et al.*, 2018).

The MIS 5e was considered an analog to pre-industrial temperature with similar atmospheric CO_2 concentration, but with distinct orbital conditions and reduced north pole ice cap coverage (Dutton *et al.*, 2015). Venancio *et al.* (2018) showed changes in upper ocean stratification in high-resolution for the record of GL-1248 marine sediment core. A thermal stratification index was constructed based on planktonic foraminifera

with distinct ecological distribution in the water column and applied to reconstruct variations on the thermocline depth according to the trade wind system. We suggested that the discrepancies in orbital eccentricity and insolation between MIS 5e and MIS1 (Figure 18E and 18F) led to differences in trade winds system intensity. Possibly the decrease of the meridional temperature gradient over the Atlantic Ocean during the warm substages of the last interglacial may have provoked less intense trade winds over the equatorial Atlantic Ocean. Weakened zonal winds potentially attenuated the accumulation of warm surface waters in western tropical Atlantic, enabling the intrusion of SACW nutrients in the photic zone. The minimal stratification corroborated with our suggestion of enhanced availability of nutrients over the MIS 5e when compared with MIS 1 (Figure 18G). Another evidence for the relevance of trade winds to reduced stratification of thermocline at the western equatorial Atlantic during the warm periods of MIS 5 interglacials was the in-phase response of GL-1248 nutricline assemblage with the *F. profunda* high abundance in the RC24-7 marine sediment core (1'20.5'S, 11'53.3'W), a coccolithophorid species associated with a deep nutricline at the eastern equatorial Atlantic (Molfino and McIntyre, 1990). Both proxies indicate that SE trade winds and SEC transport were reduced during the perihelion in June, boreal summer. Reduced transport of warm waters to the western portion of the equatorial Atlantic, consequently attenuated the piled up of water masses and triggered the proposed mechanisms. Vink *et al.* (2002) had already suggested weak trade winds as a possible mechanism that led to a shallower thermocline in the western equatorial Atlantic region.

3.4.4 Millennial-scale changes in productivity in the western equatorial Atlantic

The river outflow assemblage showed millennial-scale changes through the last glacial. The increase in the relative abundance of river outflow assemblage was linked to changes in the relative abundance of *Brigantedinium spp.* Between 65 and 30 kyr, the observed changes in river outflow assemblage seemed to match with HS4, HS5, HS5A (Figure 19A and 19B). The input of freshwaters by continental contribution increased during the last glacial with maxima during HS millennial-scale events (Govin *et al.*, 2012; Nace *et al.*, 2014). The study of Zhang *et al.* (2015) using neodymium (Nd) isotopic compositions of marine sediment cores GeoB 16224-1 and GeoB 16206-1 showed no Amazon river contribution to our study area during HS1 (period of reduced AMOC transport). Based on these findings, we assumed that the Parnaiba river was the main continental source during HS events.

Despite the match between the river outflow assemblage and HS events, no significant improvement was observed during the HS6 and HS3. For HS6, the river

outflow assemblage displayed a gradual decrease within the event, similar to the Ti/Ca ratio (Figure 19A and 19B), indicating a fluvial sediment retrenchment. In the continental part, the vegetation reflects the precipitation pattern. The millennial-scale precipitation events in northeastern Brazil was possibly the main driver of changes in vegetation structure. The increment of vegetation in the vicinity of the Parnaiba hydrographic basin might have promoted the soil stability, reducing the weathering (Dupont *et al.,* 2010; Bouimetarhan *et al.,* 2018). Prolonged wet periods probably induced the growth of trees and shrubs, which might have reduced the suspended material in the river plume. Low salinity sea surface and more light penetration benefit the widespread of neritic species (Figure 19C), as the pronounced increase of *Lingulodinium machaerophorum* (Figure S17) by the end of H6 indicated. For HS3, although there was a high relative abundance of river outflow assemblage (~80-70%) within the event, it was not synchronous with significant Ti/Ca fluctuations. The mismatch of results is not apparent. Still, we suggest that it may have occurred due to competition between species of the river outflow and nutricline assemblages as a consequence of the low sea level over the shallow continental shelf, harming the dominance of the river outflow assemblage (Figure 19B and 19E).

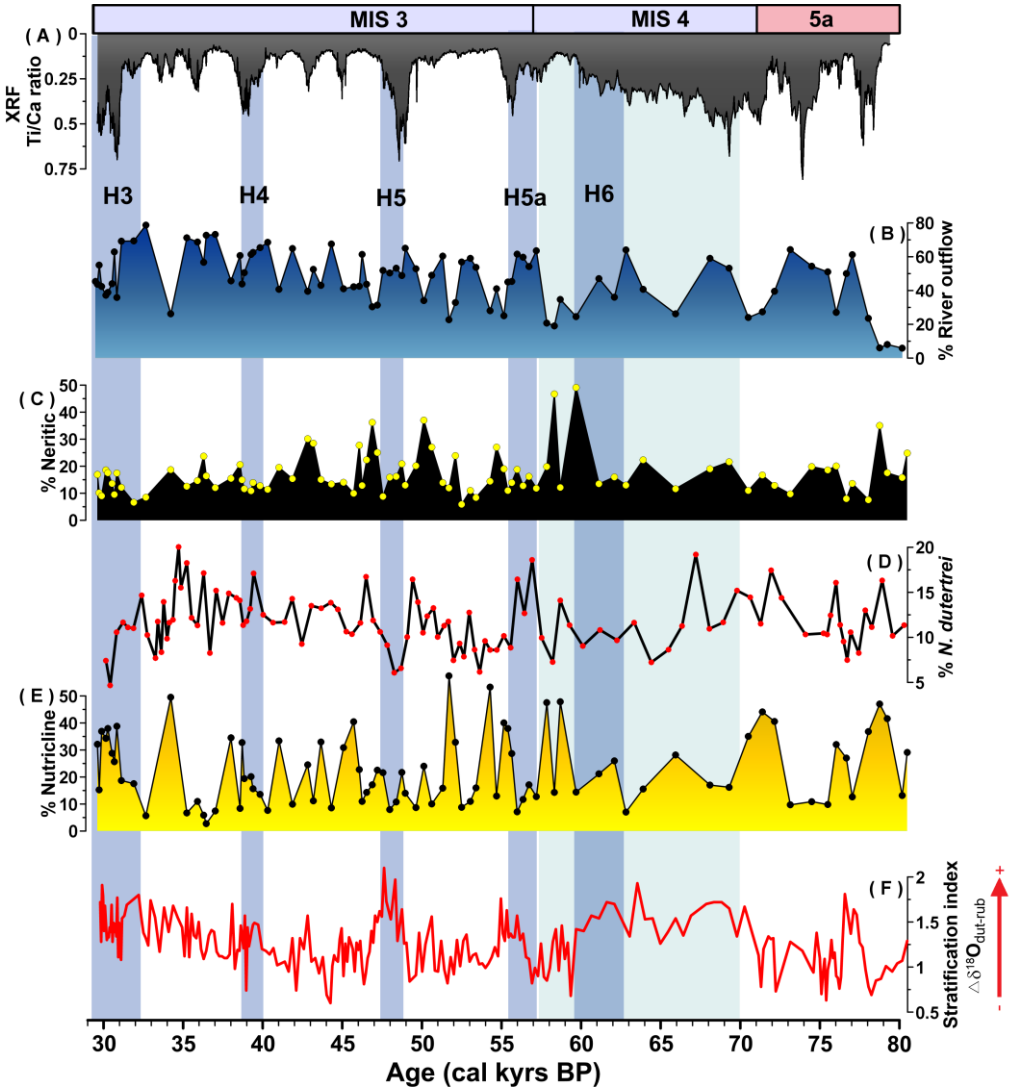

Figure 19: Millennial-scale variations in dinocyst assemblages between MIS 5a and MIS 3. A) XRF Ti/Ca ratio (Venancio *et al.*, 2018); B) Relative abundance of the river outflow assemblage; C) Relative abundance of the neritic assemblage; D) Relative abundance of *N. dutertrei*; E) Relative abundance of the nutricline assemblage; F) Stratification index $\Delta\delta^{18}O_{dut\text{-}rub}$ (Venancio *et al.*, 2018).

Modern ecological studies show that the phytoplankton size-structure might change due to variations in the nutrient source, increasing the grazing (Cuevas *et al.*, 2019). A robust input of freshwater in the adjacent ocean was possibly coupled with large amounts of dissolved inorganic nutrients, and enhanced turbulence at the sea surface creates perfect conditions to improve the primary productivity by diatoms (Smayda and Reynolds, 2001). Heterotrophs dinoflagellates are diatoms' predators and can be interpreted as an indirect primary productivity proxy. The pronounced increase of heterotrophs dinocysts over the glacial was given by the combination of more tolerance to low salinity water and light restriction. Still, another possible factor that enabled food

for heterotrophic dinocysts was the shift in the phytoplankton community (Jeong *et al*., 2004).

Even in the absence of diatoms information for the record, we may not assume low productivity over the glacial period. The specie *N. dutertrei* is endemic of the western equatorial Atlantic, known as a tracer of higher productivity, and already used to infer the vertical mixing over the glacial period (Portilho-Ramos *et al*., 2017; Cléroux *et al.*, 2013). The *N. dutertrei* feed on phytoplankton without preferences and can be viewed as an intermediate indicator between the response of the river outflow and nutricline assemblage. Despite that, other environmental features beyond productivity could be imprinted in *N. dutertrei* response, such as temperature changes and open ocean conditions. The mechanisms leading the nutricline assemblage pattern over the glacial were not evident, and changes in the relative abundances of *N. dutertrei* didn't follow the same trend of the nutricline assemblage (Figure 19D and 19E).

Despite the predominance of heterotrophic dinocysts during the glacial, the H/A ratio oscillates in the early MIS 3 (~60-45 kyr BP). The H/A ratio fluctuation indicates changes in the nutrient source in millennial-scale variability. The reductions in the nutricline assemblage during HS, except HS3, suggest that dinoflagellate productivity was low during these events. In contrast, the nutricline assemblage had improved its relative abundance (> 30%) post-HS events (H6, H5a, and H4), characterized by more potent trade winds. Portilho-Ramos *et al*. (2017) suggested that ITCZ displacements strengthened the trade winds system and promoted more wind-driven vertical mixing. The stratification index values oscillated between 0.75 and 2.0 over the glacial period (Venancio *et al.,* 2018). The peaks in the relative abundance of the nutricline assemblage might be explained by coupling more wind-driven vertical mixing post-HS events and with values that indicate a shallower thermocline (Figure 19F). Possibly more vigorous SE trade winds increased the mix-wind driven the water column and provided an increased amount of nutrients in the photic zone post-HS events. In general, our proxies pointed to a more productive glacial period than previously considered for the region (Rühlemann *et al.*, 1996; Bickert *et al.*, 1997; Mulitza *et al.*, 1998).

3.5 Conclusions

We investigated the hydrography and productivity changes in an oligotroph region over distinct past climatic backgrounds. The dinocyst assemblages showed to be sensitive to different nutrient sources and ocean-atmosphere processes. The autotrophic taxa prevailed during the interglacials, and heterotrophic taxa were more abundant over the glacial period. Singularities in dinoflagellate assemblages were observed between interglacial periods (Holocene and MIS 5e). The particular orbital features of each interglacial period created different thermal gradients throughout the Atlantic ocean and altered the trade winds' intensity between them. Two autotrophic dinocyst assemblages with distinct nutrient requirements (open ocean and nutricline) interchanged the predominance over the Holocene and MIS 5e. The antiphase between the open ocean and nutricline assemblages denoted mainly fluctuations in the availability of nutrients in the photic zone. The significant increase in the relative abundance of nutricline assemblage during the MIS 5e suggested a more productive period than MIS1. Attenuated trade winds during MIS 5e might have promoted the relaxation of thermocline stratification at western equatorial Atlantic, facilitating nutrient diffusion in the photic zone.

During the last glacial period, the enhanced gradient of temperature over the Atlantic ocean compressed climatic zones towards the equator, driving more vigorous trade winds. The displacements of ITCZ were accompanied by the reduction of Parnaíba river discharge and the intensification of SE trade winds, which enabled the northward transport of warmer sea surface waters. The strengthened of SE trade winds promoted enhanced wind-driven vertical mixing in the ocean surface and a shallower thermocline, indicated by low values of the stratification index (< 1). The ITCZ shifts probably improved the relative abundance of nutricline assemblage post-HS events, as more nutrients were available in the photic zone. The HS events were marked by the continued presence of the ITCZ over northeastern Brazil, and followed by a substantial fluvial input to the adjacent ocean. The intensified runoff might have increased the turbidity and turbulence on the sea surface. We suggest that the autotrophic phytoplankton community shifted preferentially from dinoflagellates to diatoms. Still, the heterotrophic dinocysts were benefited over the glacial period by the presence of diatoms, increased turbidity, and low salinity. The pronounced wet periods might have altered the structure of continental vegetation, with more trees and shrubs. The enhanced soil stability possibly reduced the river plume turbidity and benefited the neritic assemblage by the end of HS6. We created conceptual models of environmental processes during past intervals, as previously described in our discussions (Figure 20).

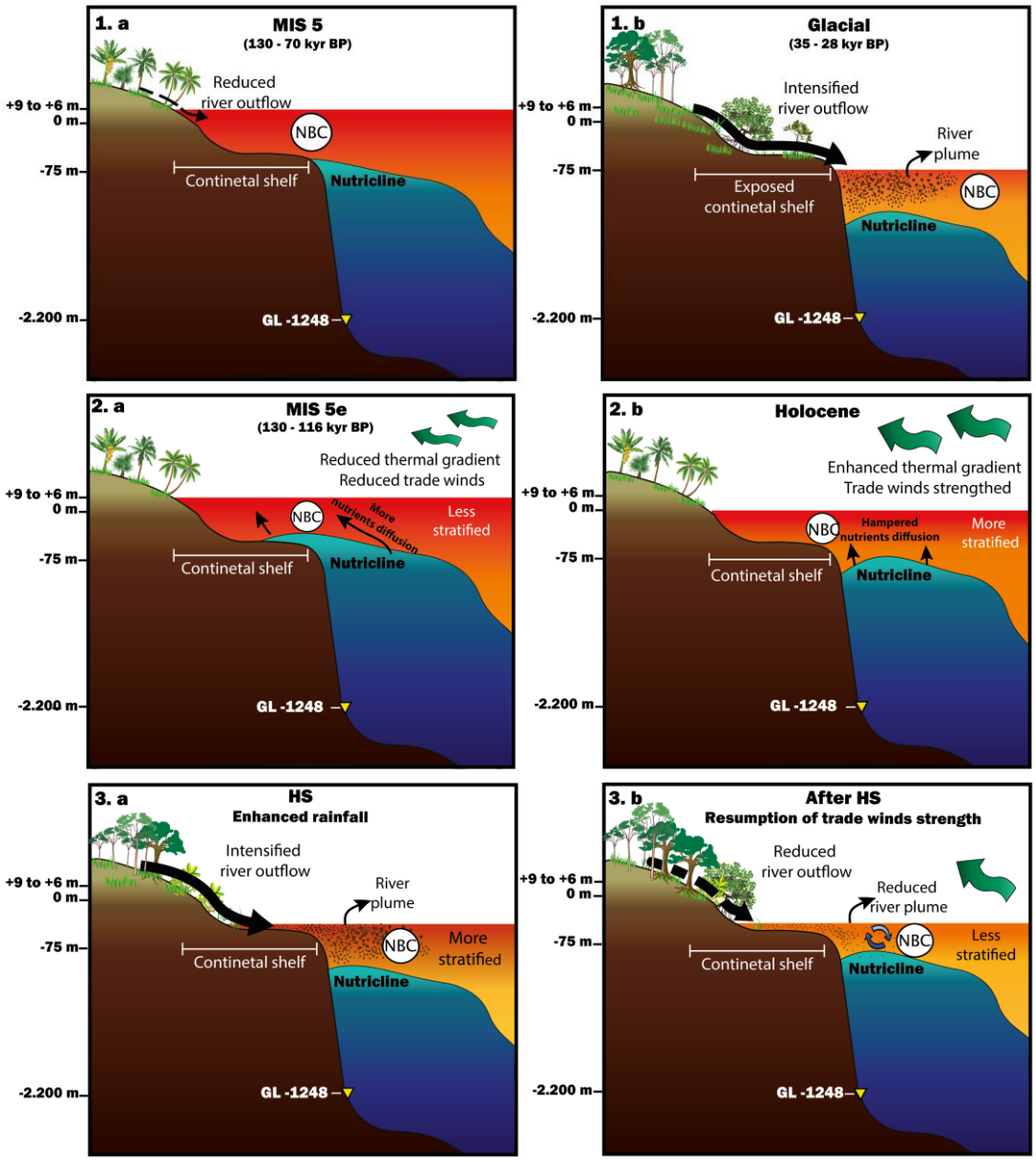

Figure 20: The conceptual model with the main environmental forces acting on three different scenarios: 1) Comparisons between MIS 5 and the last glacial hydrography, with sea-level and continental contribution discrepancies, and the NBC proximity to the continental shelf; 2) Comparisons between interglacials, with singular differences in trade winds intensity and nutrient diffusion in the photic zone; 3) Comparisons between HS and post-HS, with changes in river outflow, river plume, vegetation, and trade winds intensity. The blue arrows indicate the vertical mixing occurring in the water column. The size of the arrows is a reference to the quantity of the proposed processes. The gradient of colors in the ocean (red to orange), also represents the thermal stratification.

3.6 REFERENCES:

BENNINGHOFF, W. S. Calculation of pollen and spores density in sediments by the addition of exotic pollen in known quantities. **Pollen et Spores.** 4 (2), 332-333. 1962.

BICKERT, T., CURRY, W. B, WEFER, G. Late Pliocene to Holocene (2.6-0 Ma)

western equatorial Atlantic deep-water circulation: Inferences from benthic stable isotopes, **in Proc. ODP, Science Results.** 154, Ocean Drilling Program, College Station, TX., 239-254. 1997.

BLAAUW, M. Methods and code for 'classical' age-modeling of radiocarbon sequences. **Quaternary Geochronology.** 5 (5), 12-518. 2010.

BOYER, T.P., ANTONOV, J. I., BARANOVA, O. K., COLEMAN, C. H., GARCIA, E., GRODSKY, A., JOHNSON, D. R ., LOCARNINI, R. A. MISHONOV, A. V., O'BRIEN, T.D., PAVER, C.R., REAGAN, J.R., SEIDOV, D., SMOLYAR, I. V, AND ZWENG, M. M. World Ocean Database 2013, **NOAA Atlas NESDIS 72**, S. Levitus, Ed., A. Mishonov, Technical Ed.; Silver Spring, MD, 209 pp., http://doi.org/10.7289/V5NZ85MT. 2013.

BOUIMETARHAN, I., MARRET, F., DUPONT, L., ZONNEVELD, K. Dinoflagellate cyst distribution in marine surface sediments off West Africa (17-6°N) in relation to sea-surface conditions, freshwater input and seasonal coastal upwelling. **Marine Micropaleontology.** 2009.

BOUIMETARHAN, I., CHIESSI, C. M., GONZALEZ-ARANGO, C., DUPONT, L., VOIGT, I., PRANGE, M., AND ZONNEVELD, K. Intermittent development of forest corridors in northeastern Brazil during the last deglaciation: Climatic and ecologic evidence. **Quaternary Science Reviews.** 192, 86-96, 2018.

CLÉROUX, C., DEMENOCAL, P., ARBUSZEWSKI, J., AND LINSLEY, B. 2013. Reconstructing the upper water column thermal structure in the Atlantic Ocean, **Paleoceanography**, 28, 503–516.

CUEVAS, L. A., TAPIA, FJ, IRIARTE, J. L., GONZÁLEZ, H. E., SILVA, N., VARGAS, C. A. The interplay between freshwater discharge and oceanic waters modulates phytoplankton size-structure in fjords and channel systems of the Chilean Patagonia. **Progress in Oceanography.** 173, 103–113. 2019.

DALE, B. Dinoflagellate cyst ecology: modeling and geological applications. In: Jansonius, J., McGregor, D.G.(Eds.), **Palynology: Principles and Applications.** AASP Found. 3, 1249-1275 1996.

DA COSTA PORTILHO-RAMOS, R., BARBOSA, C. F., & RIOS-NETTO, A. M. Planktonic foraminiferal variations in the southwestern Atlantic since the last glacial–interglacial cycle. **Palaios.** 29 (1), 38-44. 2014.

DE SCHEPPER, S., FISCHER, E. I., GROENEVELD, J., HEAD, M. J., MATTHIESSEN, J. Deciphering the palaeoecology of Late Pliocene and Early Pleistocene dinoflagellate cysts. **Palaeogeography, Palaeoclimatology, Palaeoecology.** 309 (1-2), 17–32. 2011.

DE OLIVEIRA PE, BARRETO AMF, SUGUIO. K. Late Pleistocene/Holocene climatic and vegetational history of the Brazilian caatinga: the fossil dunes of the middle Sao Francisco River. **Palaeoegeography, Palaeoclimatology, Palaeoecology**, 152, 319–337. 1999.

DUPONT, L. M., SCHLÜTZ, F., EWAH, C. T., JENNERJAHN, T. C., PAUL, A., BEHLING, H. Two-step vegetation response to enhanced precipitation in Northeast Brazil during Heinrich event 1. **Global Change Biology.** 2010.

ELLEGAARD, M. Variations in dinoflagellate cyst morphology under conditions of changing salinity during the last 2000 years in the Limfjord, Denmark. **Review of Palaeobotany and Palynology.** 109 (1), 65–81. 2000.

ESPER, O.; ZONNEVELD, K. A. F.; MARRET, F. Relative abundance of dinoflagellate cysts in surface sediments and dinoflagellate counts from three sediment cores from the Atlantic sector of the Southern Ocean. **PANGAEA**. 2007.

FAEGRI K., IVERSEN J. **Textbook of Pollen Analysis**. 4th ed. (revised by K Faegri, PE Kyrland, K Krzywinski), John Wiley and Sons, Chichester, 328. 1989.

FERREIRA, F., FRONTALINI, F., LEÃO, C. J., AND LEIPNITZ, I. I. Changes in the water column structure and paleoproductivity in the western South Atlantic Ocean since the middle Pleistocene: Evidence from benthic and planktonic foraminifera. **Quaternary International.** 352, 111-123. 2014.

GAINES, G. ELBRACHTER, M. Heterotrophic nutrition. In: Taylor, F. J. R. (ed.) **The biology of dinoflagellates.** Blackwell, Oxford, 224-268. 1987.

GOVIN, A., HOLZWARTH, U., HESLOP, D., FORD KEELING, L., ZABEL, M., MULITZA, S., COLLINS, J. A., CHIESSI, CM Distribution of major elements in Atlantic surface sediments (36°N-49°S): Imprint of terrigenous input and continental weathering. **Geochemistry, Geophysics, Geosystems.** 13, 1–23. 2012.

GU, F., ZONNEVELD, K. A. F., CHIESSI, C. M., ARZ, H. W., JÜRGEN, P., BEHLING, H. Long-term vegetation, climate and ocean dynamics inferred from a 73, 500 years old marine sediment core (GeoB2107-3) off southern Brazil. **Quaternary Science Reviews.** 172, 55-71. 2017.

HARDY, W., PENAUD, A., MARRET, F., BAYON, G., MARSSET, T., DROZ, L. Dinocyst assemblage constraints on oceanographic and atmospheric processes in the eastern equatorial Atlantic over the last 44 kyr. **Biogeosciences.** 13, 4823–4841. 2016.

HAMMER, Ø., HARPER, D. A. T., AND RYAN, P. D. PAST: Paleontological Statistics Software Packyrge for Education and Data Analysis. **Palaeontologia**

Electronica. 4 (1): 9pp. 2001.

HASTENRATH, S. Exploring the climate problems of Brazil's Nordeste: a review, **Climatic Change**, Springer, 112 (2), p. 243-251, 2012.

HERBLAND A., VOITURIEZ B. Hydrological structure analysis for estimating the primary production in the tropical Atlantic Ocean. J**ournal of Marine Research**, 37 (1), 87-101. 1979.

JEONG H. J., YOO Y. D., KIM S. T., KANG N. S. Feeding by the heterotrophic dinoflagellate Protoperidinium bipes on the diatom Skeletonema costatum. **Aquatic Microbial Ecology** 36: 171–179. 2004.

LEROUX, M., The Mobile Polar High: A new concept explaining present mechanisms of meridional air-mass and energy exchanges and global propagation of paleoclimatic changes, **Global Planetary Change**, 7, 69-93. 1993.

JOHNS, W. E., LEE, T. N., BEARDSLEY, R. C., CANDELA, J., LIMEBURNER, R., CASTRO B. Annual cycle and variability of the North Brazil Current. **Journal of Physical Oceanography.** 28 (1), 103–128. 1998.

JONGMAN, R. H. G., C. J. F. TER BRAAK, AND O. F. R. VAN TONGEREN, editors. **Data Analysis in Community and Landscape Ecology**. Pudoc, Wageningen, The Netherlands. 1987.

KENNETT, J. P., SRINIVASAN, M. **Neogene Planktonic Foraminifera: A Phylogenetic Atlas**. Hutchinson Ross, Stroudsburg 273. 1983.

KIM, S., SCOURSE, J., MARRET, F., LIM, D. A 26,000-year integrated record of marine and terrestrial environmental change off Gabon, west equatorial Africa. **Palaeogeography, Palaeoclimatology, Palaeoecology.** 297, 428–438. 2010.

KUCERA, M. **Planktonic foraminifera as tracers of past oceanic environments.** In: Claude, H. M., Anne De, V. (Eds.), Developments in Marine Geology: Proxies in Late Cenozoic **Paleoceanography**. Elsevier, Montreal, 213–262. 2007.

KRAUSS, W. The warm water sphere of the North Atlantic Ocean, **Gebruder Borntraeger**, 466. 1996

KRUEGER, A., MURPHY, M., GILBERT, E., BURKE, K. Deposition and deformation in the deepwater sediment of the offshore Barreirinhas Basin, Brazil. **Geosphere.** 1–26. 2012.

LISIECKI, L. E., AND RAYMO, M. E. A Pliocene-Pleistocene stack of 57 globally distributed benthic δ18O records. **Paleoceanography.** 20. 2005.

LOEBLICH, A., TAPPAN, H. Foraminiferal Genera and Their Classification. 2. **van Nostrand Reinhold Company Publisher**. 1–212. 1988.

MALLIN, M. A., PAERL, H. W., RUDEK, J., BATES, P. W. Regulation of estuarine

primary production by watershed rainfall and river flow. **Marine Ecology Progress.** Series 93:199-203. 1993.

MARRET, F., ZONNEVELD, K. A. F. Atlas of modern organic-walled dinoflagellate cyst distribution. **Review of Palaeobotany and Palynology.** 125, 1–200. 2003.

MOLFINO, B. AND MCINTYRE, A. Precession Forcing of Nutricline Dynamics in the Equatorial Atlantic. **Science**, 249, 766-769. 1990.

MOHRIAK, W. U. Sedimentary Basins of the Brazilian Continental Margin, in: L. A. Bizzi, C. Schobbenhaus, R.M.V. e J.H.G. (Ed.), **Geologia, Tectônica e Recursos Minerais Do Brasil: Texto, Mapas & SIG.** Brasília, 87–94. 2003.

MULITZA, S., CHIESSI, C. M., SCHEFUß, E., LIPPOLD, J., WICHMANN, D., ANTZ, B., MACKENSEN, A., PAUL, A., PRANGE, M., REHFELD, K., WERNER, M., BICKERT, T., FRANK, N., KUHNERT, H., LYNCH-STIEGLITZ, J., PORTILHO-RAMOS, R. C., SAWAKUCHI, A. O., SCHULZ, M., SCHWENK, T., TIEDEMANN, R., VAHLENKYRMP, M., ZHANG, Y. Synchronous and proportional deglacial changes in Atlantic meridional overturning and northeast Brazilian precipitation. **Paleoceanography.** 2017.

MULITZA, S., RÜHLEMANN, C., BICKERT, T., HALE, W. Late Quaternary $\delta^{13}C$ gradients and carbonate accumulation in the western equatorial Atlantic. **Earth and Planetary Science Letters.** 155, 237–249. 1998.

NACE, T. E., BAKER, P. A., DWYER, G. S., SILVA, C. G., RIGSBY, C. A., BURNS, S. J., GIOSAN, L., OTTO-BLIESNER, B., LIU, Z., ZHU, J. The role of North Brazil Current transport in the paleoclimate of the Brazilian Nordeste margin and paleoceanography of the western tropical Atlantic during the late Quaternary. **Palaeogeography Palaeoclimatology Palaeoecology.** 415, 3–13. 2014.

NETO, A. V. N., DA SILVA, A. C. Seawater temperature changes associated with the North Brazil current dynamics. **Ocean Dynamics.** 64 (1), 13–27. 2013.

PARKIN, D. W. Trade-winds during the glacial cycles. **Proceedings of the Royal Society of London**, Series A 337,73-100. 1974.

PETERSON, R. G., STRAMMA, L. Upper-level circulation in the South Atlantic. **Progress in Oceanography.** 26, 1–73. 1991.

PETRÓ, S. M., PIVEL, M. A. G. COIMBRA, J. C. Paleoceanographic changes through the last 130 kyr in the Western South Atlantic based on planktonic foraminifera. **Revista Brasileira de Paleontologia.** 19(1), 3-14. 2016.

PORTILHO-RAMOS, R. C., CHIESSI, C. M., ZHANG, Y., MU, S., KUCERA, M., SICCHA, M., PRANGE, M., PAUL, A. Coupling of equatorial Atlantic surface stratification to glacial shifts in the tropical rain belt. **Nature Science.** Reports 1–8.

2017.

POSPELOVA, V., KIM, S.-J. Dinoflagellate cysts in recent estuarine sediments from aquaculture sites of southern South Korea. **Marine Micropaleontology.** 76, 37-51. 2010.

PRICE, A. M., POSPELOVA, V., COFFIN, M. R. S., LATIMER, J. S., CHMURA, G. L. Biogeography of dinoflagellate cysts in northwest Atlantic estuaries. **Ecology and Evolution.** 6(16), 5648-5662. 2016.

REIMER, P. J., BARD, E., BAYLISS, A., BECK, J. W., BLACKWELL, P. G., RAMSEY, C. B., BUCK, CE, CHENG, H., EDWARDS, R. L., FRIEDRICH, M., GROOTES, P. M., GUILDERSON, T. P., HAFLIDASON, H., HAJDAS, I., HATTÉ, C., HEATON, T. J., HOFFMANN, D. L., HOGG, A. G., HUGHEN, K. A., KAISER, K. F., KROMER, B., MANNING, SW, NIU, M., REIMER, RW, RICHARDS, DA, SCOTT, EM SOUTHON, JR, STAFF, RA, TURNEY, C. S. M., VAN DER PLICHT, J. IntCal13 and Marine13 radiocarbon age calibration curves 0–50,000 years cal BP. **Radiocarbon.** 55m (04), 1869–1887. 2013.

RICHEROL, T., ROCHON, A., BLASCO, S., SCOTT, D. B., SCHELL, T. M., BENNETT, R. J. Distribution of dinoflagellate cysts in surface sediments of the Mackenzie Shelf and Amundsen Gulf, Beaufort Sea (Canada). **Journal of Marine Research.** 74, 825-839. 2008.

RÜHLEMANN, C.; FRANK., M.; HALE, W.; MANGINI, A.; MULITZA, S.; MULLER, P. J.; WEFER, G. Late Quaternary productivity changes in the western equatorial Atlantic: Evidence from 230Th-normalized carbonate and organic carbon accumulation rates. **Marine Geology.** 135 (1-4), 127-152. 1996.

SCHULZ, M., & MUDELSEE, M. REDFIT: Estimating red-noise spectra directly from unevenly spaced paleoclimatic time series. **Computers and Geosciences**, 28(3), 421–426. 2002.

SCHMUKER, B., & SCHIEBEL, R. Planktic foraminifers and hydrography of the eastern and northern Caribbean Sea. **Marine Micropaleontology.** 46 (3-4), 387–403. 2002.

SCHOTT, F. A., STRAMMA, L., FISCHER, J. The warm water inflow into the western tropical Atlantic boundary regime, spring 1994. **Journal of Geophysical Research.** 100, 24745—24760. 1995.

SIGMAN, D. M. AND HAIN, M. P. The Biological Productivity of the Ocean. **Nature Education Knowledge**. 3 (10):21. 2012.

SMAYDA, T. J., AND REYNOLDS, C. S. 2001. Community assembly in marine phytoplankton: Application of recent models to harmful dinoflagellate blooms.

Journal of Plankton Research. 23: 447–461

STOCKMARR, J. Tablets with spores used in absolute pollen analysis. **Pollen et Spores.** 13: 615-621. 1971.

STRAMMA, L., FISCHER, J., REPPIN, J. The North Brazil Undercurrent. **Deep-Sea Research Part I**, 42 (5), 773–795. 1995.

STRAMMA, L., AND MATTHEW, E. On the water masses and mean circulation of the South Atlantic Ocean. **Journal of Geophysical Research: Oceans** 104.C9: 20863-20883. 1999.

TAYLOR F. J. R. General group characteristics, special features of interest, and a short history of dinoflagellate study. In: Taylor FJR (ed) The biology of dinoflagellates. **Botanical Monographs.** 21:1-23. 1987.

TAYLOR, F. J. R., HOPPENRATH, M., SALDARRIAGA, J. F. Dinoflagellate diversity and distribution. **Topics in Biodiversity and Conservation.** 173-184. 2008.

TER BRAAK, C. J. F., AND I. C. PRENTICE. **A theory of gradient analysis. Advances in Ecological Research**. 18:271-313. 1988.

TOLEDO, F. A., COSTA, K. B., PIVEL, M. A., CAMPOS, E. J. Tracing past circulation changes in the western South Atlantic based on planktonic foraminifera. **Revista Brasileira de Paleontologia**. 11 (3), 169-178. 2008.

VENANCIO, I. M., MULITZA, S., GOVIN, A., SANTOS, T. P., LESSA, D. O., ALBUQUERQUE, A. L. S., CHIESSI, CM, TIEDEMANN, R., VAHLENKAMP, M., BITCKET, T., SCHULZ, M. Millennial- to orbital-scale responses of western equatorial Atlantic thermocline depth to changes in the trade wind system since the Last Interglacial. **Paleoceanography and Paleoclimatology.** 2018.

VERLEYE, T., MERTENS, K., YOUNG, M. D., DALE, B., MCMINN, A., SCOTT, L. ZONNEVELD, K. A. F., LOUWYE, S. "Average Process Length Variation of the Marine Dinoflagellate Cyst Operculodinium Centrocarpum in the Tropical and Southern Hemisphere Oceans: Assessing Its Potential as a Palaeosalinity Proxy." **Marine Micropaleontology.** 86-87: 45–58. 2012.

VINK, A., ZONNEVELD, K. A. F., WILLEMS, H. Organic-walled dinoflagellate cysts in western equatorial Atlantic surface sediments: Distributions and their relation to environment. **Review of Palaeobotany and Palynology.** 112, 247–286. 2000.

VINK, A., BRUNE, A., HÖLL, C., ZONNEVELD, K. A. F., WILLEMS, H. On the response of calcareous dinoflagellates to oligotrophy and stratification of the upper water column in the equatorial Atlantic Ocean. **Palaeogeography Palaeoclimatology Palaeoecology.** 178, 53–66. 2002.

WAELBROECK, C., LABEYRIE, L., MICHEL, E., DUPLESSY, J. C., MCMANUS, J. F.,

LAMBECK, K., LABRACHERIE, M. Sea-level and deep water temperature changes derived from benthic foraminifera isotopic records. **Quaternary Science Reviews.** 21 (1–3), 295–305. 2002.

WANG, X., AULER, A. S., EDWARDS, R. L., CHENG, H. Wet periods in northeastern Brazil over the past 210 kyr linked to distant Wet periods in northeastern Brazil over the past 210 kyr linked to distant climate anomalies. **Nature.** 432. 740-743. 2004.

WOLFF, E. W., CHAPPELLAZ, J., BLUNIER, T., RASMUSSEN, S. O., & SVENSSON, A. Millennial-scale variability during the last glacial: The ice core record. **Quaternary Science Reviews.** 29 (21–22), 2828–2838. 2010.

WRIGHT, D. G., PAWLOWICZ, R., MCDOUGALL, T. J. FEISTEL, R. AND MARION, G. M. Absolute Salinity, "Density Salinity" and the Reference-Composition Salinity Scale: present and future use in the seawater standard TEOS-10. **Ocean Science**, 7, 1 - 26. 2011.

ZHANG, Y., CHIESSI, CM, MULITZA, S., ZABEL, M., TRINDADE, R. I. F., HOLLANDA, M. H. B. M., DANTAS, E. L., GOVIN, A., TIEDEMANN, R., WEFER, G. Origin of increased terrigenous supply to the NE South American continental margin during Heinrich Stadial 1 and the Younger Dryas. **Earth Planetary Science Letters**. 2015.

ZONNEVELD, K. A. F., AND POSPELOVA, V. A determination key for modern dinoflagellate cysts. **Palynology.** 39 (3), 387-409. 2015.

ZONNEVELD, K. A. F., MARRET, F., VERSTEEGH, G., BOGUS, K., BONNET, S., BOUIMETARHAN, I., CROUCH, E., DE VERNAL, A., ELSHANAWANY, R., EDWARDS, L., ESPER, O., FORKE, S., GRØSFJELD, K., HENRY, M., HOLZWARTH, U., KIELT, J-F., KIM, S-Y., LADOUCEUR, S., LEDU, D., LIANG, C., LIMOGES, A., LONDEIX, L., LU, S.-H.; MAHMOUD, M. S., MARINO, G., MATSOUKA, K., MATTHIESSEN, J., MILDENHAL, D. C., MUDIE, P., NEIL, H. L.; POSPELOVA, V., QI, Y., RADI, T., RICHEROL, T., ROCHON, A., SANGIORGI, F., SOLIGNAC, S., TURON, J-L., VERLEYE, T., WANG, Y., WANG, Z., YOUNG, M. "Atlas of modern dinoflagellate cyst distribution based on 2405 datapoints". **Review of Palaeobotany and Palynology.** 191: 1–197. 2013.

ZONNEVELD, K. A. F., VERSTEEGH, G. J. M., KASTEN, S., EGLINTON, T. I., EMEIS, K-C., HUGUET, C., KOCH, B. P., DE LANGE, G. J., DE LEEUW, J. W., MIDDELBURG, J. J., MOLLENHAUER, G., PRAHL, F., RETHEMEYER, J., WAKEHAM, S. Selective preservation of organic matter in marine environments; processes and impact on the fossil record. **Biogeosciences.**, 7, 483-511. 2010.

ZONNEVELD, K. A. F., BOCKELMANN, F., HOLZWARTH, U. Selective preservation of organic-walled dinoflagellate cysts as a tool to quantify past net primary production and bottom water oxygen concentrations. **Marine geology.** 237, 109–126. 2007.

ZONNEVELD, K. A. F., & BRUMMER, G. J. A. (Palaeo-)ecological significance, transport, and preservation of organic-walled dinoflagellate cysts in the Somali Basin, NW Arabian Sea. Deep-Sea Research Part II: **Topical Studies in Oceanography.** 47 (9–11), 2229–2256. 2000.

4 CONCLUSIONS AND FUTURE CHALLENGES

The marine core GL-1248, retrieved from the continental slope and under the influence of the Parnaíba river discharge, recorded ecological responses over the last 130kyrs. Palynological analysis of pollen grains and spores enables us to infer changes in the continental environment, carried by the river outflow to the seabed. Synchronically, changes in dinoflagellate cysts assemblages allowed us to identify autochthonous oscillations in past primary productivity of the surface of the ocean. The ITCZ displacements are a crucial component in the precipitations patterns in Northeastern Brazil, and the ecological responses were guided by past shifts of the ITCZ over northeastern Brazil. The pulses of the Parnaiba River discharge was the integrative guiding line between reconstructed the vegetation of Parnaíba Hydrographic Basin, as well as inferences of the hydrography and paleoproductivity changes in the adjacent ocean.

Based on the information presented, the following conclusions are given:

- We used the delta coverage to infer the prevalence of vegetation type in northeastern Brazil according to water availability. The ITCZ was considered the primary source of moister in the region, whereas gains in the delta coverage reflected the improvement of rainforest vegetation and more wet period. The reconstructed rainforest lowland appeared to be sensible to HS precipitation events. Still, the spectral analyses have shown rainforest periodicity was better aligned with orbital cycles (precession and obliquity). At the same time, the open vegetation is more susceptible to changes according to millennial time-scale events. This work reinforced the concept of ecological corridors, and we suggest that the species' dispersion and genetic-flow through northeastern Brazil must also be modulated by orbital forcing.
- The dinocysts assemblages of open ocean and river outflow displayed a glacial-interglacial distribution pattern, dictated by the oscillation of sea level. Over the glacial period, the nutricline assemblage shifted in anti-phase to past ITCZ displacements, and the enhancement of the assemblage was related to the strength of the trade wind system. During the interglacials, two autotrophs dinocyst assemblages with different nutrient requirements interchange during the MIS5. We suggested that past productivity changed according to the variability of nutrients in the photic zone led by ocean-atmosphere processes. We also highlighted the significant discrepancies in tradewinds' strength

between the current and past interglacials periods, as longs as attenuated trade wind system led to oligotrophic conditions in the western equatorial Atlantic.

The reconstruction of past vegetation and ocean surface hydrography and paleoproductivity over the last ~130 kyr provide new perspectives of long-term environmental changes. The climate has changed over geological time, and the planet orbital conditions might relate semi-arid conditions in northeastern Brazil for long. Still, the anthropogenic climate disturbances created by excessive emissions of greenhouse gases hampers future predictions. However, the effects of global warming and anthropogenic impacts are already evident in our daily lives. The actual coverage of dense vegetation represents less than 15% (MAPBIOMAS, 2015). If our data can be compared to current standards, the forest vegetation has only experienced equivalent values under drought climate events. The non-attendance of containment actions for future climatic damage or the absence initiatives to preserve the local environment may enhance environmental degradation, poverty to the local population, and immeasurable losses to the biodiversity of northeastern Brazil. Different fields of knowledge should cooperate to integrate better information about the patterns biodiversity spread in South America. Regarding the investigations carried out in the adjacent ocean, studies on the ecology and motile capacity of dinoflagellates in the water column can be enriching for future interpretations regarding the distribution of dinocyst in marine sediment cores.

4.1 REFERENCES:

ARAGÃO, L. E. O. C., POULTER, B., BARLOW, J. B., ANDERSON, L. O., MALHI, Y., SAATCHI, S., PHILLIPS, O. L., GLOOR, E. Environmental change and the carbon balance of Amazonian forests. **Biological Reviews**, 89(4), 913–931. 2014.

BEHLING, H., ARZ, HW, PÄTZOLD, J., WEFER, G. Late Quaternary vegetational and climate dynamics in northeastern Brazil, inferences from marine core GeoB 3104-1. **Quaternary Science Reviews**, 19 (10), 981-994. 2000.

BEHLING, H., COHEN, MCL, AND R. J. LARA, RJ Late Holocene mangrove dynamics of the Marajó Island in Amazonia, northern Brazil. **Vegetation History and Archaeobotany**, 13, 73-80. 2004.

BEREITER, B., EGGLESTON, S., SCHMITT, J., NEHRBASS-AHLES, C., STOCKER, T.F., FISCHER, H., KIPFSTUHL, S., CHAPPELLAZ, J., 2015. Revision of the EPICA Dome C CO2 record from 800 to 600 kyr before present. **Geophys. Res**. Lett. 42, 542–549. 2015.

BERGER, A., LOUTRE, M. F. Climate 400,000 years ago, a key to the future? in Earth's Climate and Orbital Eccentricity: The Marine Isotope Stage 11 Question, edited by A. W. Droxler, R. Z. Poore, and L. H. Burckle, Geophys. Monogr. Ser., vol. 137, pp. 17–26, **AGU**, Washington, D. C. 2003.

BUTT, N., SEABROOK, L., MARON, M., LAW, B. S., DAWSON, T. P., SYKTUS, J., MCALPINE, C. A. Cascading effects of climate extremes on vertebrate fauna through changes to low latitude tree flowering and fruiting phenology. **Global Change Biology**, 21, 3267–3277. 2015.

BOUIMETARHAN, I., CHIESSI, C. M., GONZALEZ-ARANGO, C., DUPONT, L., VOIGT, I., PRANGE, M., ZONNEVELD, K. Intermittent development of forest corridors in northeastern Brazil during the last deglaciation: Climatic and ecologic evidence. **Quaternary Science Reviews**, 192, 86-96, 2018.

CAESAR, L., RAHMSTORF, S., ROBINSON, A., FEULNER, G. Observed fingerprint of a weakening Atlantic Ocean overturning circulation**. Nature**, 556 191–6. 2018

CASTRO, A. A. J. F., MARTINS, F. R. & FERNANDES, A. G. The woody flora of cerrado vegetation in the State of Piauí, Northeastern Brazil. **Edinburgh Journal of Botany**. 55: 455-472. 1998.

DUPONT, LM, SCHLÜTZ, F., EWAH, CT, JENNERJAHN, TC, PAUL, A., BEHLING, H. Two-step vegetation response to enhanced precipitation in Northeast Brazil during Heinrich event 1. **Global Change Biology.** 2010.

DUTTON, A., CARLSON, A. E., LONG, A. J., MILNE, G.A., CLARK, P. U., DECONTO, R., HORTON, B. P., RAHMSTORF, S. AND RAYMO, M. E. Sea-level rise due to

polar ice-sheet mass loss during past warm periods, **Science**, 349, 6244, 2015.

EPICA Community Members. Eight glacial cycles from an Antarctic ice core. **Nature** 429, 623–628. 2004.

HARRISON, R. D. Repercussions of El Niño: drought causes extinction and the breakdown of mutualism in Bor-neo. **Proceedings of the Royal Society B**, 267, 911–91. 2000.

HAUG, G. H., HUGHEN, K. A., SIGMAN, D. M., PETERSON, L. C., RÖHL, U. Southward migration of the intertropical convergence zone through the Holocene. **Science**. (5533), 1304–1308. 2001.

IBGE, INSTITUTO BRASILEIRO DE GEOGRAFIA E ESTATÍSTICA. **Mapa de Biomas e de Vegetação do Brasil**. Disponível em: <http://www.ibge.org.br/>. 2004.

IPCC: Climate Change 2014: Synthesis Report. Contribution of Working Groups I, II and III to the Fifth Assessment Report of the Intergovernmental Panel on Climate Change [Core Writing Team, R.K. Pachauri and L.A. Meyer (eds.)]. IPCC, Geneva, Switzerland, 151 pp. 2014.

JENNERJAHN T.C., ITTEKOT V., ARZ H.W., BEHLING H., PÄTZOLD J., WEFER G. Asynchronous terrestrial and marine signals of climate change during Heinrich Events. **Science**, 306, 2236–2239. 2004.

JOUZEL, J., MASSON-DELMOTTE, V., CATTANI, O., DREYFUS, G., FALOURD, S., HOFFMANN, G., MINSTER, B., NOUET, J., BARNOLA, J.M., CHAPPELAZ, J., FISCHER, H., GALLET, J. C., JOHNSEN, S., LEUENBERGER, M., LOULERGUE, L., LUETHI, D., OERTER, H., PARRENIN, F., RAISBECK, G., RAYNAUD, D., SCHILT, A., SCHWANDER, J., SELMO, E., SOUCHEZ, R., SPAHNI, R., STAUFFER, B., STEFFENSEN, J.-P., STENNI, B., STOCKER, T. F., TISON, J.-L., WERNER, M., AND WOLFF, E. W. Orbital and Millennial Antarctic Climate Variability over the Past 800.000 Years, **Science**, 317, 5839, 2007.

KIRTMAN, B., POWER, S. B, ADEDOYIN, J. A, BOER, GJ, BOJARIU, R., CAMILLONI, I., DOBLAS-REYES, F. J, FIORE, A.M., KIMOTO, M., MEEHL, G. A, PRATHER, M., SARR, A., SCHÄR, C., SUTTON, R., VAN OLDENBORGH, G. J, VECCHI G., WANG H. J. Near-term Climate Change: Projections and Predictability. In: Climate Change 2013: The Physical Science Basis. Contribution of Working Group I to the Fifth Assessment Report of the Intergovernmental Panel on Climate Change. [STOCKER, TF, QIN, D., PLATTNER, G.-K., M. TIGNOR, ALLEN, SK, BOSCHUNG, J., NAUELS, A. XIA, Y. BEX, V. AND MIDGLEY, P.M. (eds.)]. **Cambridge University Press**, Cambridge, United Kingdom and New York, NY, USA. 2013.

LI, S., OTTO, F. E. L., HARRINGTON, L.J., SPARROW, S. N., WALLOM, D. C. H. A pan-South-America assessment of avoided exposure to dangerous extreme precipitation by limiting to 1.5 °C warming. **Environmental Research Letters**, 15, 5. 2020.

LOUTRE, M. F., BERGER, A. Marine Isotope Stage 11 as an analogue for the present interglacial. **Global and Planetary Change**, 36(3), 209–217. 2003.

LÜTHI, D., LE FLOCH, M., BEREITER, B., BLUNIER, T., BARNOLA, J.-M., SIEGENTHALER, U., STOCKER, T. F. High-resolution carbon dioxide concentration record 650,000–800,000 years before present. **Nature**, 453(7193), 379–382. 2008.

MALLIN, M. A., PAERL, H. W., RUDEK, J., AND BATES, P. W. Regulation of estuarine primary production by watershed rainfall and river flow. **Marine Ecology Progress Series.** 93:199-203. 1993.

MULITZA, S., RÜHLEMANN, C., BICKERT, T., HALE, W. Late Quaternary $\delta^{13}C$ gradients and carbonate accumulation in the western equatorial Atlantic. **Earth and Planetary Science Letters.** 155, 237–249. 1998.

MULITZA, S., CHIESSI, C. M., SCHEFUß, E., LIPPOLD, J., WICHMANN, D., ANTZ, B., MACKENSEN, A., PAUL, A., PRANGE, M., REHFELD, K., WERNER, M., BICKERT, T., FRANK, N., KUHNERT, H., LYNCH-STIEGLITZ, J., PORTILHO-RAMOS, R. C., SAWAKUCHI, A. O., SCHULZ, M., SCHWENK, T., TIEDEMANN, R., VAHLENKYRMP, M., ZHANG, Y. Synchronous and proportional deglacial changes in Atlantic meridional overturning and northeast Brazilian precipitation. **Paleoceanography**. 2017.

PHILLIPS, O. L., ARAGAO, L. E. O. C., LEWIS, S. L., FISHER, J. B., LLOYD, J., LOPEZ-GONZALEZ, G., TORRES-LEZAMA, A. Drought sensitivity of the Amazon rainforest. Science, 323, 1344–1347. 2009.

PRICE, A. M., POSPELOVA, V., COFFIN, M. R. S., LATIMER, J. S., CHMURA, G. L. Biogeography of dinoflagellate cysts in northwest Atlantic estuaries. **Ecology and Evolution.** 6(16), 5648-5662. 2016.

PRIMACK, R. B. **Essentials of Conservation Biology**. Sunderland, MA: Sinauer, 1993.

PROJETO MAPBIOMAS – Coleção v. 4.1 da Série Anual de Mapas de Cobertura e Uso de Solo do Brasil, acessado em 06 de março de 2020 através do link:https://mapbiomas.org/

OGAYA, R., PEÑUELAS, J. Species-specific drought effects on flower and fruit production in a Mediterranean holm oak forest. **Forestry**, 80, 351–357. 2007.

OLSON, D. M., E. DINERSTEIN, E. D. WIKRAMANAYAKE, N.D. BURGESS, G. V. N. POWELL, E. C. UNDERWOOD, J. A. D'AMICO, I. ITOUA, H.E. STRAND, J. C. MORRISON, C. J. LOUCKS, T. F. ALLNUTT, T. H. RICKETTS, Y. KURA, J. F. LAMOREUX, W. W. WETTENGEL, P. HEDAO, K. R. KASSEM. Terrestrial Ecoregions of the World: A New Map of Life on Earth (PDF, 1.1M) **BioScience** 51:933-938. 2001.

RISSER, P. G. The status of the science examining ecotones. **BioScience.** 45: 318–325. 1995.

RUDDIMAN, W. F. Earth's Climate: Past and Future**. New York: W.H. Freeman**. 2001.

RÜHLEMANN, C.; FRANK., M.; HALE, W.; MANGINI, A.; MULITZA, S.; MULLER, P. J.; WEFER, G. Late Quaternary productivity changes in the western equatorial Atlantic: Evidence from 230Th-normalized carbonate and organic carbon accumulation rates. **Marine Geology.** 135 (1-4), 127-152. 1996.

SIGMAN, D. M., HAIN, M. P. The Biological Productivity of the Ocean. **Nature Education Knowledge**, 3(10):21. 2012.

SIQUEIRA, V. A., PAIVA, R. C. D. D., FLEISCHMANN, A. S., FAN, F. M., RUHOFF, A. L., PONTES, P. R. M., COLLISCHONN, W. Toward continental hydrologic–hydrodynamic modeling in South America. **Hydrology and Earth System Sciences**, 22(9), 4815-4842. 2018.

VENANCIO, I. M., MULITZA, S., GOVIN, A., SANTOS, T. P., LESSA, D. O., ALBUQUERQUE, A. L. S., CHIESSI, CM, TIEDEMANN, R., VAHLENKAMP, M., BITCKET, T., SCHULZ, M. Millennial- to orbital-scale responses of western equatorial Atlantic thermocline depth to changes in the trade wind system since the Last Interglacial. **Paleoceanography and Paleoclimatology**. 2018.

VINK, A., BRUNE, A., HÖLL, C., ZONNEVELD, K. A. F., WILLEMS, H. On the response of calcareous dinoflagellates to oligotrophy and stratification of the upper water column in the equatorial Atlantic Ocean. **Palaeogeography Palaeoclimatology Palaeoecology.** 178, 53–66. 2002.

WEBSTER, P. J., FASULLO, J. T. A hydrological definition of Indian monsoon onset and withdrawal. **Journal Of Climate,** 16, 3200-3211. 2003.

YOON, J.H., ZENG, N. An Atlantic influence on Amazon rainfall. **Climate Dynamics** 34(2–3): 249– 264, 2010.

ZHANG, Y., CHIESSI, C. M., MULITZA, S., ZABEL, M., TRINDADE, R. I. F., HOLLANDA, M. H. B. M., DANTAS, E. L., GOVIN, A., TIEDEMANN, R., WEFER, G. Origin of increased terrigenous supply to the NE South American continental margin during Heinrich Stadial 1 and the Younger Dryas. **Earth Planetary**

Science Letters. 2015.

5 Supplementary material:

Table S1 - All pollen grains types identified in GL-1248 marine core and their classification.

Group	Structure	Pollen type
Open Vegetation	Herbs	Asteraceae
	Herbs	Polygalaceae Polygala
	Herbs	Amaranthaceae Alternathera
	Herbs	Amaranthaceae Gompherena-Pfaffia-type
	Herbs	Amaranthaceae/ Chenopodiaceae
	Herbs	Poaceae
	Herbs	Asteraceae subf. Asteoideae
	herbs	Lamiaceae
	herbs	Lauraceae
	Herbs	Euphorbiaceae
	Herbs	Asteraceae subf. Cichorioideae
	Herbs	Asteraceae Trichocline
	herb	Scrophulariaceae
	herb to tree	Turneraceae Turnera Panamensis
	herb	Zygophyllaceae Kallstroemia
	herbs	Anthemideae Matricaria
	herb, shrub	Caryocaraceae
	Shrubs	Lythraceae Cuphea
	Herbs	Fabaceae
	Herbs	Fabaceae Bauhinia
	Herbs	Fabaceae Dioclea
	Herbs	Fabaceae Mucuna
	Herbs	Rubiaceae Borreria
	Trees and shrubs	Cactacea
	Trees and shrubs	Anacardiaceae
	Trees and shrubs	Combretaceae
	Trees	Verbenaceae Aegiphila
	Trees	Vitaceae vitis tiliifolia
	Trees	Apocynaceae
	Trees and shrubs	Malvaceae
	Trees and shrubs	Rubiaceae Faramea
	Trees and shrubs	Rubiaceae Psychotria
	Trees and shrubs	Rubiaceae Spermacouceae
	Trees and shrubs	Mimosaceae
	Trees and shrubs	Araliaceae Didymopanax

Group	Structure	Pollen type
Rainforest	Trees and shrubs	Rubiaceae
	Trees and shrubs	Bignoniaceae
	Trees and shrubs	Arecaceae
	Trees and shrubs	Arecaceae Mauritia
	Trees and shrubs	Cannabaceae Celtis
	Trees and shrubs	Euphorbiacea Alchornea
	Trees and shrubs	Melastomatacea/ Combretaceae
	Trees and shrubs	Moraceae-Urticaceae
	Trees and shrubs	Burseraceae Protium
	Trees and shrubs	Symphonia Globulifera
	Trees	Urticaceae Cecropia
	Trees and shrubs	Sapotaceae
	Trees	Myrtaceae
	Trees and shrubs	Dilleniaceae Doliocarpus type
	Trees and shrubs	Bombacaceae
	Shrub or epiphyte	Piperaceae piper
	Trees and shrubs	Meliaceae
	Trees and shrubs	Sapindaceae
	Trees and shrubs	Sapindaceae Allophylus
	Trees and shrubs	Sterculiaceae
	Trees and shrubs	Theaceae Gordonia
	Trees and shrubs	Rutaceae Zanthoxylum
	Trees and shrubs	Salicaceae Salix
	Trees	Clusiaceae Symphonia globulifera
	Trees and shrubs	proteacea
	Trees and shrubs	Flacourtiaceae
	Trees and shrubs	Flacourtiaceae Banara
	Trees	Phytolaccaceae Gallesia
	Trees and shrubs	Annonaceae
	Shrubs	Solanaceae Solanum
	Shrubs	Malpighiaceae
	Shrubs	Malpighiaceae 1
	Shrubs	Malpighiaceae Byrsonima
	Shrubs	Malpighiaceae small type
	Liana	Convolvulaceae
	Liana	Curcubitaceae
	herb to tree	Boraginaceae Cordia
	Herbs	Euphorbiaceae Sebastiana brasiliensis
	herbs	Acanthaceae Justicia pectoralis
	herb	Acanthaceae
	herb	Maranthaceae

Group	Structure	Pollen type
Mountain vegetation	Trees and shrubs	Chloranthaceae Hedyosmum
	Trees and shrubs	Podocarpaceae Podocarpus
	Trees and shrubs	Aquifoliaceae Ilex
	Trees and shrubs	Myrsinaceae Myrsine
	Trees and shrubs	Symplocaceae Symplocos tenuifolia-type
	Trees and shrubs	Cunoniaceae Weinmannia
	Trees and shrubs	Ericaceae
Wetland	Aquatics	Alismataceae Sagittaria
	Aquatics	Onagraceae Ludwigia
	Herbs	Lentibulariaceae utricularia foliosa
	Herbs	Cyperaceae
	Herbs	Iridaceae
Mangrove	Tree	Acanthaceae Avicennia
	Tree	Rhizophoraceae Rhizophora
	Herbs	Polygonaceae
	liana	Convolvulaceae Ipomoea
Exotic	Trees and shrubs	Betulaceae Alnus
	Trees and shrubs	Plantaginaceae Plantago*
	Trees and shrubs	Pinaceae Pinus
UNK	Trees and shrubs	Caricaceae
	Trees and shrubs	Ulmeaceae
	epiphytas	Loranthaceae
	epiphytas	Marcgraviaceae
	epiphytas	Menispermaceae
	Lianas	Celastraceae Hippocrateaceae volubilis
	Lianas	Bromeliaceae
	Lianas	Marcgraviaceae
	Herb to tree	Boraginaceae

Table S2 - Compilation of GL-1248 marine core dinocysts information. The species names, abbreviations, nutritional requirements, ecological affinities, selective preservation (S-cyst and R-cyst groups), and geographic distribution.

Species	Abbreviation	Nutritional requirements	Ecological affinities	Selective preservation	Geographic distribution
Polysphaeridium zoharyi	Open ocean	P. zoh	autotrophic	R-cyst	coastal
Pentapharsodinium dalei	Open ocean	P. dal	autotrophic	R-cyst	coastal
Operculodinium centrocarpum	Open ocean	O. cen	autotrophic	M-cyst	cosmopolitan
Spiniferites bentorii	Open ocean	S. ben	autotrophic	M-cyst	coastal
Spiniferites membranaceus	Open ocean	S. mem	autotrophic	M-cyst	coastal
Spiniferites pachydermus	Open ocean	S. pac	autotrophic	M-cyst	coastal
Lingulodinium machaerophorum	Neritic	L. mac	autotrophic	M-cyst	coastal
Operculodinium centrocarpum reduced processes	Neritic	O. cen reduced	autotrophic	M-cyst	cosmopolitan
Nematosphaeropsis labyrinthus	Neritic	N. lab	autotrophic	R-cyst	coastal
Impagidinium aculeatum	Neritic	I. acu	autotrophic	R-cyst	open sea
Impagidinium paradoxum	Neritic	I. par	autotrophic	R-cyst	open sea
Impagidinium strialatum	Neritic	I. str	autotrophic	R-cyst	open sea
Selenopemphix quanta	Neritic	S. qua	hetertrophic	R-cyst	coastal
Echinidinium delicatum	Neritic	E. del	hetertrophic	**S-cyst**	coastal
Selenopemphix nephroides	River outflow	S. nep	hetertrophic	R-cyst	coastal
Trinovantedinium applanatum	River outflow	T. app	hetertrophic	R-cyst	coastal
Protoperidinium americanum	River outflow	P. ame	hetertrophic	**S-cyst**	coastal
Brigantedinium spp	River outflow	Brig Spp	hetertrophic	**S-cyst**	cosmopolitan
Echinidinium transparantum	Nutricline	E. tra	hetertrophic	**S-cyst**	coastal
Echinidinium aculeatum	Nutricline	E. acu	hetertrophic	**S-cyst**	coastal
Echinidinium granulatum	Nutricline	E. gra	hetertrophic	**S-cyst**	coastal
Pyxidinopsis reticulata	Nutricline	P. ret	autotrophic	M-cyst	cosmopolitan
Spiniferites mirabilis	Nutricline	S. mir	autotrophic	M-cyst	coastal
Tuberculodinium vancampoae	Nutricline	T. van	autotrophic	M-cyst	coastal
Operculodinium israelianum	Nutricline	O. isr	autotrophic	R-cyst	coastal
Impagidinium patulum	Nutricline	I. pat	autotrophic	R-cyst	open sea
Impagidinium sphaericum	Nutricline	I. sph	autotrophic	R-cyst	open sea
Impagidinium velorum	Nutricline	I. vel	autotrophic	R-cyst	open sea
Dalella chathamensis	Nutricline	D. cha	autotrophic	R-cyst	coastal

Pollen diagram of the marine core GL 1248

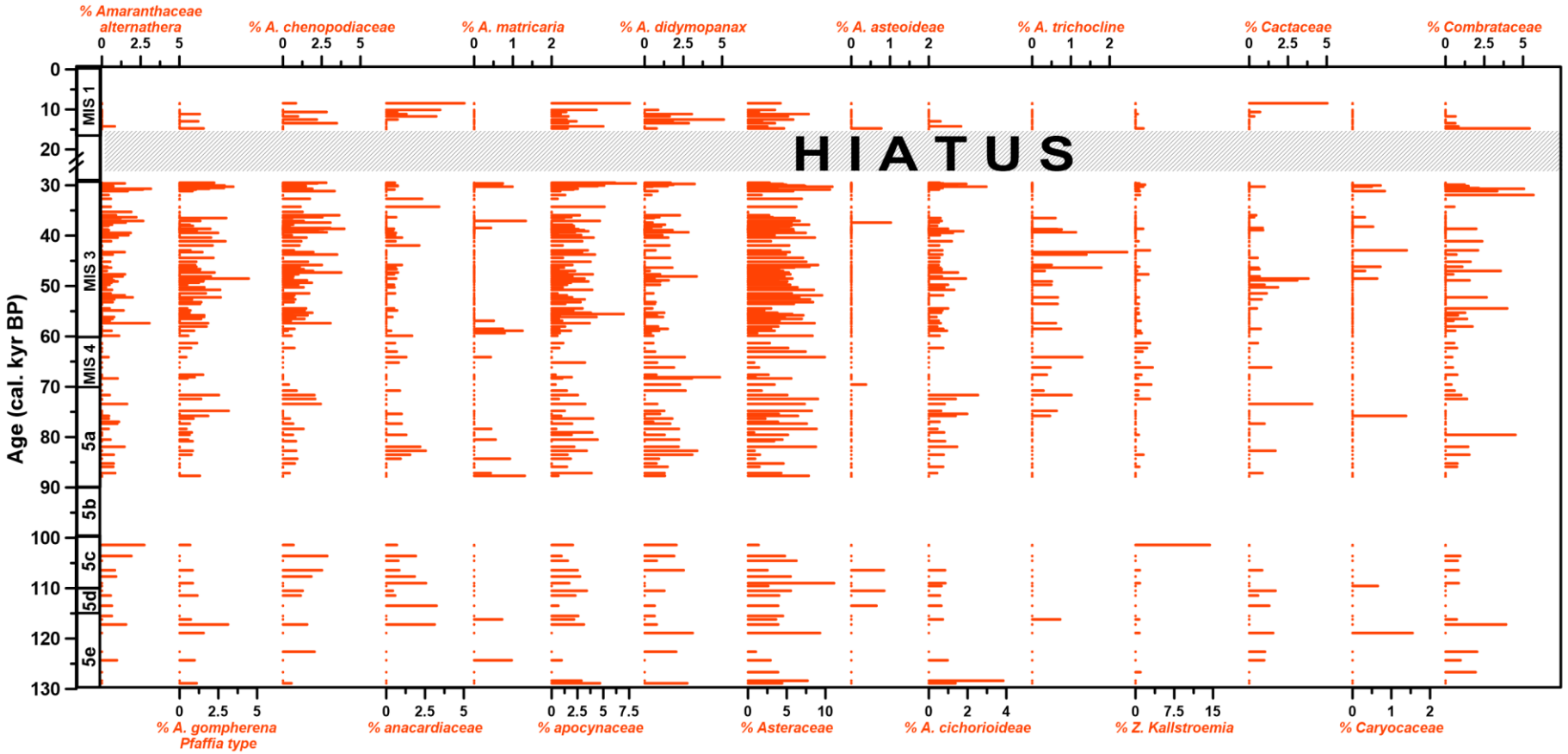

Figure S1: Open vegetation pollen diagram part 1, represented by the following pollen types: *Amaranthaceae Alternathera, Amaranthaceae Gompherena-Pfaffia type, Amaranthaceae/ Chenopodiaceae, Anacardiaceae, Anthemideae, Matricaria, Apocynaceae, Araliaceae Didymopanax, Asteraceae, Asteraceae subf. Asteoideae, Asteraceae subf. Cichorioideae, Asteraceae Trichocline, Cactacea, Caryocaraceae, Combrataceae.*

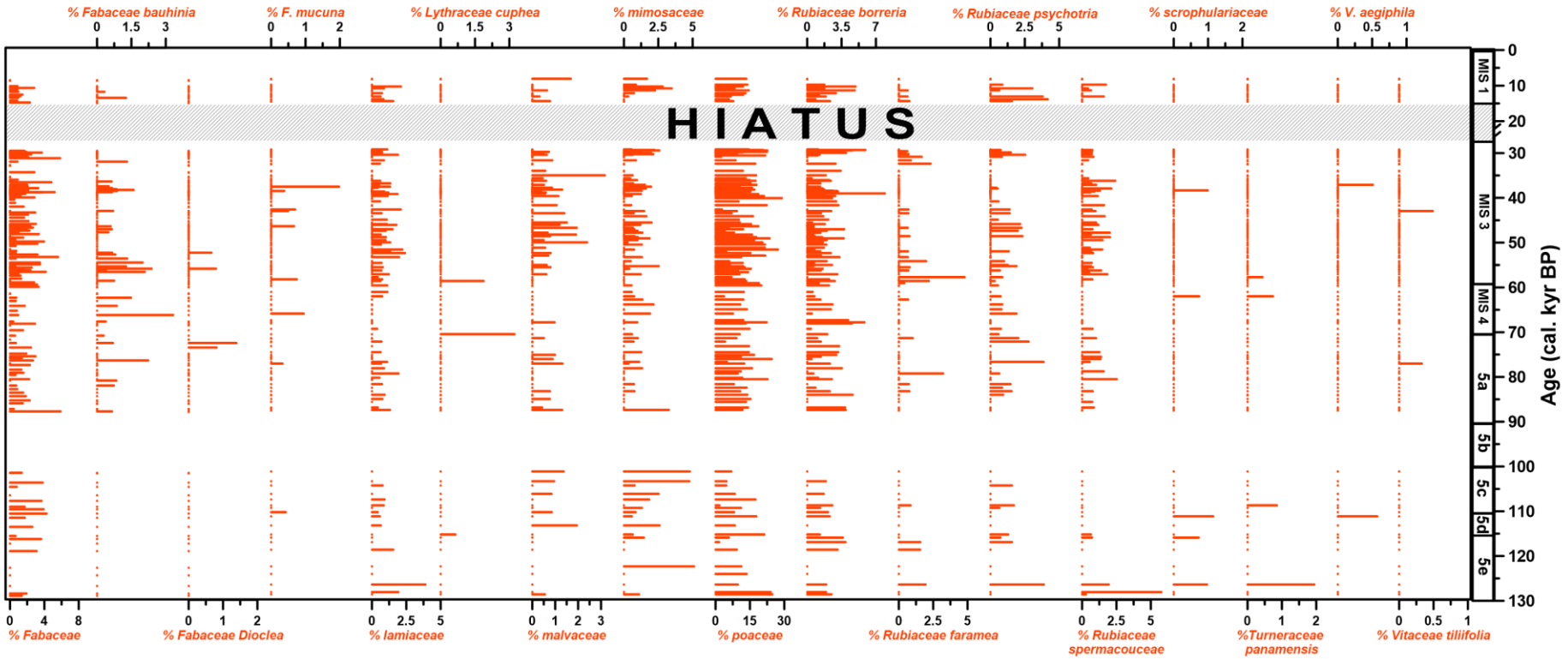

Figure S2: Open vegetation pollen diagram part 2, represented by the following pollen types: *Fabaceae, Fabaceae bauhinia, Fabaceae dioclea, Fabaceae mucuna, lamiaceae, Lythraceae cuphea, malvaceae, mimosaceae, poaceae, Rubiaceae borreria, Rubiaceae faramea, Rubiaceae psychotria, Rubiaceae Spermacouceae, scrophulariaceae, Turneraceae Turnera Panamensis, Verbenaceae Aegiphila, Vitaceae vitis tiliifolia.*

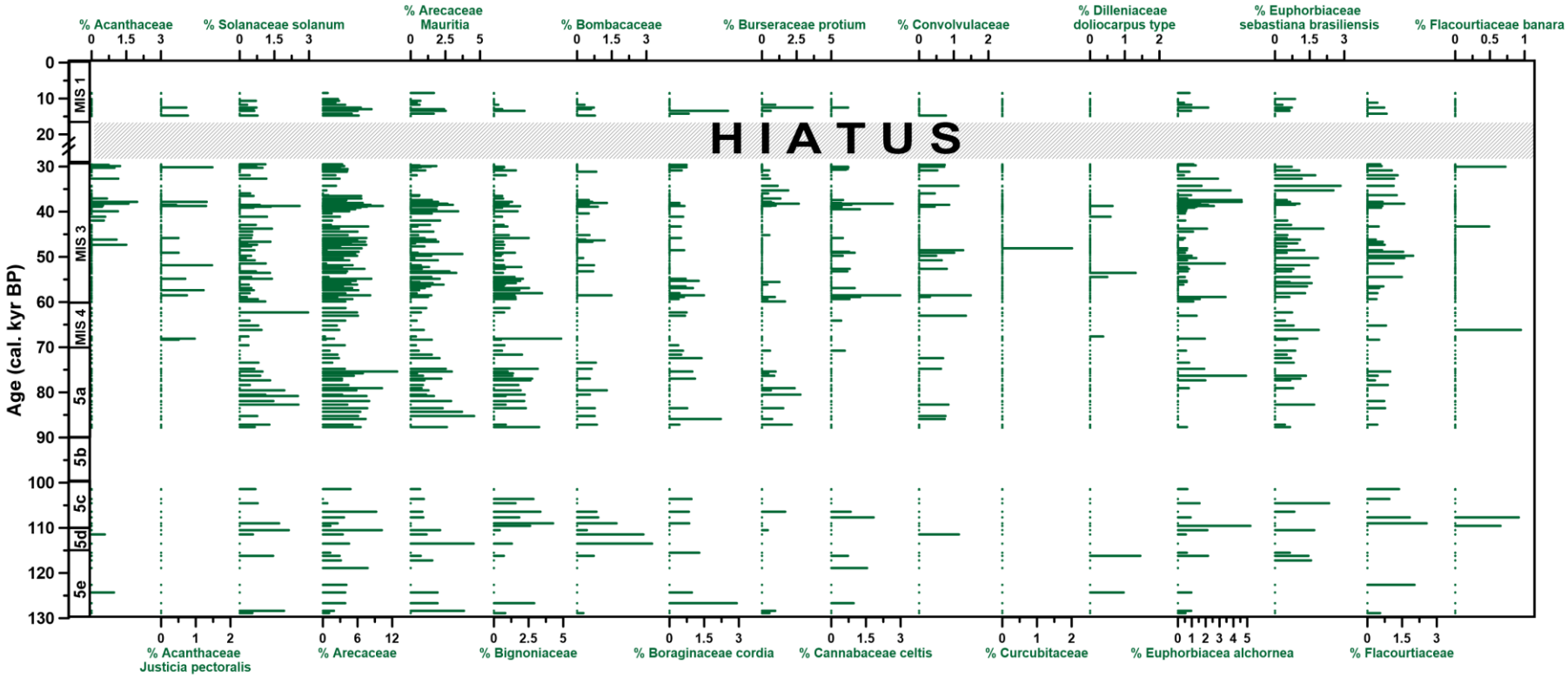

Figure S3: Rainforest lowland pollen diagram part 1, represented by the following pollen types: Acanthaceae, Acanthaceae Justicia pectoralis, Solanaceae Solanum, Arecaceae, Arecaceae Mauritia, Bignoniaceae, Bombacaceae, Boraginaceae, Cordia, Burseraceae Protium, Cannabaceae Celtis, Convolvulaceae, Curcubitaceae, Dilleniaceae Doliocarpus type, Euphorbiacea Alchornea, Euphorbiaceae Sebastiana brasiliensis, Flacourtiaceae, Flacourtiaceae Banara.

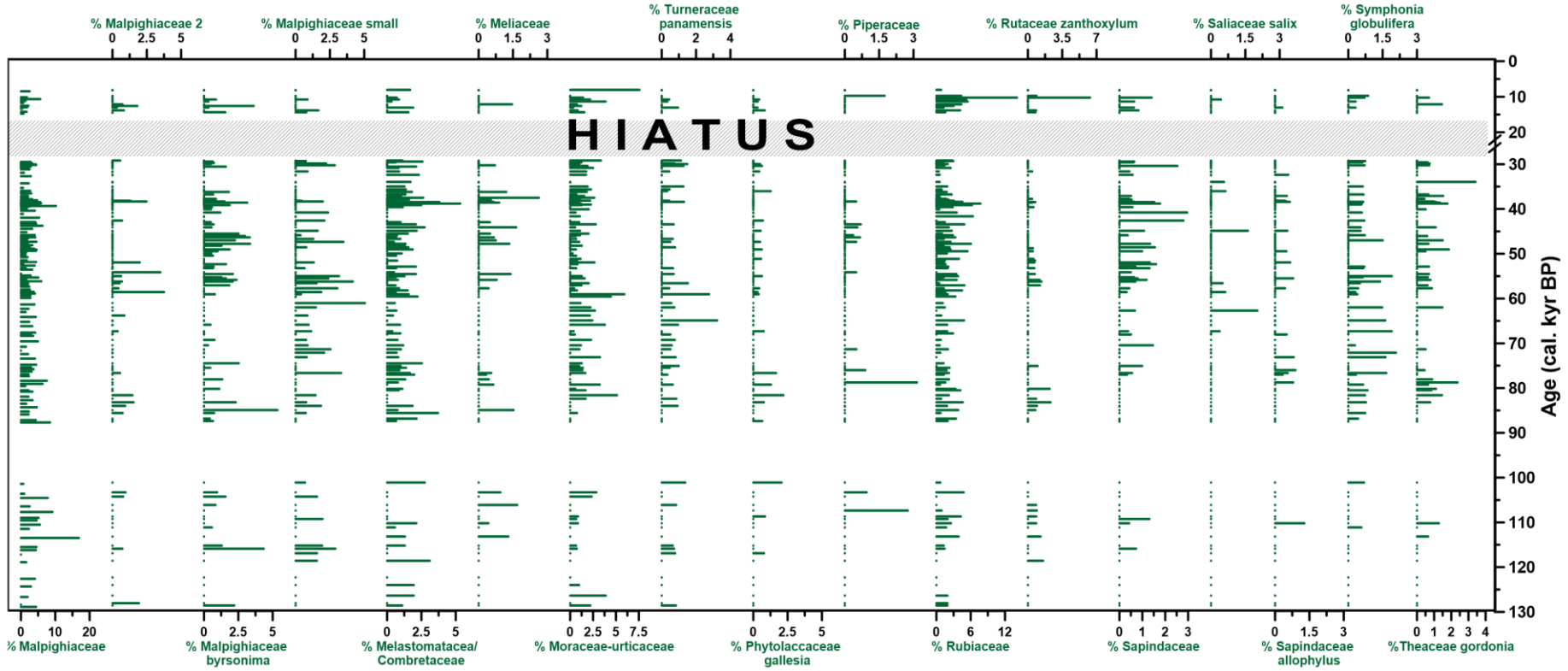

Figure S4: Rainforest lowland pollen diagram part 2, represented by the following pollen types: Malpighiaceae, Malpighiaceae 2, Malpighiaceae byrsonima, Malpighiaceae small type, Melastomataceae/ Combretaceae, Meliaceae, Moraceae-Urticaceae, Phytolaccaceae Gallesia, Piperaceae, Rubiaceae, Rutaceae Zanthoxylum, Salicaceae salix, Sapindaceae allophylus, Symphonia Globulifera, Theaceae Gordonia.

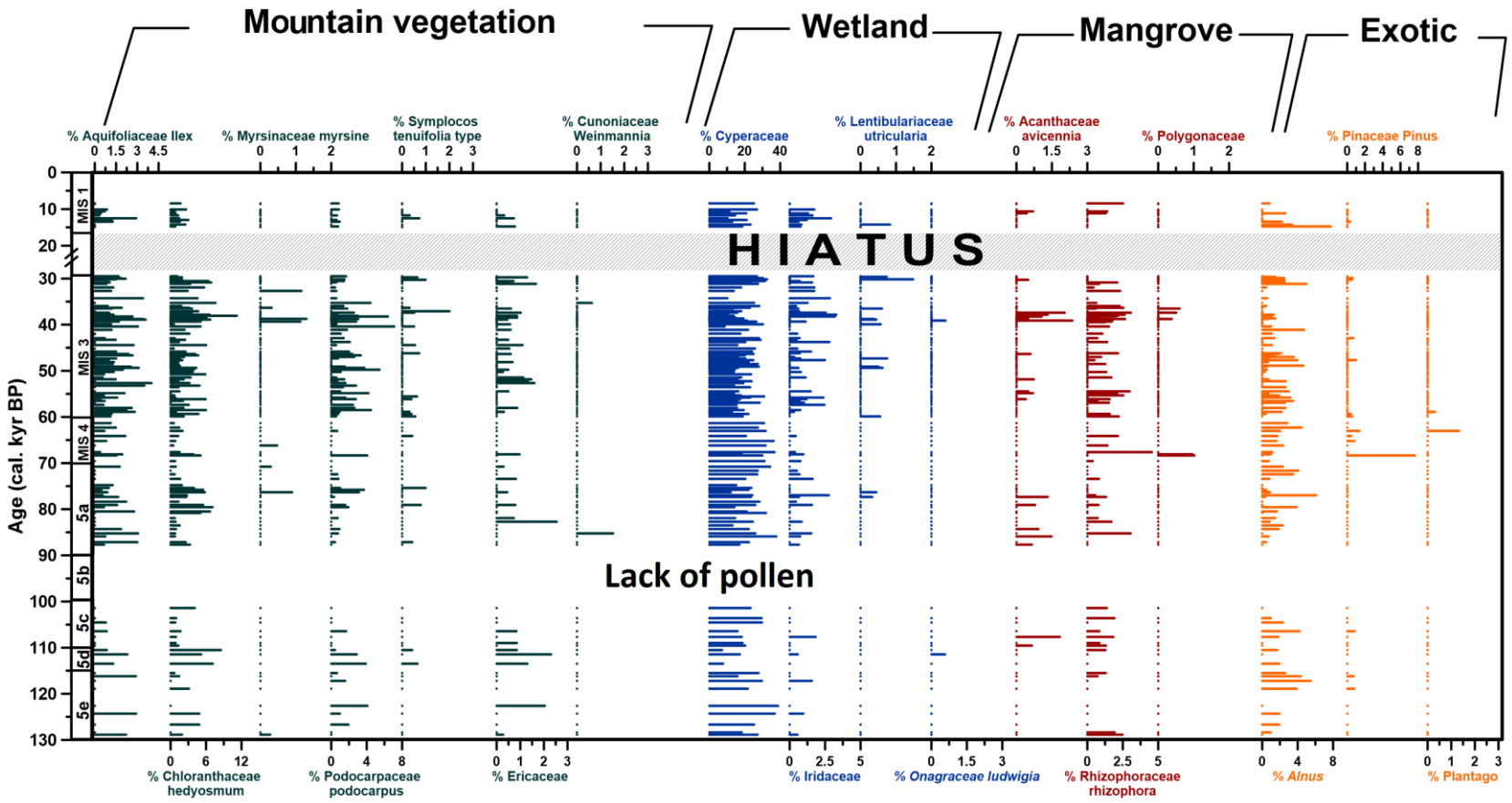

Figure S5: Pollen diagram with the groupings mountain vegetation, wetland, mangrove, and exotic, represented by the following pollen types*:* Aquifoliaceae Ilex, Chloranthaceae hedyosmum, Myrsinaceae Myrsine, Podocarpaceae podocarpus, Cunoniaceae Weinmannia, Symplocaceae symplocos tenuifolia type, Ericaceae, Cyperaceae, Iridaceae, Lentibulariaceae Utricularia, Onagraceae ludwigia, Acanthaceae Avicennia, Rhizophoraceae Rhizophora, Polygonaceae, Alnus, Plantaginaceae Plantago, Pinaceae Pinus.

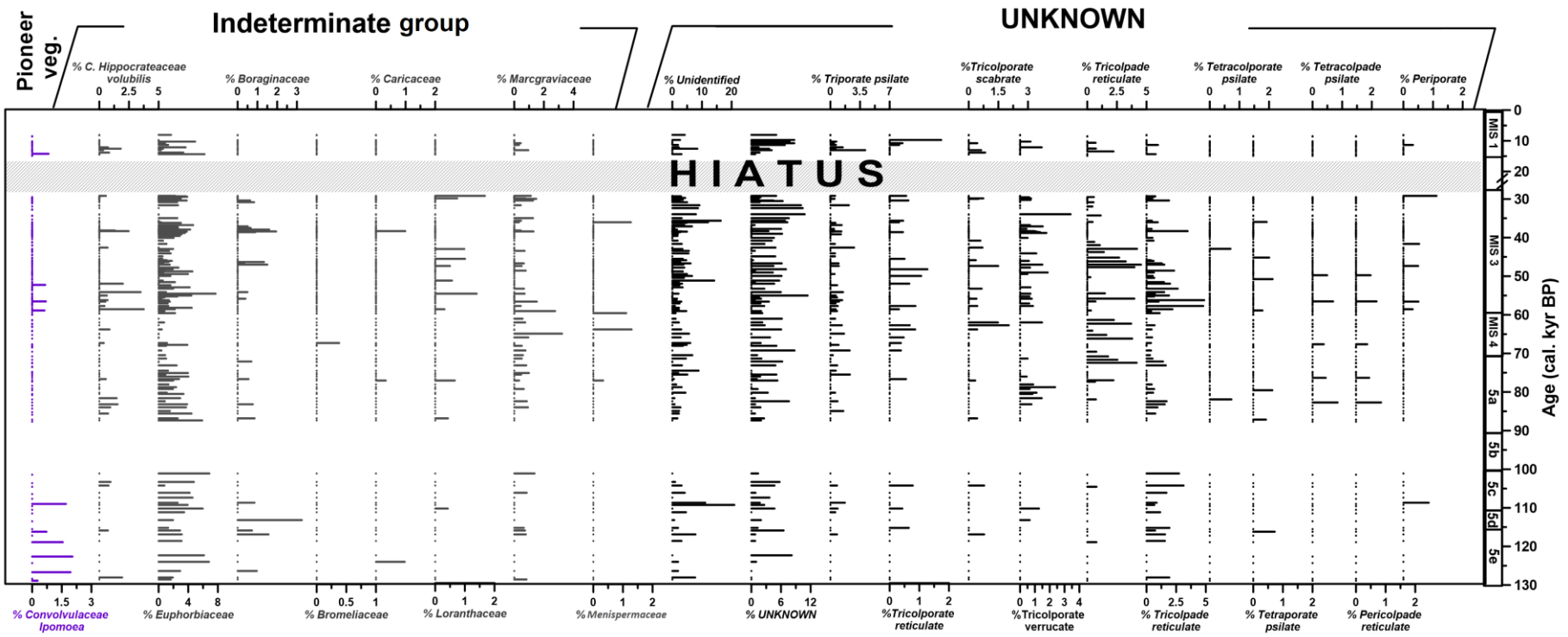

Figure S6: Pollen diagram with the groupings pioneer vegetation, indeterminate vegetation, and unknown types, represented by the following pollen types: *Convolvulaceae Ipomoea, Celastraceae Hippocrateaceae volubilis, Euphorbiaceae, Boraginaceae, Bromeliaceae, Caricaceae, Loranthaceae, Marcgraviaceae, Menispermaceae, unidentified pollen types, unknown, Triporate psilate, Tricolporate reticulate, Tricolporate scabrate, Tricolporate verrucate, Tricolporate equinate, Tricolporate psilate, Tricolpade reticulate, Tricolpade psilate, Tetracolporate psilate, Tetraporate psilate, Tetracolpade psilate, Pericolpade reticulate, Periporate*

Spore diagram of the marine core GL 1248

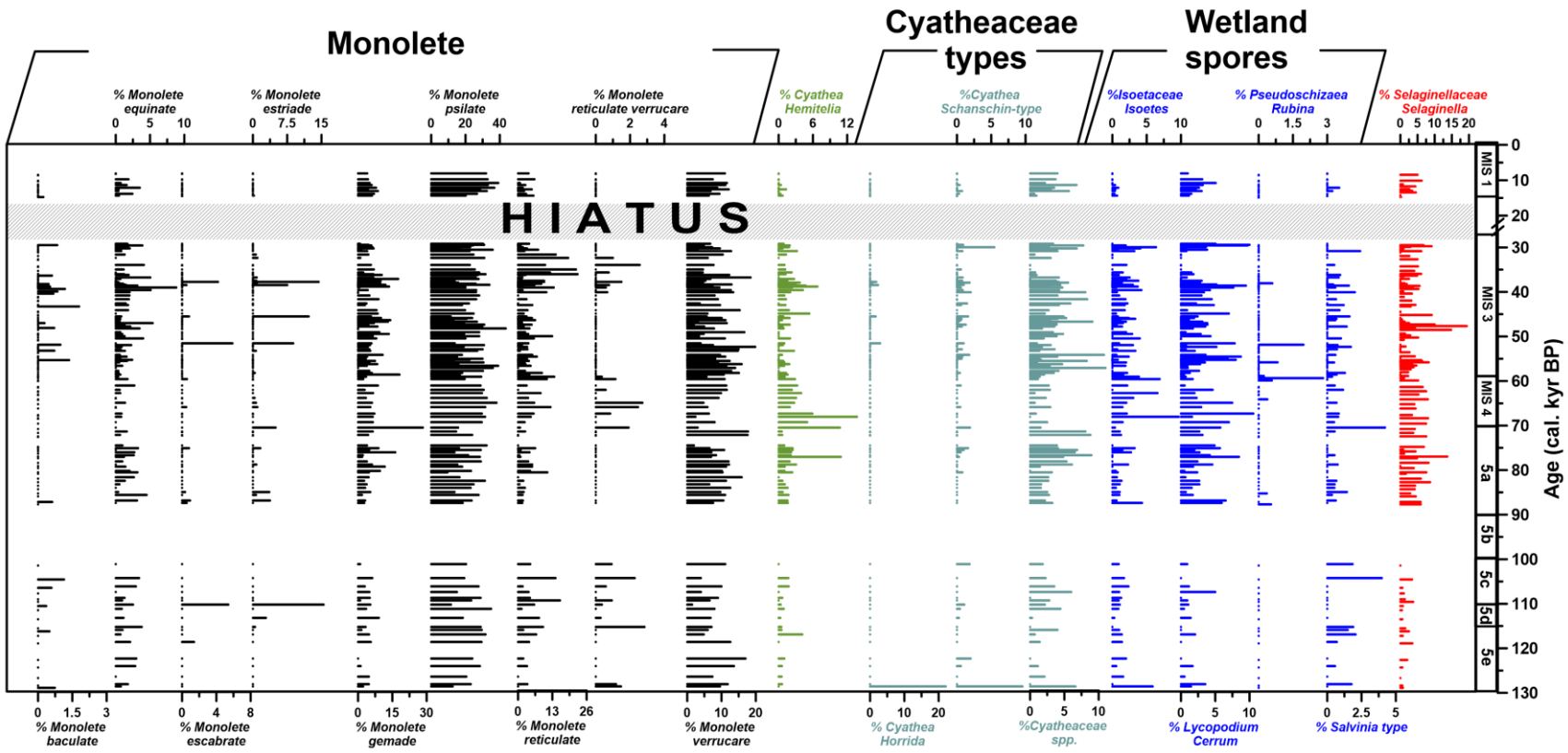

Figure S7: Spore diagram part 1, with the groupings monolete, Cyatheaceae spp., and wetland spores, represented by the following pollen types: *Monolete baculate, Monolete equinate, Monolete escabrate, Monolete estriade, Monolete gemade, Monolete reticulate, Monolete reticulate, verrucare, Monolete verrucare, Cyathea Hemitelia, Cyathea Horrida, Cyathea Schanschin-type,* Cyatheaceae spp., *Isoetaceae Isoetes, Lycopodium Cerrum, Pseudoschizaea Rubina, Sabinia type, Selaginellaceae Selaginella.*

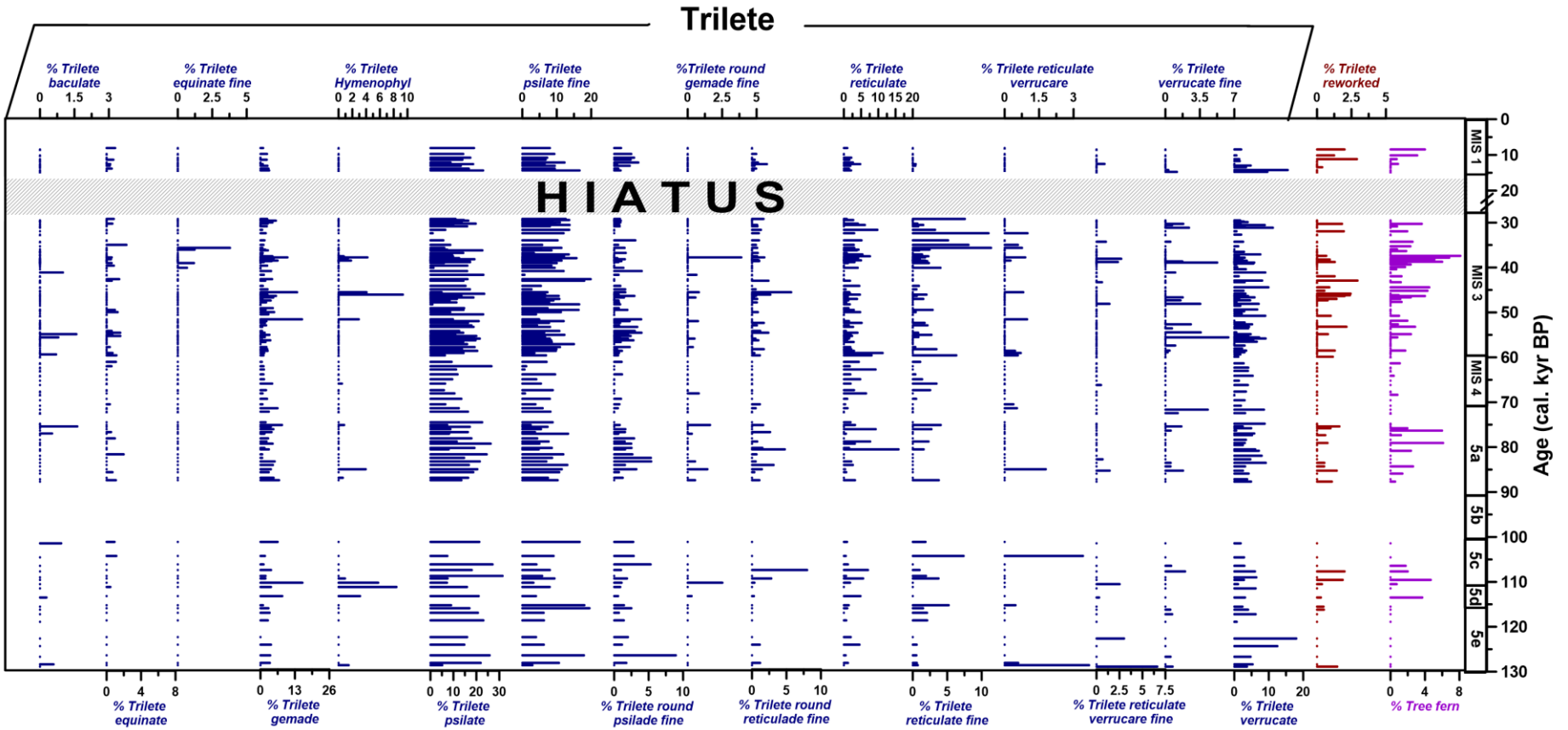

Figure S8: Spore diagram part 2, with the trilete types represented by the following pollen types: Trilete baculate, Trilete equinate, Trilete equinate fine, Trilete gemade, Trilete Hymenophyl, Trilete psilate, Trilete psilate fine, Trilete round psilade fine, Trilete round gemade fine, Trilete round reticulade fine, Trilete reticulate, Trilete reticulate fino, Trilete reticulate verrucare, Trilete reticulate verrucare fine, Trilete verrucate, Trilete verrucate fine, Trilete reworked, Tree fern.

List of the photographs of selected pollen grains and spores

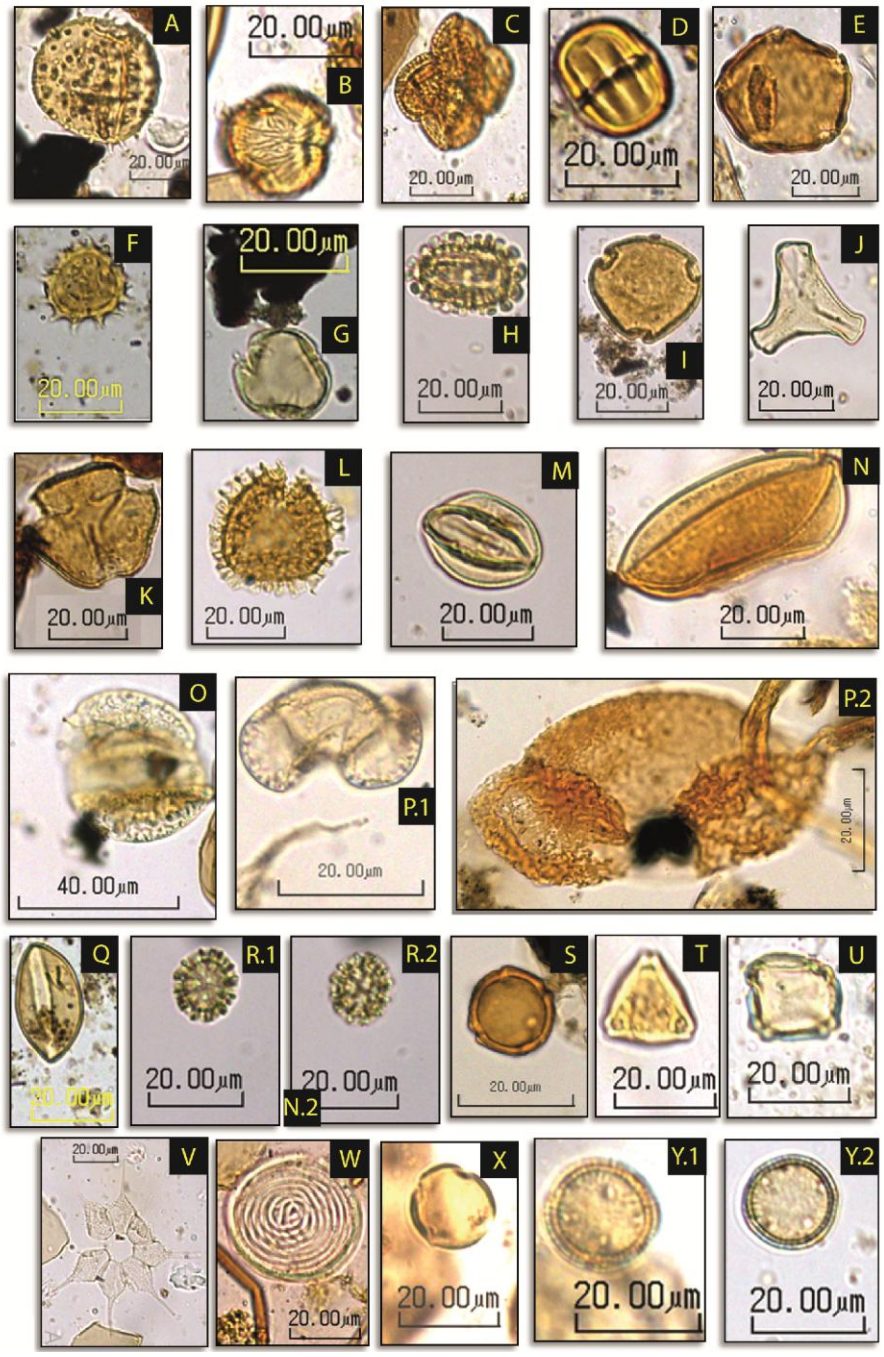

Figure S9: Pollen types: A- Arecaceae Mauritia, B- anacardiaceae, C-Hippocratea volubilis,D- Polygala sp. Polygalaceae, E- Clusiaceae Symphonia globulifera, F- Asteraceae, G- Euphorbiacea Alchornea, H- ilex, I-Symplocos, J- loranthaceae, K- Fabaceae, L- Lycopodium cerrum, M- Euphorbiaceae Sebastiana brasiliensis, N- Iridaceae, O- Pinus, P- Podocarpus, P.2- Podocarpus reworked, Q- Arecaceae, R.1- Amaranthaceae gompherena pfaffia type, R.2- Amaranthaceae gompherena pfaffia type, S- malpighiaceae, T- sapindaceae, U- alnus, V- pediastrum, W- pseudoschizaea spp., X- Myrsinaceae, Y.1- Rubiaceae spermacoceae, Y.2- Rubiaceae spermacoceae.

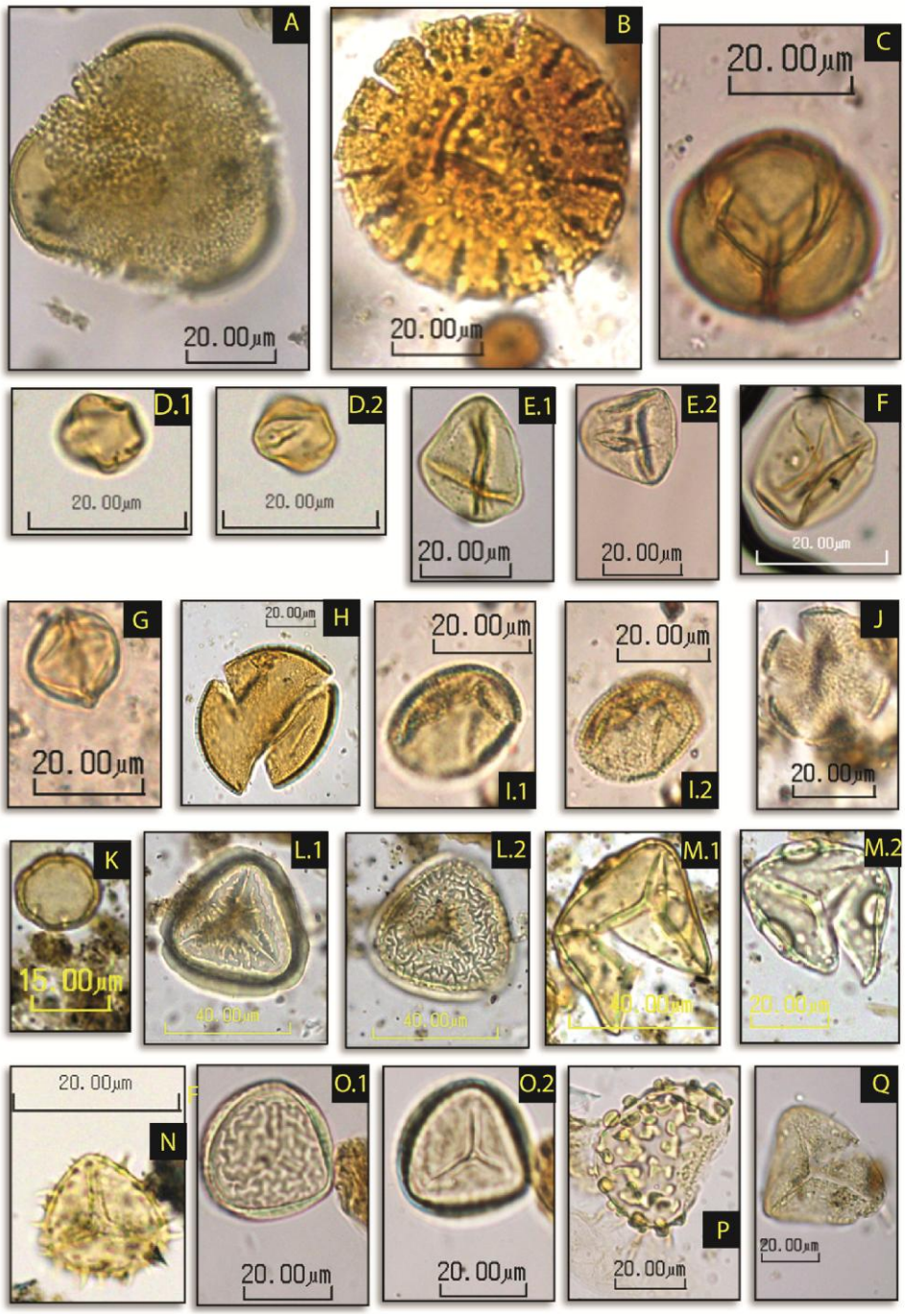

Figure S10: Pollen types: A- Ipomoea, B- borreria latifolia type, C- Ericaceae, D.1- Rhamnaceae, D.2- Rhamnaceae, E.1- cyperaceae, E.2- cyperaceae, F- poaceae, G- rhizophora, H- Verbenaceae, I.1- hedyosmum, I.2- hedyosmum, J- lamiaceae, K- borreria, L.1- Tree fern, L.2- Tree fern, M.1-broken Cyathea hemitelia, M.2- broken Cyathea hemitelia, N- Selaginellaceae selaginella, O.1- Cyatheaceae spp., O.2- Cyatheaceae spp., P- Monolete gemade, Q- Trilete reticulate fine.

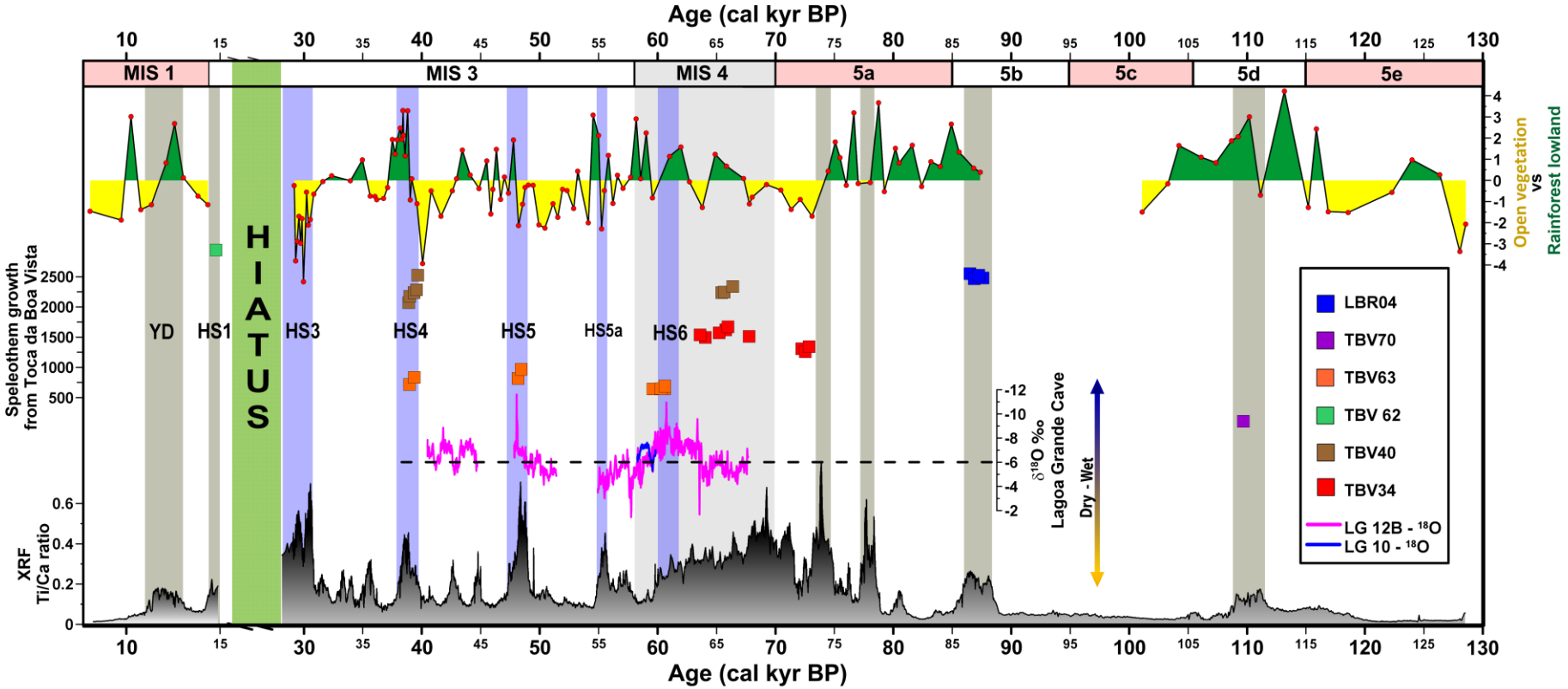

Figure S11: Delta coverage, positive values indicate an increase in rainforest lowland (filled in green) and negative values indicate an increase in open vegetation (filled in yellow); Speleothems grow phases from Toca da Boa Vista (TBV) and Lagoa dos Bretões (LBR) (Wang *et al.,* 2004); Two speleothems from Lapa Grange cave, central west of Brazil, LG - 12B (in pink) and LG - 10 (in blue) (Strikis *et al.,* 2018); (E) GL-1248 XRF Ti/Ca ratio (Venancio *et al*., 2018). The Heinrich Stadials (HS), are marked in blue, and the MIS 4 is highlighted in gray.

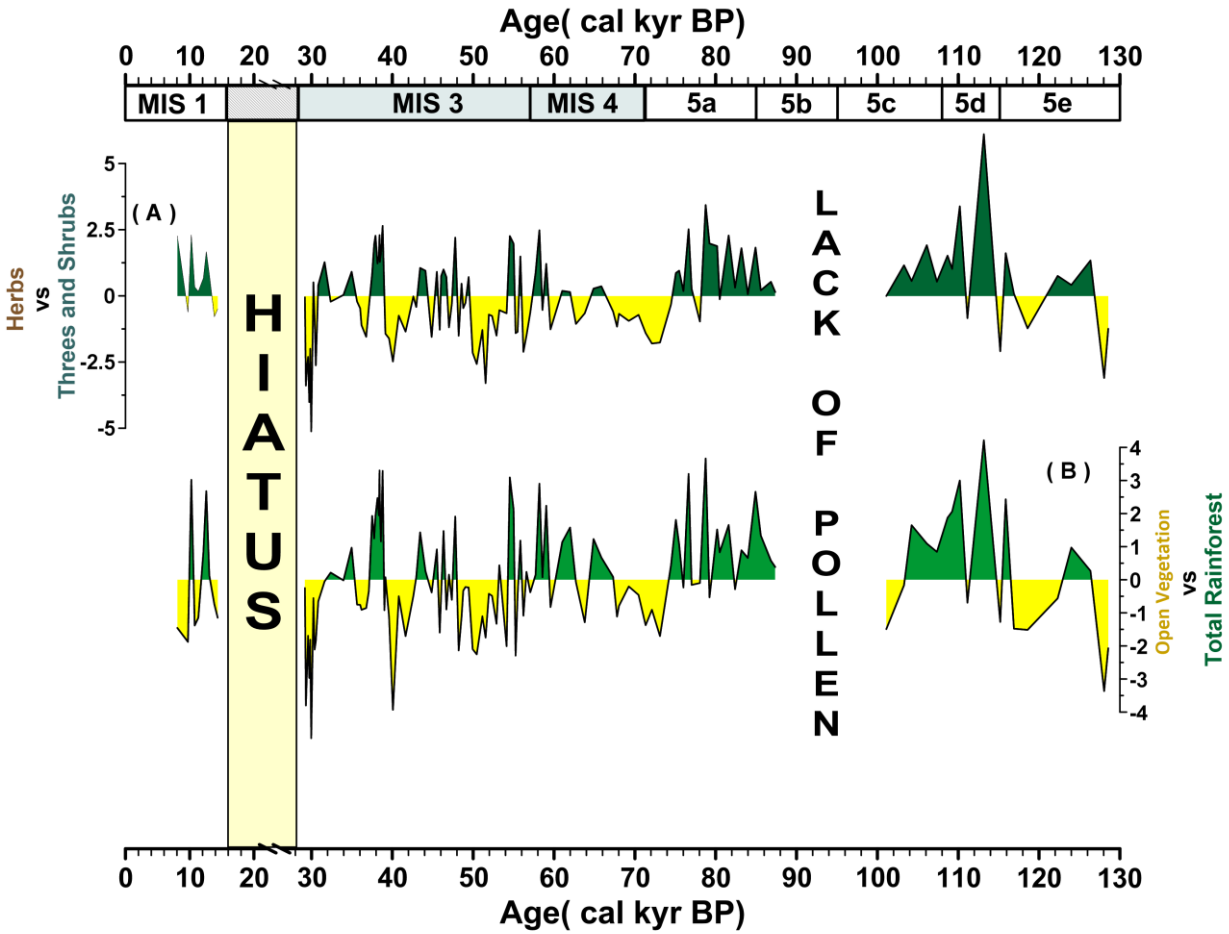

Figure S121: Comparison between (A) Delta structure; positive values indicate an increase in threes and shrubs (filled in green), and negative values indicate an increase of herbs (filled in yellow); (B) Delta coverage, positive values indicate an increase in rainforest lowland (filled in green), and negative values indicate growth of open vegetation (filled in yellow).

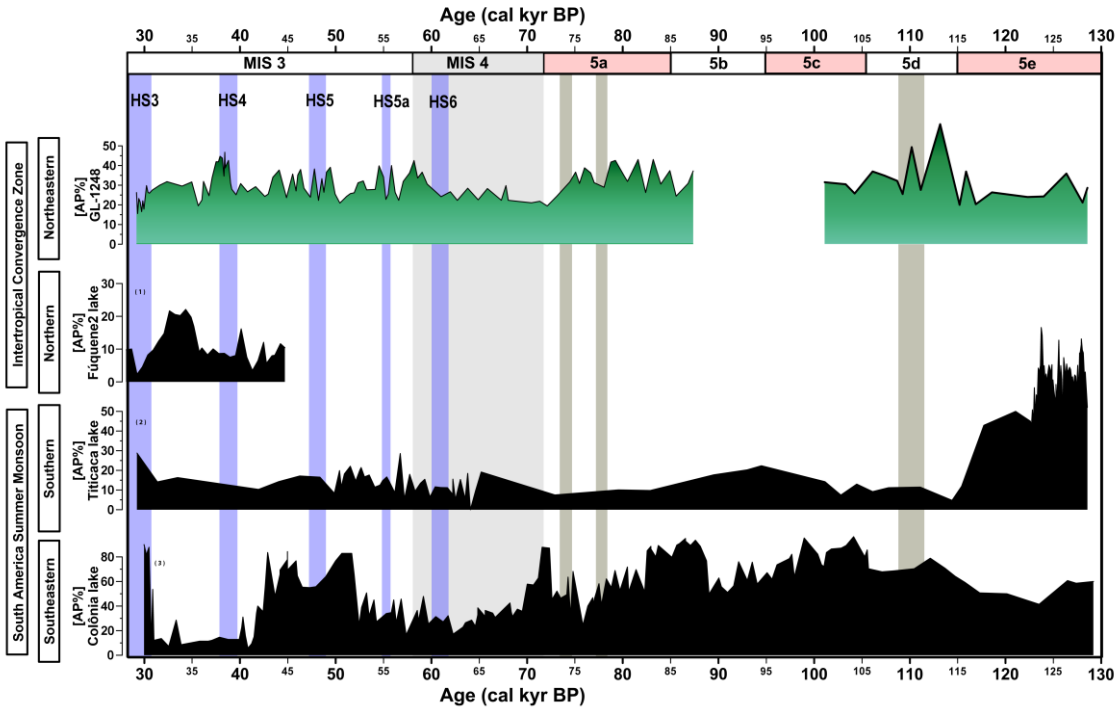

Figure S13: Distinct sites of South America and the vegetation response to different sources of moisture into the continent (SASM and ITCZ shifts) during the Pleistocene. 1-Fúquene2 (05°27′N 73°46′W) (van der Hammen and Hooghiemstra, 2003); 2-Titicaca (16°20′S, 65°59′W) (Paduano et al., 2003, Hanselman *et al.,* 2011); 3-Colônia basin (23°52′S, 46°42′W) (Rodriguez-zorro *et al.,* 2020).

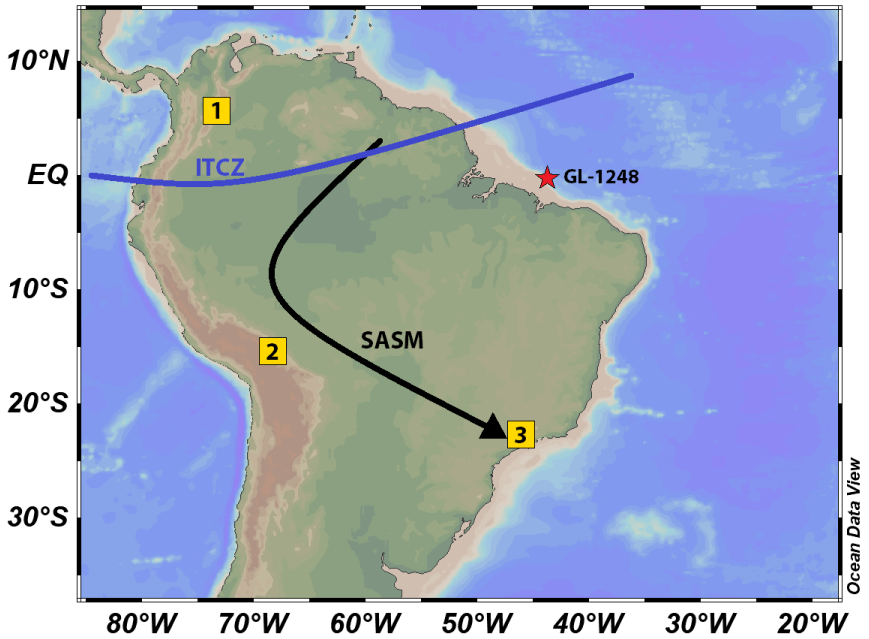

Figure S14: Pollen record over South America and different sources of moisture into the continent (SASM and ITCZ). 1 - Fúquene2 (05°27′N 73°46′W) (van der Hammen and Hooghiemstra, 2003); 2 - Titicaca (16°20′S, 65°59′W) (Paduano et al., 2003, Hanselman *et al.,* 2011); 3 - Colônia basin (23°52′S, 46°42′W) (Rodriguez-zorro *et al.,* 2020); Red star - GL-1248 (this study).

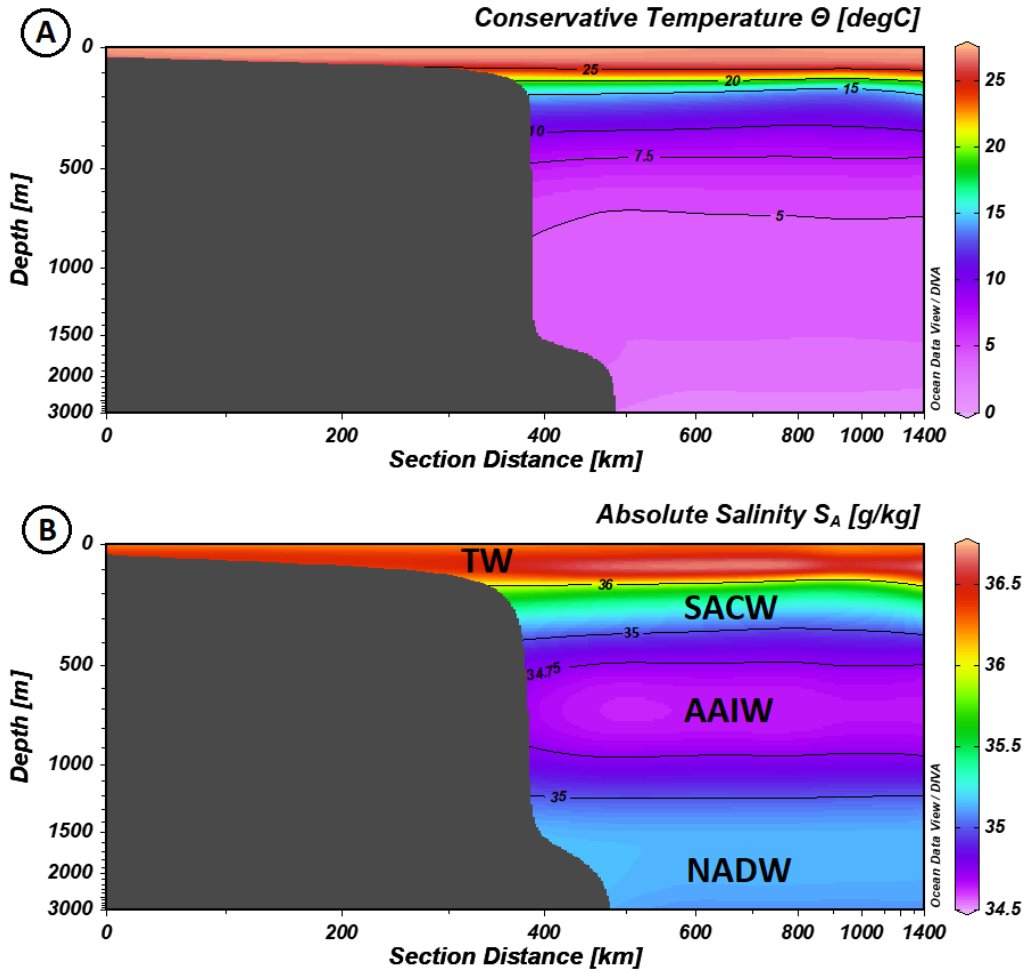

Figure S15 - Bathymetric profile of Barreirinhas bight and its present oceanographic conditions a) conservative temperature and b) absolute salinity, based on the World Ocean Atlas WOA13 (Boyer *et al.,* 2013) and converted toTEOS-10 Standard. We highlight the average salinity and depth of the main water masses salinity (Tropical Water – TW; South Atlantic Central Water – SACW; Antarctic Intermediate Water – AAIW; North Atlantic Deep Water – NADW), following Stramma and England (1999) and adapted for TEOS-10 using Wright *et al.,* (2011).

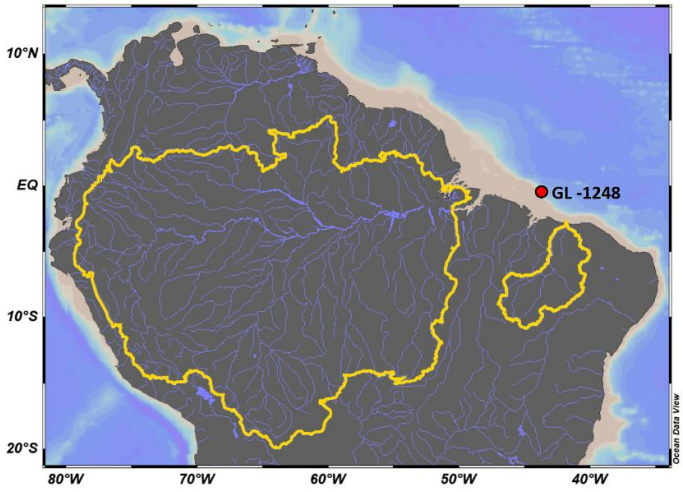

Figure S16 – Comparative size between Amazon and Parnaíba Hydrographic Basins.

Dinocysts diagram of the marine GL 1248

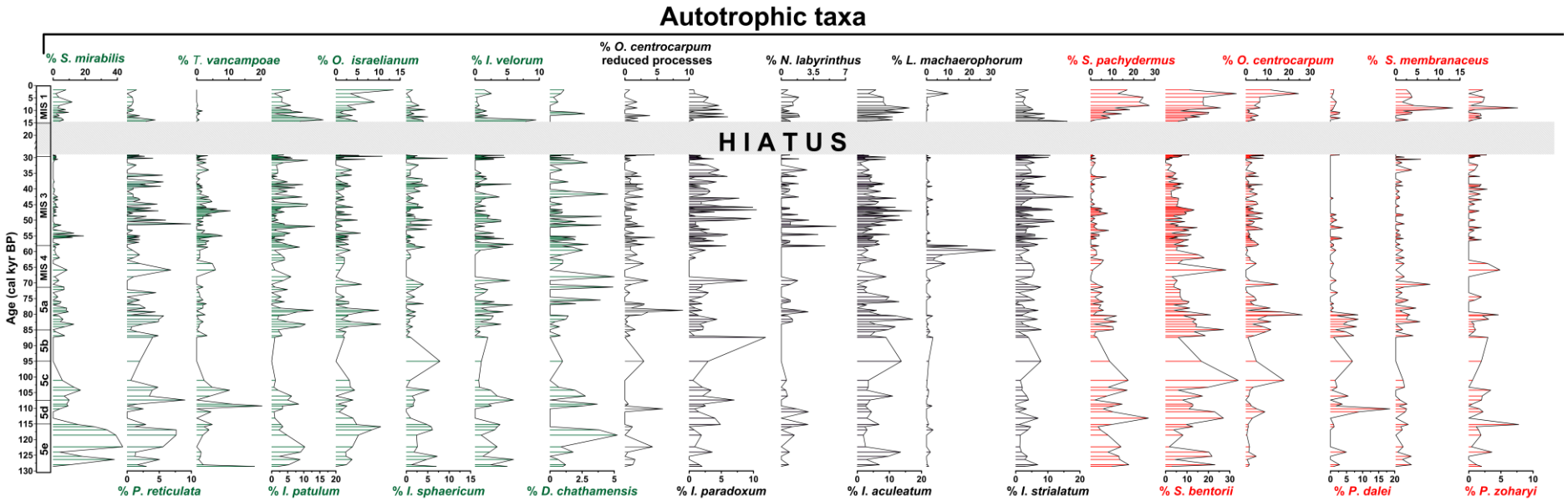

Figure S1227 - Selection of major (> 5%) non-heterotrophic dinocyst species represented in relative abundance. In black the species established in the Neritic assemblage in green the species that were established as Nutricline assemblage and in red the species that were established as Open ocean assemblage.

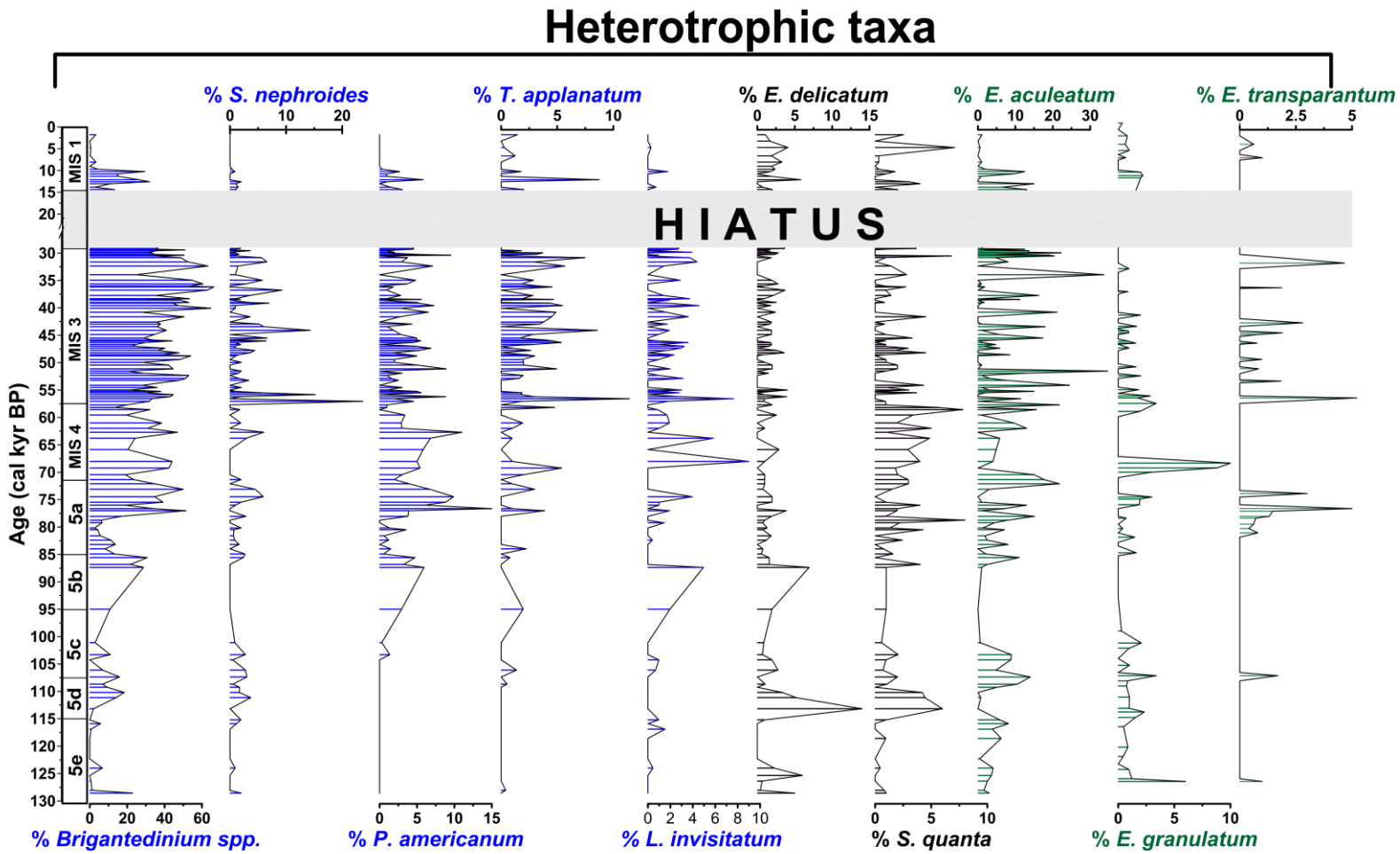

Figure S18 - Selection of major (> 5%) heterotrophic dinocyst species represented in relative abundance. In blue species that were established as River outflow assemblage, in black, the species established in the Neritic assemblage and in green the species that were established as Nutricline assemblage.

Planktonic diagram of the marine GL 1248

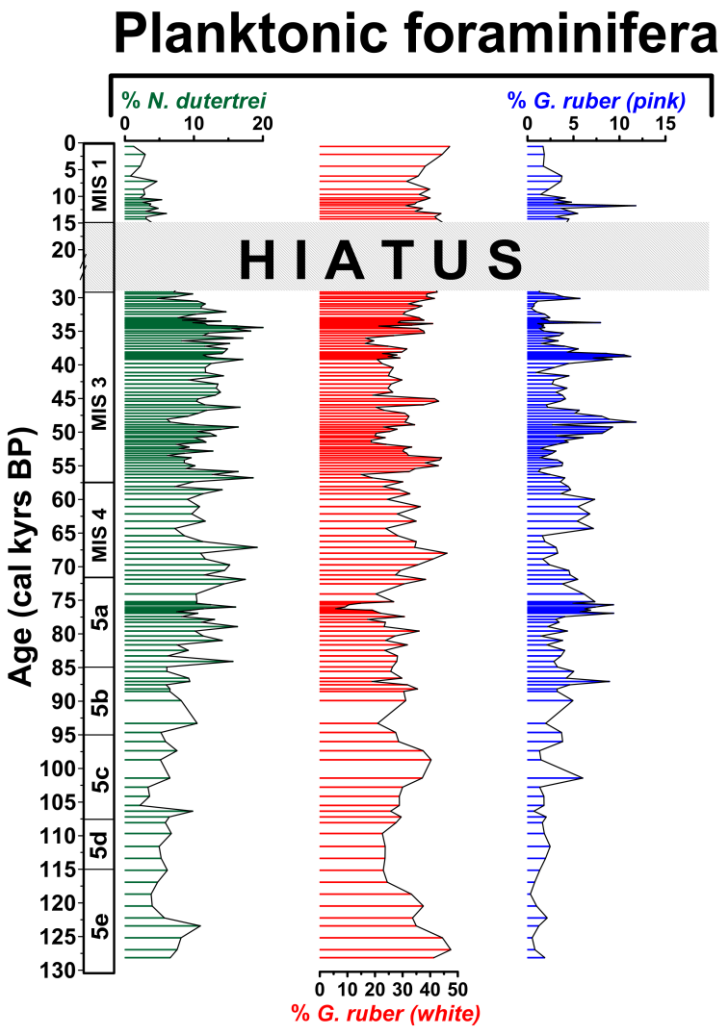

Figure S19 - GL-1248 marine core planktonic foraminifera species represented in relative abundance. In green, the species that were related to enhanced productivity (*N. dutertrei*), in red, the species related to oligotrophic conditions (*G. ruber* (white)), and in blue species related to low salinity (*G. ruber* (pink)).

List of the photographs of selected dinocysts

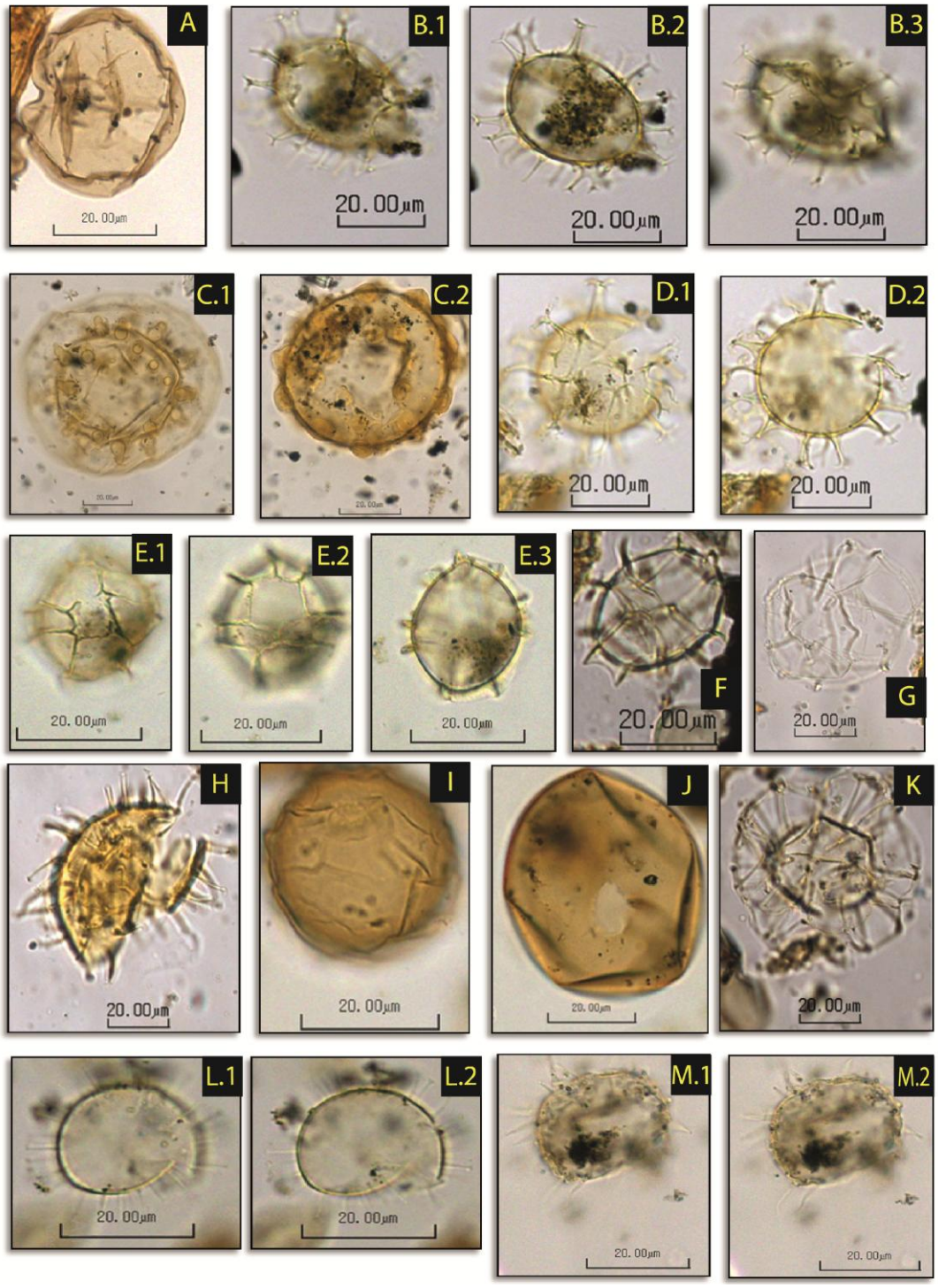

Figure S20- Dinocysts types: A- *Selenopemphix nephroides,* B.1- *Spiniferites bentorii,* B.2- *Spiniferites bentorii,* B.3- *Spiniferites bentorii,* C.1- *Tuberculodinium vancampoae*, C.2- *Tuberculodinium vancampoae*, D.1- *Spiniferites pachydermus,* D.2- *Spiniferites pachydermus*, E.1- *Impagidinium paradoxum,* E.2- *Impagidinium paradoxum,* E.3- *Impagidinium paradoxum,* F- *Impagidinium aculeatum*, G- *Dalella chathamensis*, H- *Polysphaeridium zoharyi*, I- *Protoperidinium americanum*, J- *Brigantedinium spp*, K- *Nematosphaeropsis labyrinthus*, L.1- *Pentapharsodinium dalei*, L.2- *Pentapharsodinium dalei*, M.1- *Lingulodinium machaerophorum,* M.2- *Lingulodinium machaerophorum*